RANGE SAFETY DATA REPORT #4-65
June 17, 1965

GEORGE C. MARSHALL **SPACE FLIGHT CENTER**
HUNTSVILLE, ALABAMA

RANGE SAFETY DATA FOR SATURN SA-10

By

G. W. Solmon and E. L. Leonard

GPO PRICE $ _____

CFSTI PRICE(S) $ _____

Hard copy (HC) ___2.50___

Microfiche (MF) ___.75___

ff 653 July 65

N66 32794

RANGE SAFETY SECTION
FLIGHT MECHANICS BRANCH
FLIGHT EVALUATION AND OPERATIONS STUDIES DIVISION
AERO-ASTRODYNAMICS LABORATORY

National Aeronautics and Space Administration

NASA

S67-37995

C - Form 454 (Revised September 1961)

GEORGE C. MARSHALL SPACE FLIGHT CENTER

Range Safety Data Report #4-65

RANGE SAFETY DATA FOR SATURN SA-10

G. W. Solmon and E. L. Leonard

$N66-32794$

ABSTRACT

The purpose of this report is to present range safety
data for the Saturn SA-10 vehicle. This study is based on the
standard trajectory to be published by R-AERO-FM. It has
a firing azimuth of 95.2 degrees east of true north and
goes into orbit at an alitude of 289 nautical miles. The
standard and dispersions have been provided on magnetic tape.

One of the primary objectives for the SA-10 vehicle is
to place the Pegasus (Micrometeoroid) satellite into a
circular orbit. Other primary vehicle objectives are the
further flight testing of the S-I and S-IV structure, pro-
pulsion, control systems, S-I/S-IV separation sequence,
and closed loop guidance during S-IV flight. Additional
vehicle objectives are to obtain Apollo boilerplate data,
further tests of the Launch Escape System (LES), and
general Apollo development.

The reliability analysis of the S-IV-8 and S-IV-10
stages was performed by Douglas Aircraft, and is presented
in the Appendix.

Author

GEORGE C. MARSHALL SPACE FLIGHT CENTER

Range Safety Data Report #4-65

June 17, 1965

RANGE SAFETY DATA FOR SATURN SA-10

by

G. W. Solmon and E. L. Leonard

RANGE SAFETY SECTION
FLIGHT MECHANICS BRANCH
FLIGHT EVALUATION AND OPERATIONS STUDIES DIVISION
AERO-ASTRODYNAMICS LABORATORY

(U) TABLE OF CONTENTS

(U) LIST OF ILLUSTRATIONS

(U) DEFINITION OF SYMBOLS

Symbol	Definition
t_c (sec)	Time of engine cutoff
α (deg)	Angle of attack
XYZ (meters)	Magnitudes of the components of the missile's displacement in the earth-fixed X, Y, Z axis, respectively.
$\dot{X}\dot{Y}\dot{Z}$ (meters/sec)	Magnitudes of the components of the missile's velocity in the earth-fixed X, Y, Z axis, respectively.
F (newtons)	Thrust, including gain due to altitude
θ (deg)	Angle measured between the local vertical and the velocity vector (theta)
A (deg)	Aiming azimuth of the missile measured clockwise from North
χ (deg)	Pitch attitude angle as measured by missile hardware (chi)
m (kg)	Mass of vehicle
q (newtons/m^2)	Dynamic Pressure
ρ (kg/m^3)	Density of the air, a function of altitude
V_e (m/sec)	Velocity of missile relative to the earth
M	Mach number
A_T (m/sec^2)	Longitudinal load factor
h (meters)	Altitude
θ_r (deg)	Arc tan $DZZe / \sqrt{(DXXe)^2 + (DYYe)^2}$
θ_v (deg)	Arc tan $DYYe/DXXe$

GEORGE C. MARSHALL SPACE FLIGHT CENTER

RANGE SAFETY DATA FOR SATURN SA-10

by

G. W. Solmon and E. L. Leonard

SUMMARY

The data presented in this report are for the Saturn
SA-10 vehicle, with a firing azimuth of 95.2 degrees east
of true north.

This report is based on a standard trajectory to be
published by R-AERO-FM, with other pertinent information
furnished by R-P&VE and Douglas Aircraft Company.

The data submitted consists of booster and Launch
Escape System impact areas, effects of range safety
termination, land impact probabilities, injury probabilities,
and turning rate effects. Graphs of turning rates and
earth-fixed velocity as a function of time, after malfunction
is introduced, are given for the S-I and S-IV stages.

Data consisting of standard, ± 3 σ dispersions, and
booster free flight trajectories have been forwarded to the
Cape on magnetic tape as requested by Range Safety.

The iterative guidance was used in the second stages
for the standard and $\pm$ 3 σ dispersion trajectories.

SECTION I. INTRODUCTION

The purpose of this report is to present range safety data for Saturn SA-10 vehicle. The data presented herein are based on the final standard trajectory to be published by R-AERO-FM.

The engines to be used for the first stage in Saturn SA-10 have a sea level thrust of 188,000 pounds (836,000 newtons) each. The inner four engines have a fixed cant angle of 3° to the missile axis. The outer engines, which are free to swivel for control, are canted 6° to the missile axis. The second stage has six RL-10A3 engines which have a vacuum thrust of 15,000 pounds (66,700 newtons) each.

This report was based on the trajectory having an aiming azimuth of 95.2 degrees East-of-North with an insertion altitude of 535 kilometers.

SECTION II. DESCRIPTION

A. Standard Trajectory Variations

The variations of the standard trajectory are listed below:

(1) 3σ Maximum $\begin{bmatrix} +2\% \text{ F}, +1\% \text{ } \dot{m}, +E_X \text{ Wind}, -3,500 \text{ lbm in 1st Stage} \\ +2\% \text{ F}, +1\% \text{ } \dot{m}, -1,000 \text{ lbm in 2nd Stage} \end{bmatrix}$

(2) 3σ Minimum $\begin{bmatrix} -2\% \text{ F}, -1\% \text{ } \dot{m}, \quad -E_x \text{ Wind}, +3,500 \text{ lbm in 1st Stage} \\ -2\% \text{ F}, -1\% \text{ } \dot{m}, +1000 \text{ lbm in 2nd Stage} \end{bmatrix}$

(3) 3σ Lateral $\begin{bmatrix} +E_z \text{ Wind, Motor \#4 out at 100 sec in 1st Stage} \\ \text{No crossrange guidance in 2nd Stage} \end{bmatrix}$

(4) Extreme Lateral $\begin{bmatrix} +E_z \text{ Wind, Motor \#4 out at 0 sec} \end{bmatrix}$

(5) Steepest $\begin{bmatrix} +2\% \text{ F}, +1\% \text{ } \dot{m}, \text{ Headwind}, -3,500 \text{ lbm} \end{bmatrix}$

(6) Flattest $\begin{bmatrix} \text{Motor \#4 out at 0 sec, Tailwind} \end{bmatrix}$

In addition to impacts given every second on the Cape Tape, impacts will be given in tabular form every 20 seconds until near orbital conditions, thereafter, at 1 second intervals for the standard, 3σ maximum, and 3σ minimum. The following parameters will be given in the tables: instantaneous cutoff time, geodetic latitude, longitude, remaining flight time, and range along the surface of the earth from launch to impact. Tables are on pages 43-48.

B. (U) Effects of Range Safety Flight Termination

If the vehicle, for purposes of range safety, is to be destroyed in early flight phase, the most probable pieces, according to P&VE and DAC, are considered to be the following:

	Mass (kg)	Area (sq. m)	Velocity Increment (m/sec)	Drag Curve to be used Figure #
(a) S-I Stage (1)	54,940	33.47 (cs)	2.0	3
(b) S-IV Stage (1)	6,271	24.52 (cs)	2.0	4
(c) 4-Engine Cluster (1)	2,818	4.26 (m)	9.0	5
(d) Single Engine (8)	880	1.12 (m)	7.2	6
(e) Instrument Canister (1)	228	1.03 (cs)	7.0	7
(f) Fragment of S-I Barrel Section (2)	227	3.68 (p)	95.1	8
(g) Fragment of S-I Tail Shroud (2)	136	.68 (p)	29.6	8
(h) Fragment of S-I Heat Shield (2)	34	.18 (p)	30.5	8
(i) LES (1)	1,285	.34 (cs)	9.0	9
(j) Command Module Without LES	4,203	12.02 (cs)	9.0	10
(k) Fragment of S-I Barrel Sections (1)	23	.40 (p)	95.0	8
(l) 70" Diameter Tank	1,768	2.48 (cs)	30.0	12
(m) Turbopump Assembly	181	5.06 (cs)	9.0	13
*(n) Forward Interstage Skin	134	17.19 (p)	141.0	8
(o) Forward Dome Skin	453	48.77 (p)	66.0	8
(p) Cylindrical Tank Skin	97	7.90 (p)	95.0	8
(q) Common Bulkhead	244	19.97 (p)	80.0	8
(r) Aft Interstage and Skirt Skin	151	17.19 (p)	125.0	8
(s) Upper Portion of Aft Dome	37	3.25 (p)	105.0	8
(t) Lower Portion of Aft Dome	116	15.79 (p)	140.0	8

NOTE: Figure in parenthesis after (a) through (i) indicates number of pieces.

cs - cross sectional; m- mean; p - planiform

For the maximum and minimum distance pieces, the approximate drag can be calculated as $D = C_D q A$. The C_D curves are given in Figures 3 - 13.

*Pieces (n) through (t) are representative pieces given by DAC for the S-IV stage. (see Appendix.)

4

C.   (U) Tracking Equipment

SA-10 has the following onboard antenna locations:

VHF Telemetry Antenna Sta. 909.929	S-I Stage 5.75° II→ I 5.75° II→III 5.75° IV→ III 5.75° IV→I
VHF Telemetry Antenna Sta. 1483.084	IU Stage 5°10' II→III 5°10' IV I
Command Antenna Sta. 868.6	S-I Stage 5°30' I→ IV , 5°30' I→II 5°30' III→II 5°30' III→IV
Command Antenna Sta. 1471.889	IU 28°07'30" I——→ IV 28°07'30" III→II
ODOP Receiving Antenna Sta. 1483.424	33°45' I→ IV
ODOP Transmitting Antenna Sta. 1483.424	33°45' IV→I
Altimeter Antenna Sta. 1474.414	Fin I
MISTRAM Antenna Sta. 1467.934	11°15' IV→I 4°38'30" IV→III
Command Antenna System Sta. 1384.157	Fins II & IV (Transverse) Fins I & III (Longitudinal)
Telemetry Antenna System Sta. 1423.092	S-IV Stage Fins I & III (Transverse) Fins II & IV (Longitudinal)
Television Antenna Sta. 872.459	2°40' IV-I
Radar Antenna Sta. 1466.596	39°22'30" I→ IV
Azusa Antenna Sta. 1475.721	11°14' I→IV

D. (U) Wind Disturbances

For this analysis, the winds considered are the 3 σ winds published by W. W. Vaughan, M-AERO-F-53-63, "Cape Canaveral, Florida, Wind Profile Envelopes for Selected Flight Azimuth," March 28, 1963. (See Figure 1.)

E. (U) Vehicle Velocity Turning Angle Investigation

The vehicle velocity vector turning data for the standard is presented in Figures 19-72 . These figures give the reorientation of the total velocity vector in the lateral direction as a function of time once the malfunction (engine gimbal deflection) in yaw is introduced.

In the past, an investigation was made of the reorientation of the velocity vector in the vertical plane (X_e, Y_e). Gravity was removed at the time the malfunction (engine gimbal deflection) was introduced in pitch. Under these conditions, there is no significant difference in turning rates in the lateral direction and the pitch plane; thus, only lateral turning rates are given. The lateral turning rates are symmetrical; hence, the vehicle was only yawed to the right.

When yaw turning rates are investigated, the engine gimbal deflection angle in pitch (beta p) is set at zero degrees deflection. The yaw malfunction chosen is held fixed throughout any specific investigation. These turning rates can be translated to the ± 3 σ trajectories given on tape by use of the following time equivalent relations.

Standard Trajectory, Time of Turning Rate (sec)	Maximum Trajectory, Time of Turning Rate (sec)	Minimum Trajectory, Time of Turning Rate (sec)
30	29	32
80	76	83
130	126	133
190	190	190
410	410	410

The relative velocity of the turning rate cases is given as a function of time in Figures 73-126.

F. (U) Downrange Land Impact Probability

Statistical data in regard to impact resulting from malfunctions which occur during the late phase of the second stage is presented. For these calculations, it was assumed that first stage functioned properly and that second stage failed to reach orbital conditions. It was assumed that the probability of the vehicle dropping short is approximately .13 for the second stage; this is based on data given in Appendix ' by DAC for the S-IV stage. The instantaneous impact time ($\triangle$ t) over land on the 95.2° standard trajectory is approximately 4.9 sec.

A 3 σ corridor was determined for the overland flight (Figure 16) by taking the root sum square of the following: impacting the vehicle after it turned with a maximum rate until alpha yaw had reached 180°; impacting the 3 σ lateral case; assuming that the vehicle had exploded, taking the most critical piece, injecting a $+E_z$ wind and the velocity increment in the +Z direction and impacting the piece.* These results are shown in the table below.

WIDTH OF RIGHT SIDE OF 3 σ CORRIDOR IN N. MI.			
Turning Rates (Vacuum) Right Side Cross Range (n.mi.)	Wind + $\triangle$ Velocity (Drag Considered) Right Side Cross Range (n.mi.)	Motor #4 out 100 sec (Vacuum) Right Side Cross Range (n.mi.)	Resultant For Right Side Σ (RCR)
20	55	10	59.4

*Piece (o) in paragraph B.

The probability of impacting on land can be calculated as follows:

$$P_I = \frac{\triangle t}{T_B} \; X \; P_F$$

P_I - probability of impacting on land

$\triangle t$ - dwell time

T_B - total burn time of second stage

P_F probability of any failure causing the 2nd stage to drop short

$$P_I = \frac{4.9}{480.1} \; X \; .13 = 1.3 \; X \; 10^{-3}$$

Impact probabilities for individual countries are as follows:

Land Area	Dwell Time	Impact Probability
Angola	2.8	7.6×10^{-4}
Rhodesia and Nyasaland	1.5	4.1×10^{-4}
Bechuanland	.1	2.6×10^{-5}
Mozambique	.3	8.1×10^{-4}
Madagascar	.2	5.3×10^{-5}

G. Probability of Injuring a Person

The probability of injuring a person downrange can be determined in the following manner:

$$P_{IP} = P_I \times \frac{N}{L_A} \times A_L$$

P_{IP} - probability of injuring person

$\frac{N}{L}$ - population density of country (people per sq. mi.)

A_L - lethal area (sq. mi.)

Based on Appendix by Douglas, the S-IV stage has approximately 3,000 sq. ft. of lethal area. This includes the additional area contributed by the piece falling at an angle of $15°$ to the vertical and the projected lethal effect on a person.

A sample calculation: Forward Interstage Assembly: $A = 185 \text{ ft}^2$;

Number of pieces = 8 $\frac{A}{Pieces} = \frac{185}{8} = 23.12$

Assuming this piece to be square, one side = $\sqrt{23.12} = 4.808$ ft.

Assume an average man is 6 ft. tall and this piece comes in at 15° to the vertical. The lethal area of this piece is increased by tan. 15° (6 ft.) (4.808) = 7.7 ft^2. Adding this to 23.12 ft^2 and multiplying by 8 pieces, we get the total lethal area as 246.5 ft^2 for the forward interstage assembly. Then, in addition, we should assume that the dense pieces could impact on hard surfaces, giving an estimated splatter effect of an additional 2,000 sq. ft. Thus, the approximate total lethal area of the S-IV-10 stage is conservatively estimated to be 5,000 sq. ft.

The probability of injuring a person by overflying land is:

$$P_{IP} = .0013 \ X \ 20 \ X \ \frac{5,000}{27,878,400} = 4.7 \ X \ 10^{-6}$$

Probability of injuring Person for individual countries:
    (3 σ deviation) (Sectors 1 and 2, Figure 16)

$$P_{IP} = P_I \ X \ \frac{N}{L} \ X \ A_L$$

Country	P_I	$\frac{N}{L_A}$ (People per sq. mi.)	Probability of Injuring a Person
Angola	7.6X10^{-4}	25	3.4 X 10^{-6}
Rhodesia & Nyasaland	4.1X10^{-4}	12	8.8 X 10^{-7}
Bechvanaland	2.6X10^{-5}	1	4.7 X 10^{-9}
Mozambique	5.3X10^{-5}	25	3.6 X 10^{-7}
Madagascar	5.3X10^{-5}	21	2.0 X 10^{-7}

Disregarding hardware limitations and the likelihood of occurence, it was desired to determine the absolute maximum lateral deviation that could be obtained from a malfunction that could occur after reaching the "gate" (IIP reaches land). The vehicle was assumed to instantaneously yaw (ϕ y) to the left and also have a variation in the pitch (ϕ_p) plane. If we assume fuel depletion with these maximum deviation conditions, the following impacts are obtained.

	Variations		Impact*	
Case	ϕ_P	ϕ_y	Geodetic Latitude	Longitude
1	5	-70	-16.1	-34.4
2	5	-80	-6.7	-14.2
3	-5	-70	-16.3	-35.0
4	-5	-80	-10.8	-22.3
5	-15	-70	-14.0	-30.0

These are sketched in Figure 16. Then, in addition to the above probabilities, we have the following impact and injury probability in sectors 3 and 4.

Country	P_I	$\frac{N}{L_A}$	Probability of Injuring a Person
Angola	1.9×10^{-6}	25	8.5×10^{-9}
South West Africa	9.1×10^{-7}	24	2.9×10^{-9}
Union South Africa	3.3×10^{-7}	24	1.4×10^{-9}
Bechvanaland	7.0×10^{-7}	1	1.3×10^{-10}
Basutoland	1.1×10^{-7}	50	9.9×10^{-10}
Mozambique	2.2×10^{-7}	17	6.7×10^{-10}
Madagascar	1.3×10^{-7}	25	5.8×10^{-10}
Rhodesia & Nyasaland	1.0×10^{-6}	12	2.2×10^{-9}

The probability of impacting outside of sectors 3 and 4 in Figure is Zero with the present propellant loading and range safety action being taken before the vehicle reaches the "gate."

*Based on superimposed corridor from SA-8.

H.   Sequence of Events

Given below are the times that the major events occur during the nominal case:

Nominal Sequence of Events

Time of Event (From Liftoff)	Remarks
0.0	Liftoff
9.0	Initiate Roll and Pitch Simultaneously
14.2	Terminate Roll
137.7	S-I Stage Propellant Level Sensors Enabled
138.0	Tilt Arrest
141.7	S-I Stage Level Sensor Signal
143.52	Inboard Cutoff (S-I Stage)
149.52	Outboard Cutoff (S-I Stage)
150.22	Ullage Rocket Ignition(S-IV Stage)
150.32	Separation, Immediately Followed by Retro Ignition (S-I Stage)
152.02	S-IV Mainstage Ignition
162.32	Jettison Ullage Rocket Casing and LES
168.0	Initiate Active Guidance
595.0	Signal from Sequencer to Arm LOX Depletion Cutoff Capability
632.085	S-IV Stage Main Engine Cutoff
642.085	End of Powered Flight

I. Booster Impact

Further cursory investigation by R-P&VE-V on the re-entry of the S-I boost stage after separation confirms that the major pieces of it will remain intact as it re-enters the atmosphere. However, they state it is possible for thin metal pieces (panels, etc.) weighing less than 50 lbm to break loose from the S-I stage upon re-entry. Based on this, the following booster impact analysis has been performed.

The booster and a representative piece as described (thin metal piece) were impacted. .The applicable drag was used for the trajactories and the appropriate winds were applied. Figure 17 gives an ellipse of the impact dispersion points, which are as follows: -

Booster

Trajectory	Latitude	Longitude
Standard	27.2019	70.7510
Maximum	27.0480	69.9469
Minimum	27.3036	71.2720
3 σ Lateral	26.9707	71.2810

50 lbm Barrel Section

Standard	27.2100	70.7923
Maximum	27.0742	20.0439
Minimum	27.3388	71.5496
3 σ Lateral	26.9380	71.4710

J. LES Impact

An analysis concerning LES impact has been performed and Figure 17 gives the ellipse. The ellipse was determined as follows. The LES was ejected 10.3 seconds after ignition of the S-IV-10 stage from the ± 3 σ dispersion trajectories given on magnetic tape. The impacts were as follows:

Trajectory	Latitude	Longitude
Standard	26.9446	69.3584
3 σ Maximum	26.7964	68.6319
3 σ Minimum	27.0937	70.0891
3 σ Lateral	26.7359	70.1045

K. Pad Area Study

For this study the effects of Vehicle turning rates, velocity increment due to destruct and a wind from 67.5° E of N were combined to give the maximum deviation toward the industrial area. The results of this study indicate that, to avoid any impact of maximum distance pieces due to destruct, on critical areas, the wind profile given in Figure 1-A should not be exeeded. The probability of the 67.5° E of N wind, exceeding the profile given in Figure 1-A is less than 10% based on R-AERO-Y's wind profile for the month of August.

A P P E N D I X

by

DAC

14

RANGE SAFETY FLIGHT TERMINATION SYSTEM

4. RANGE SAFETY FLIGHT TERMINATION SYSTEM

4.1 Description and Function

The RSFT (range safety flight termination) system (figures 4-1 and 4-2), (electrical and ordnance), is a dual system which provides a high degree of reliability. Each system is capable of imposing a condition of·zero thrust, and causing fuel dispersion in the event of erratic performance of the vehicle. In addition to various antenna systems and wire bundles, the RSFT system consists of the following major components:

    a. Power supplies

    b. Command destruct receivers

    c. RSFT system controller

    d. Power distribution boxes

    e. EBW electronic firing units

    f. Safety and arming device

    g. EBW detonators

    h. Explosive harness assemblies

    i. Linear shaped charges

Refer to Section 3, Explosive Ordnance and Associated Electrical Systems, for description and function of the aforementioned items.

The ordnance portion of the system consists of EBW detonators, explosive harness assemblies, and linear shaped charges. The detonators, through the safety and arming device, detonate small charges in the ends of the explosive harness assemblies. The harness assemblies propagate the detonation to the linear shaped charges mounted on the side of the LH2 tank and the bottom of the LOX tank. Exploding the shaped charges ruptures the tanks, allowing the propellants to disperse. In addition, an explosive harness interconnection is provided between the destruct systems of the S-I and S-IV stages. This interconnection is singular on the S-I stage side of the explosive interconnection blocks.

The RSFT electrical circuitry is located in the forward section of the S-IV stage and consists of the power supplies, destruct system controller, power distribution box and the EBW electronic firing units. A separate circuit controlled from the ground permits switching the safety and arming device from one position to another.

19 April 1965

Accidental detonation of the linear shaped charges during preflight checkout operations on the launch pad is prevented for most of the time by the safety and arming device which maintains an out of line condition in the explosive trains. However, the switching function of the device which is singular, is relegated to the launch pad and is switched to the arm condition just before liftoff, but is monitored both electrically and visually on a panel in the blockhouse. The firing units are charged only after launch in the event of a decision to initiate flight termination.

4.2 Operation

4.2.1 Final Arming Prior to Launch

The EBW electronic firing units (2) will not be charged on the ground. A "not ready" condition of the firing units will be indicated on the S-IV, stage destruct panel (figure 4-3). The safety and arming device will be cycled to the armed position approximately 3 minutes prior to liftoff and the conditions verified on the S-IV destruct panel.

4.2.2 Arming After Launch

If after liftoff, the vehicle deviates from the predicted flight path to the extent that a hazardous condition exists, the RSFT system in the S-IV stage delivers the required flight termination command by decoding frequency-modulated signals received from a ground transmitter. These UHF signals are received by the S-IV stage antenna system, provides omnidirectional coverage about the vehicle regardless of its attitude. Two command destruct receivers are located in the forward interstage area of the S-IV stage. Each receiver relays a signal to the S-IV stage destruct system controller. The signal from either receiver is capable of activating the controller for the detonation of the linear shaped charges.

4.2.3 Range Safety Flight Termination

Range safety flight termination is initiated by the range safety officer if after liftoff, the vehicle deviates from the predicted flight path to the extent that a hazardous condition exists. The following sequence is initiated by closing the destruct switch in the launch control center:

19 April 1965

a. The command transmitter sends an FM, audio-coded signal to the vehicle.

b. The receiving antennas transfer the signal to the command destruct receiver.

c. The command destruct receiver demodulates and decodes the signal; the commands are fed to the command destruct controller.

d. The command destruct controller initiates engine cutoff through the flight sequencer and subsequently triggers the firing units.

e. The firing units activate the high voltage detonators.

f. The detonators explosion is propagated by the explosive harness assemblies and the linear shaped charges. Explosion of the linear shaped charges mounted on the outside of the LH2 and LOX tanks, ruptures the tanks permitting fuel dispersion.

19 April 1965
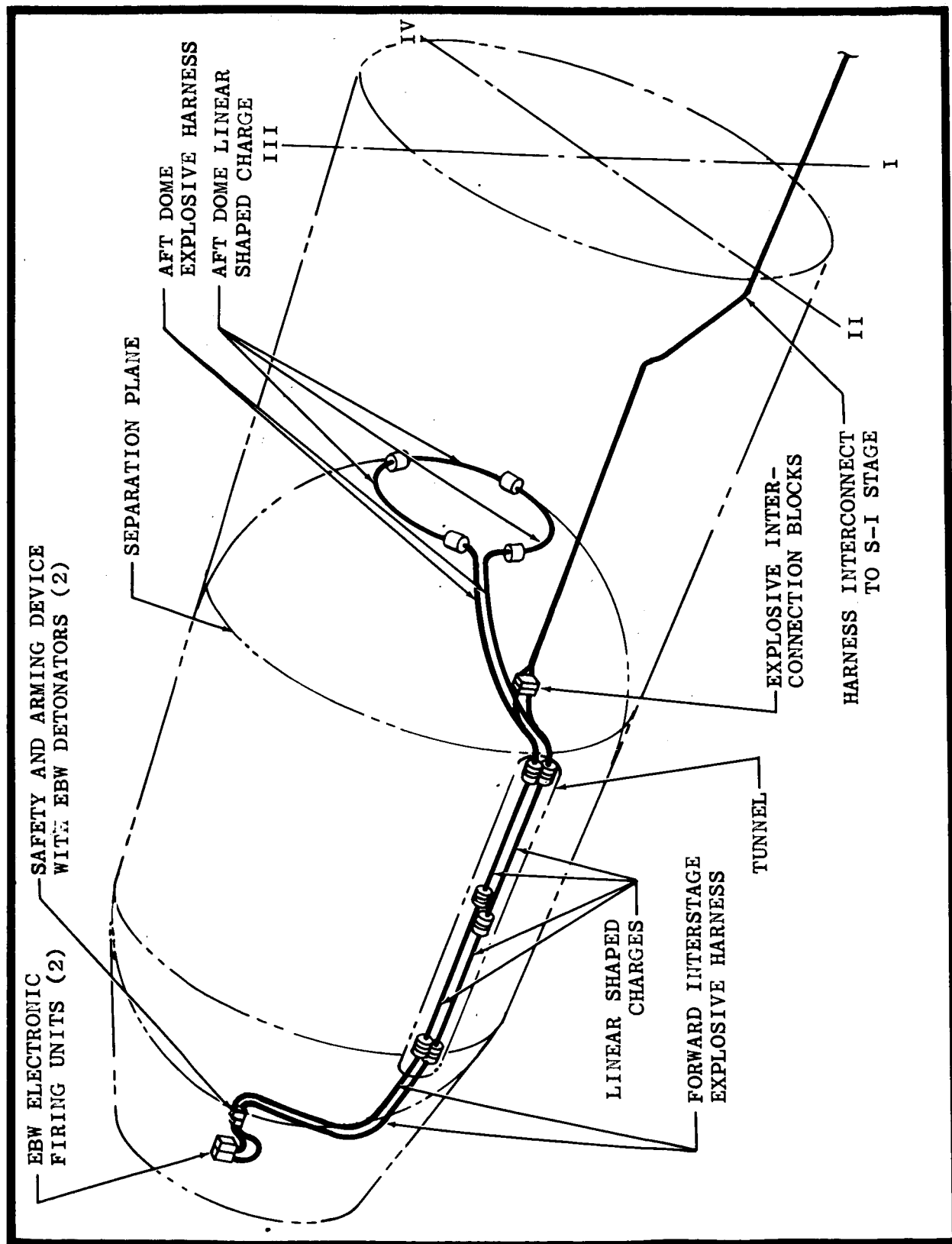
Figure 4-1 Range Safety Flight Termination System

19 April 1965
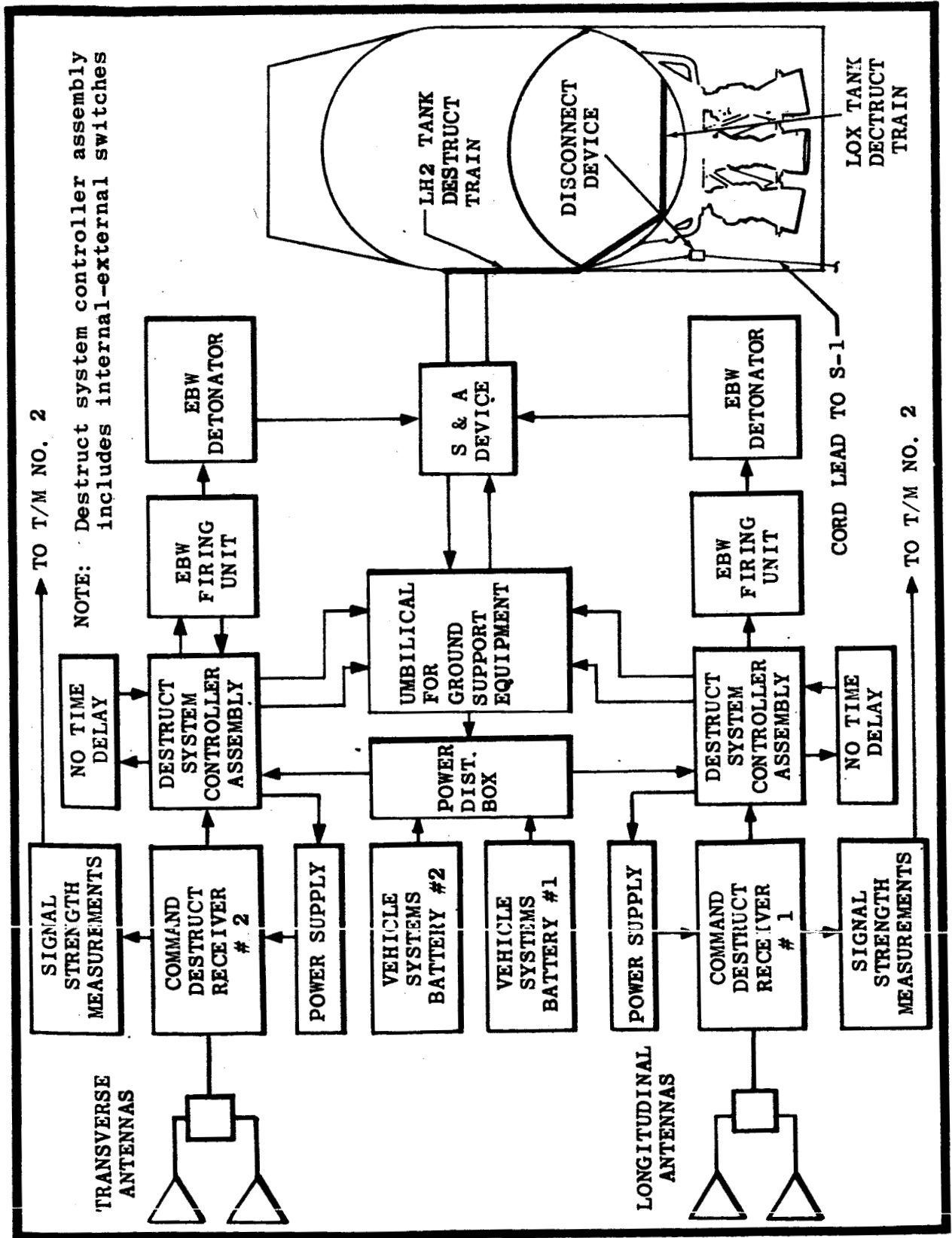
Figure 4-1

Figure 4-2 Range Safety Flight Termination System Block Diagram

19 April 1965
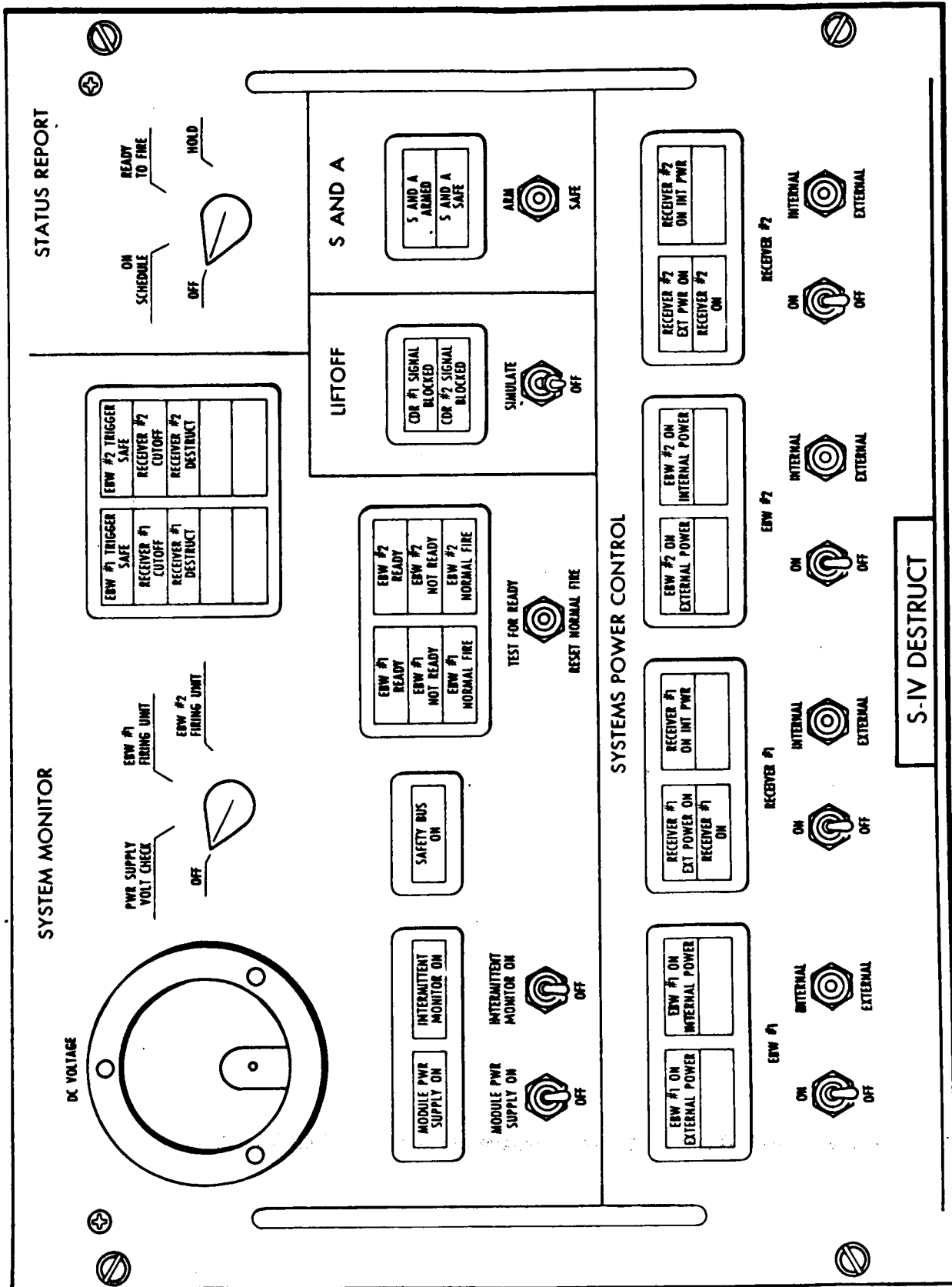
Figure 4-2

Figure 4-3 S-IV Stage Destruct Panel

SECTION 5

EFFECTS OF RANGE SAFETY FLIGHT TERMINATION

5. EFFECTS OF RANGE SAFETY FLIGHT TERMINATION (RSFT)

5.1 General

The S-IV stage can be destroyed in flight by the range safety flight termination (RSFT) system. In order to discuss the destructive effect of the system on the stage, the stage total flight time has been divided into three flight phases (1) before S-I/S-IV separation, (2) after S-I/S-IV separation with S-IV stage propellant tanks nearly full, and (3) after S-I/S-IV separation with S-IV stage propellant tanks nearly empty.

5.2 Effects of RSFT Before Stage Separation

Initiation of RSFT before stage separation will result in one of three situations: (1) the stage will break up and its propellants will detonate, (2) the stage will break up but its propellants will not detonate, and (3) the stage will not break up. DAC believes that stage breakup will occur and the propellants will mix and detonate and that breakup will be caused either by aerodynamic loads, tumbling inertial loads, or by forces created by the destruction of the S-I stage. However, the possibility that the stage may break up and not detonate is considered, as is the possibility that the stage may not break up at all.

5.2.1 Stage Breaks Up With Propellant Detonation

Breakup of the S-IV stage with propellant detonation can occur only as a result of S-I stage destruction and propellant explosion. In this case, the debris falling from the stage will consist of the following pieces: (It is recommended that for range safety purposes, it be assumed that all debris will survive re-entry into the atmosphere).

> a. Skin pieces (maximum size 10 ft^2) originating from the skin sections described in figure 5-1 and tables 5-1 and 5-2.
>
> b. Individual RL10A-3 rocket engines, including hydraulic actuators.
>
> c. Ullage rockets-loaded.
>
> d. Ullage rockets-expended.
>
> e. Helium heater.
>
> f. Base heat shield.

19 April 1965

Section 5
Effects of Range Safety Flight Termination

g. Electronics rack and units (1 piece) located on the forward interstage assembly.

h. Electronics units, such as the instrumentation signal conditioning equipment, located outside of the thrust structure.

i. Thrust structure (including electric equipment and accessories inside, and that portion of the aft dome that extends below the thrust structure junction; excluding engines, external electronic packages, helium heater, and control helium sphere).

j. Cold helium spheres.

k. LH2 tank makeup helium sphere.

l. Pneumatic control helium sphere

It should be emphasized that the number of pieces are estimates only, based primarily on data obtained from vehicles previously destroyed in flight. More accurate estimates can be obtained only by conducting full-scale tests.

5.2.2 Stage Breaks Up Without Propellant Detonation

If the stage breakup does occur without a propellant detonation, breakup would be caused by aerodynamic and tumbling inertial loads. The propellants will vaporize at ambient pressure, and temperature and the following skin pieces and components will fall as debris. (This debris will not have had energy imparted to it.)

a. Skin pieces from the S-IV stage.

b. Individual RL10A-3 rocket engines, including their hydraulic actuators (only if the engines break off at the thrust structure).

c. RL10A-3 rocket engine, thrust structure, helium heater, and portion of aft dome extending below thrust structure junction (only if engines do not break off at thrust structure).

d. Ullage rockets-loaded.

e. Electronics rack and units (one piece) located on forward interstage assembly (only if rack breaks off at the forward interstage assembly).

19 April 1965

f. Electronics units, such as the instrumentation signal conditioning equipment, located outside of the thrust structure (only if the units break off at the thrust structure).

g. Thrust structure, including electronic equipment accessories mounted inside and at that portion of the aft dome extending below the thrust structure junction; excluding engines, external electronics packages, helium heater and control helium sphere (only if the excluded units break off at the thrust structure).

h. Cold helium spheres.

i. LH2 tank pressure makeup sphere.

j. Pneumatic control helium sphere.

k. Helium heater.

l. All structure forward of DAC station 337.781, including useful load.

m. Base heat shield.

5.2.3 Stage Does Not Break Up

If the stage does not break up, the only pieces of debris that may be released by the explosives will be very small pieces of skin plus the side tunnel cover.

5.3 Effects of RSFT After Stage Separation With Propellant Tanks Nearly Full

It is believed that initiation of RSFT when the propellant tanks of the S-IV stage are nearly full, will not cause stage breakup since the forces created by the RSFT explosives are probably not strong enough to deflect the stage and cause tumbling. Furthermore, the hydrostatic pressures of the propellants will probably not burst the tanks. Although burning of the propellants may not occur, the propellants will vaporize at ambient pressure and temperature. The only pieces that may be released by the explosives will be very small pieces of skin and the side tunnel cover.

5.4 Effects of RSFT After Stage Separation With Propellant Tanks Nearly Empty

It is believed that initiation of RSFT when the propellant tanks are nearly empty will cause stage breakup because of forces created by the release of

large volumes of compressed gases from the tanks. This stage breakup should be less extensive than stage breakup before separation when the propellants do not detonate. It is anticipated that the pieces dispersed at this time will be as follows:

a. Skin pieces from the S-IV stage.

b. Individual RL10A-3 rocket engines, including their hydraulic actuators (only if the engines break off at the thrust structure).

c. RL10A-3 rocket engines, thrust structure, helium heater, and portion of aft dome extending below thrust structure junction (only if engines do not break off at thrust structure).

d. Ullage rockets-loaded.

e. Ullage rockets-expended.

f. Electronics rack and units (one piece) located on the forward interstage assembly (only if the rack breaks off at the forward interstage assembly).

g. Electronic units, such as the instrumentation signal conditioning equipment located outside of the thrust structure (only if the units break off at the thrust structure).

h. Thrust structure, including electronic equipment and accessories mounted inside and at that portion of the aft dome extending below the thrust structure junction; excluding engines, external electronics packages, helium heater and control helium sphere (only if the excluded units break off at the thrust structure).

i. Cold helium spheres.

j. LH2 tank makeup helium bottle.

k. Pneumatic control sphere.

l. Helium heater.

m. All structure forward of DAC station 337.781, including useful load.

n. Base heat shield.

5.5 <u>Fragment Velocity Increments Before Stage Separation</u>

A theoretical method for determining the velocity increments imparted to the S-IV stage components or stage fragments (pieces) by initiation of the flight termination system was developed. By assuming that the velocity increment imparted to a reference piece was known, a relationship between the increment of the reference piece to the increment of all other pieces was established regardless of their density, thickness, and curvature. The relationship was made with the following equation:

(1) $\Delta V = F \dfrac{g}{w} \Delta t$

where:

ΔV = the velocity increment imparted to a piece

F = the forces exerted on a piece due to stage explosion or breakup

g = gravitational acceleration

W = piece weight

Δt = the time increment during which the forces (F) act on a piece

Assuming:

(2) $F = PA$

where:

P = the pressure acting upon a piece due to stage breakup or propellant detonation. (P is assumed constant for all pieces.)

A = the effective area of a piece; i.e., the projected area of the piece

and that:

(3) $W = A'T\rho$

where:

ρ = piece density

T = piece thickness

A' = piece actual surface area; i.e., the piece side which is oriented toward the pressure source

Then, combining equations (1), (2), and (3)

(4) $V = \dfrac{PAg\,\Delta t}{\rho A'T}$

It may be seen from equation (4) that the velocity increment (V) is directly
proportional to the ratio of the projected area of the piece to its actual
surface area (A/A'), a ratio that is a function of the piece shape. It may
be assumed that pieces of the S-IV stage will have three basic shapes: flat,
spherical, and cylindrical. The ratio of the piece shape projected area to
the actual surface area ($\frac{A}{A'}$) may be determined as follows:

    a. flat piece

        $\dfrac{A}{A'} = 1$

    b. spherical piece

        $\dfrac{A}{A} = \dfrac{r - h/2}{r}$ (for $h \leqslant r$)
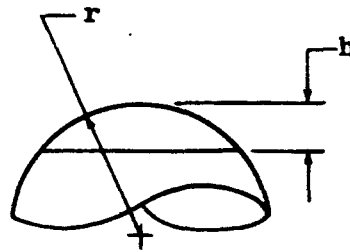
where:

        r = radius of the spherical section

        h = height of the spherical section

    c. cylindrical piece

        $\dfrac{A}{A'} = \dfrac{2\sin\ \theta/2}{\theta}$
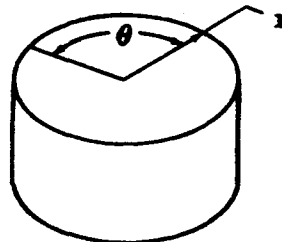
where:

        θ = central angle of the cylindrical section (radians)

Effects of RSFT

The ratio of the velocity increments imparted to two pieces is:

(5) $\dfrac{\Delta V_1}{\Delta V_2} = \dfrac{V_1 (A/A')_2 (\rho T)_1}{(\rho T)_2 (A/A')_1}$

The various stage pieces are separated into two categories for this study.
These categories are: (1) skin pieces such as those originating from the
cylindrical tank wall, etc., and (2) specific pieces such as helium spheres,
ullage rockets, etc. The stage skin is divided into several sections as

19 April 1965

indicated in figure 5-1. It has been shown that the velocity increment
imparted to any skin piece is a function of the area ratio (A/A') and the
density-thickness product (T). Each skin section is assumed to have a
density-thickness product (T) which is constant throughout the section.
Therefore, skin pieces from any given section will receive velocity
increments which are a function only of their area ratio. Skin pieces from
any given section are assumed to be approximately square. The density-
thickness products of the specific pieces were found by dividing the total
piece weight by an assumed area for each piece, where the assumed area is
representative of the piece projected area. Therefore, all specific pieces
have area ratios (A/A') equal to one. The skin sections and the specific
pieces considered, are listed in table 5-2 along with their density-
thickness products, assumed shapes, skin piece maximum size, specific piece
weight, and specific piece representative areas.

Use of the reference piece velocity increment together with equation (6),
the area ratio equations and the piece density-thickness product data of
table 5-2, permits determination of the estimated velocity increments
imparted to skin pieces and the specific pieces.

The assumptions that all pieces feel the same pressure (P), and the values
assumed for the density-thickness product (T) of pieces such as the engines
and ullage rockets, are not totally correct. However, it is considered that
use of these assumptions would result in determination of piece velocity
increments that are within the accuracy of the reference piece velocity
increment determination.

5.5.1 Propellant Tank Pieces With Propellant Detonation

It has been assumed that a 1.000 ft/sec velocity increment is imparted to
a 1 sq ft piece of the LH2 tank wall (reference piece). Assuming this
velocity increment, the total kinetic energy of all the LH2 tank wall
fragments is approximately:

$$\Sigma KE = \frac{w}{2g} v^2$$

$$= \frac{1383}{2 \times 32} \times 1.000^2$$

$$= 2.17 \times 10^7 \text{ ft/lbs}$$

The energy released by 1 lb of oxygen reacting with hydrogen is 3.9 x 106 ft/lbs. If it is assumed that 1 percent of this energy is transformed into kinetic energy of the fragments, then there are 3.9×10^4 ft/lbs of energy available per lb of oxygen. Therefore, to obtain 1,000 ft/sec velocity, 560 lb of oxygen must react rapidly with hydrogen or $\frac{2.17 \times 10}{3.9 \times 10^4}$. To summarize, if 0.7 percent of the total oxygen available detonates, and if the energy transfer is 1 percent efficient (both percentage values are intuitively assumed to be reasonable), the tank skin fragments will receive a velocity of 1,000 ft/sec. Therefore, it appears that a velocity as high as 1,000 ft/sec is reasonable.

The velocity increment of 1,000 ft/sec imparted to the reference piece (1 sq ft piece of cylindrical tank wall), together with equation (6), the area ratio equations, and the piece density-thickness product data of table 5-2, were utilized to compute the estimated velocity increments imparted to the skin pieces and the specific pieces. The estimated velocity increments imparted to the specific pieces are presented in figure 5-2.

5.5.2 Stage Pieces Without Propellant Detonation

Pieces dispersed by the S-IV stage breaking up without propellant detonation will have no appreciable velocity increments imparted to them.

5.5.3 Stage Pieces Without Breakup

The few pieces which will be dispersed by initiation of RSFT without stage breakup, will have no significant velocity increments imparted to them.

5.6 Fragment Velocity Increments After Stage Separation With Propellant Tanks Nearly Full

Initiation of the RSFT after stage separation and with the stage propellant tanks nearly full, will not result in stage breakup, and debris which will be dispersed at this time will have no significant velocity increments imparted to them.

5.7 Fragment Velocity Increments After Stage Separation With Propellant
     Tanks Nearly Empty

At time of destruct, the shaped charge will cut a slot along the LH2 tank
wall. The tank wall, now unsupported in this region, will start to break
up and the pieces will be accelerated. This acceleration will be accompa-
nied by venting of the gases. For the purpose of estimating the velocity
of the pieces, it is assumed that there is no gas leakage for the first
one-half in. of travel and that the gas pressure is decreased instantaneously
to zero after one-half in. of travel.

$$\text{Initial radius of LH2 tank } (r_o) = 110 \text{ in.}$$

$$\text{Final radius of LH2 tank } (r_1) = 110.5 \text{ in.}$$

$$\text{LH2 tank volume } (V) = \pi r^2 h$$

$$\frac{V_1}{V_0} = \frac{\pi r_1^2 h}{\pi r_o^2 h} = r_1^2 = 1.009$$

The kinetic energy transmitted to the wall during the first one-half in. of
travel will be:

$$K.E. = \rho_o V_o \ \ln \frac{V_1}{V_o}$$

Effects of RSFT

$$= 40 \times 144 \times 4270 \ \ln 1.009$$

$$= 40 \times 144 \times 4270 \times 0.009$$

$$= 2.2 \times 10^5 \text{ ft/lbs}$$

The approximate velocity of the fragments, therefore, will be:

$$K.E. = 1/2 \frac{w}{g} v^2$$

$$v = \sqrt{\frac{2KEg}{w}}$$

$$= \sqrt{\frac{2 \times 2.2 \times 10^5 \times 32}{1380}}$$

$$= \sqrt{10,200}$$

$$= 101 \text{ ft/sec}$$

The velocity increment of 100 ft/sec imparted to the reference piece
(1 sq ft piece of cylindrical tank wall), together with equation (6), the
area ratio equations and the piece density-thickness product data of
table 5-2, were utilized to compute the estimated velocity increment
imparted to skin pieces and the specific pieces.

5.8 General Comments

The velocity increment of a given skin section, as shown in figure 5-2
varies a maximum of 10 percent with an increase of piece surface area from
1 ft^2 to 100 ft^2. The skin pieces anticipated for the propellant detonation
type of breakup before stage separation are considerably smaller (10 sq ft)
than those for the pressure vessel explosive type of breakup after separa-
tion. It may also be seen from figure 5-2 that the velocity increment
variation between constant density-thickness product skin pieces is
negligible for a propellant detonation type of breakup. It is concluded
that the velocity increment imparted to any skin piece is a strong function
of the density-thickness product of the piece and is nearly independent of
piece surface area.

5.9 Possibility of Engine Ignition in the Event of Destruct Action

In order to obtain engine ignition, the engine prestart and start valves
must be open, an ignition source must be available, and adequate propellant
pump inlet conditions must be achieved. The RF arm and cutoff command
(which is common to both stages) to the command destruct receivers causes
an "All Engine Cutoff Command" to be generated in the S-IV stage. This
command electrically disables all engine prestart, start, and ignition
circuits.

Therefore, S-IV engine ignition will not occur if destruct action is taken
during the S-I boost phase, unless both the S-I and S-IV command destruct
receivers subsystems fail. The latter possibility is extremely remote.

TABLE 5-1
SKIN DESCRIPTIONS

SKIN SECTION	LOCATION	CONSTRUCTION
I	Forward Interstage Assembly	1-in. aluminum honeycomb
II	Forward Dome	1/4-in. aluminum plate, partially waffled and reduced (3/4-in. insulation inside tank).
IIIa	Cylindrical Tank	1/2-in. aluminum plate, waffled (3/4-in. insulation inside tank).
IIIb	Common Bulkhead	1-in. aluminum and fiberglass honeycomb.
IIIc	Center Portion of Aft Dome	1/4-in. aluminum plate, partially reduced.
IV	Aft Interstage Assembly and Aft Skirt Assembly	1.6-in. aluminum honeycomb.
V	Lower Portion of Aft Dome	0.086-in. aluminum plate.
VI	Upper Portion of Aft Dome	1/4-in. aluminum plate, waffled (3/4-in. insulation inside tank).

NOTE: .Refer to figure 5-1 for location of skin sections.

Table 5-1   19 April 1965

TABLE 5-2 (Sheet 1 of 2)

STAGE PIECE CHARACTERISTICS

Piece	Shape and Area	Weight (lbs)	Item density-thickness product (ρT-lb/ft²)	Item velocity increment due to pressure vessel explosion (ΔVE-ft/sec)	Number of items due to pressure vessel explosion	Item velocity increment due to propellant detonation (ΔVPE-ft/sec)	Number of items due to propellant detonation
Forward Interstage Assembly	Cylindrical A=185 ft² (max)	---	1.6	See figure 5-2	8	See figure 5-2	106
Forward Dome	Spherical A=525 ft² (max)	---	1.9	See figure 5-2	12	See figure 5-2	100
Cylindrical Tank	Cylindrical A=85 ft² (max)	---	2.5	See figure 5-2	35	See figure 5-2	100
Common Bulkhead	Spherical A=215 ft² (max)	---	2.5	See figure 5-2	1	See figure 5-2	43
Center Portion of Aft Dome	Spherical A=5 ft² (max)	---	2.5	See figure 5-2	1	See figure 5-2	40
Aft Interstage Assembly and Aft Skirt Assembly	Cylindrical A=185 ft² (max)	---	1.8	See figure 5-2	4	See figure 5-2	203
Lower Portion of Aft Dome	Spherical A=170 ft² (max)	---	1.5	See figure 5-2	1	See figure 5-2	50
Upper Portion of Aft Dome	Spherical A=35 ft²	---	2.3	See figure 5-2	1	See figure 5-2	40
Individual Main Engine (includes hydraulic actuators)	Flat, A=5.6 ft²	410	73.2	3	6	30	6
Ullage Rockets (loaded)	Flat, A=2.4 ft²	110	45.8	5	---	50	4
Ullage Rockets (expended)	Flat, A=2.4 ft²	50	20.8	12	4	120	---
Electronics Rack and Units (1 piece) located on forward interstage assembly	Flat, A=9.9 ft²	90	9.1	27	1	270	1
Electronics Units Located Outside of Engine Thrust Structure	Flat, A=0.5 ft²	13	26.0	10	37	100	37
Electronics Units Located Outside of Engine Thrust Structure	Flat, A=0.8 ft²	6	7.5	33	1	330	1

Refer to figure 5-1 for location of skin sections.

STAGE PIECE CHARACTERISTICS

Piece	Shape and Area	Weight (lbs)	Item density-thickness product (ρT-lb/ft^2)	Item velocity increment due to pressure vessel explosion (ΔVE-ft/sec)	Number of items due to pressure vessel explosion	Item velocity increment due to propellant detonation (ΔVPE-ft/sec)	Number of items due to propellant detonation
Thrust Structure (includes electronic packages mounted inside, and that portion of aft dome extending below the thrust structure junction; excluding engines, external electronics packages, helium heater and sphere)	Flat, A = 177.0 ft^2	1,660	9.4	27	1	270	1
Cold Helium Bottles	Flat, A = 2.9 ft^2	55	18.9	13	3	130	3
LH2 Tank Pressurization Makeup Helium Bottle	Flat, A = 1.5 ft^2	44	29.3	9	1	90	1
Control Helium Spheres	Flat, A = 2.9 ft^2	85	29.3	9	1	90	1
Backup Pressure Helium Spheres	Flat, A = 2.8 ft^2	105	37.5	7	10	70	1
Helium Heater	Flat, A = 0.5 ft^2	40	80.0	3	1	30	1
All Structure Forward of Station 337 (includes 8,000 lbs of useful load)	Flat, A = 264.0 ft^2	10,600	40.2	6	1	---	---
All Structure Forward of Station 337 (includes 25,000 lbs of useful load)	Flat, A = 264.0 ft^2	27,600	104.5	2	1	---	---
Base Heat Shield	Flat, A = 20.0 ft^2	260	13.0	19	1	190	7
Engine Section (includes engines, thrust structure, helium heater, and portion of aft dome extending below thrust structure junction)	Flat, A = 177.0 ft^2	4,485	25.4	10	1	---	---

Refer to figure 5-1 for location of skin sections.

Table 5-2   19 April 1965
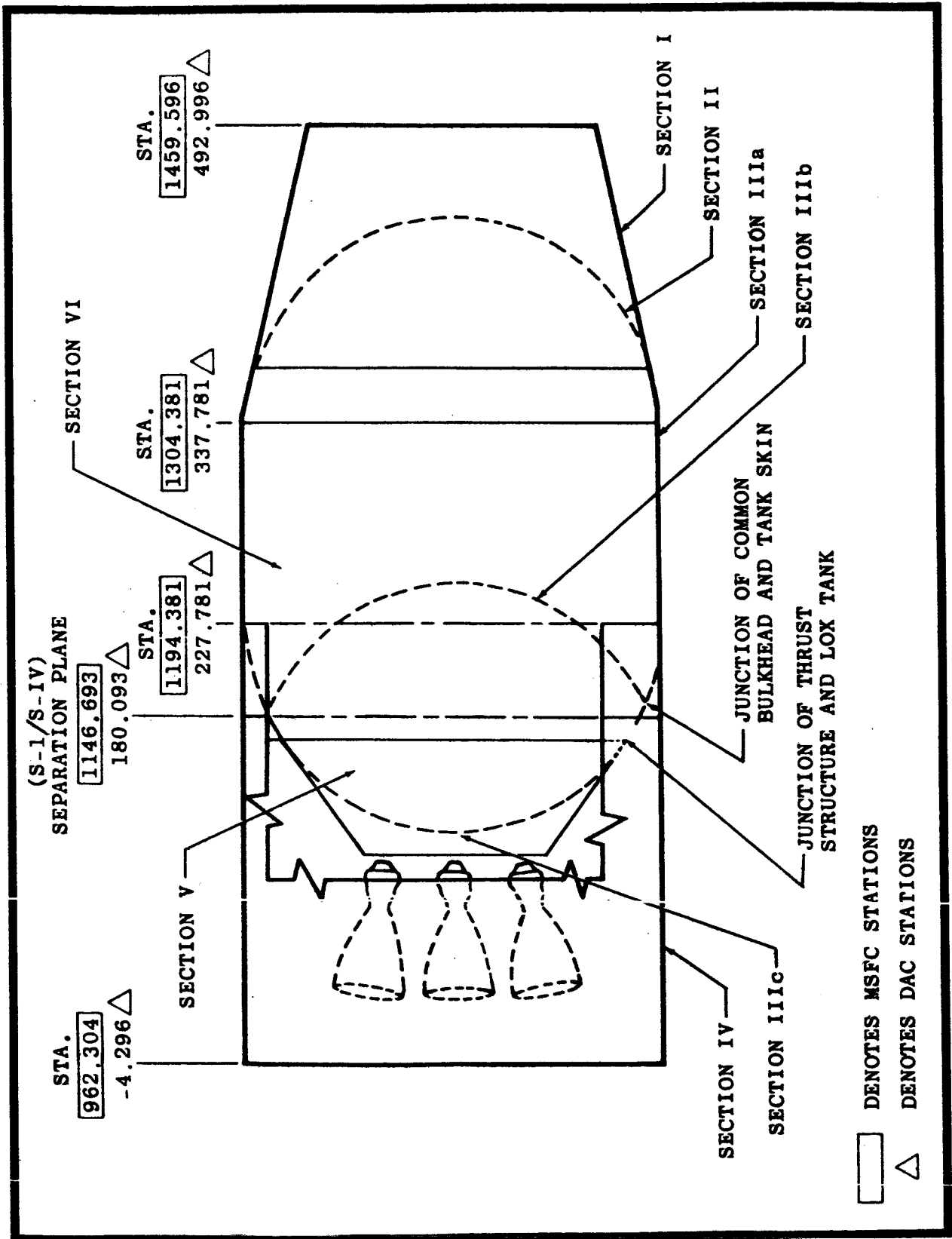
Figure 5-1 Locations of Skin Sections
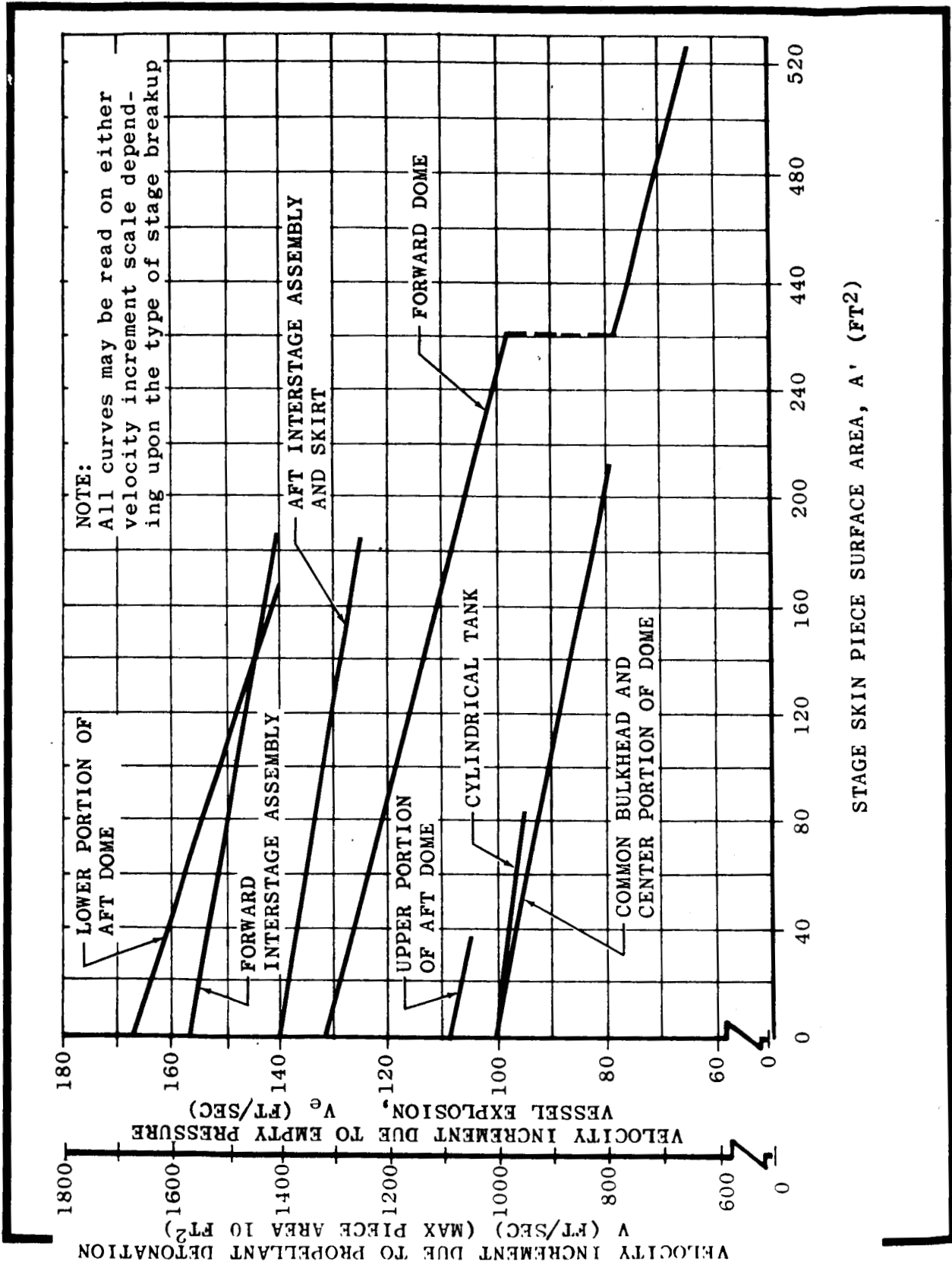
Figure 5-2 Skin Piece Velocity Increments

Figure 5-2   19 April 1965

SECTION 6

PROBABILITY PREDICTIONS

6. PROBABILITY PREDICTIONS

In considering the possible abort situations during S-IV stage flight, it is necessary to predict the probability of various events which are related to stage loss and the operation of the range safety flight termination system in the S-IV stage. The probability predictions of these events are included in tables 6-1, 6-2, and 6-3 and are based upon the ground rules and the information contained in the DSV-4 Reliability Mathematical Model, DAC drawing No. 7859475, change letter C, and the Mathematical Model Supplement, DAC drawing No. 1A68943. It should be noted that the ground rules assume that the S-IV stage has one-engine-out and one-flight-control-subsystem-out capability which is concurrently applicable for the same engine, but not for different engines. For comparison, table 6-1 also includes the no-engine-out probability prediction. The aforementioned documents reflect a general S-IV stage rather than a specific configuration; as of this report data, the specific reliability predictions for the S-IV stage are not available.

6.1 Vehicle Loss and Mission Loss--Definition

Two types of overall loss are considered in the Reliability Mathematical Model--Failure Effect Analysis; namely, vehicle loss and mission loss. For the purpose of this report, vehicle loss is defined as the result of stage loss attributed to stage breakup or explosion. Mission loss is defined as the result of a stage loss attributed to the loss of engine thrust or excessive deviation from the intended flight path. The latter definition differs from the mathematical model definition since it is assumed here that RSFT action will be accomplished before the stage breaks up.

6.2 Discussion of Results

Table 6-1 includes the predictions for the complete S-IV stage system. Item (2) indicates that stage loss may occur 3.7 times out of 100 missions. Item (3) indicates that vehicle loss probability is not affected by the change in engine-out status. Vehicle loss may occur 6 times out of 100 missions. Item (5) shows the percentage of stage loss that may result in vehicle loss (explosion or breakup) before RSFT action. For example, 4.6 percent indicates that 1 out of 22 stage losses is a vehicle loss type. Due to the

extremely short failure reaction time (refer to Mathematical Model for specific FRT's), in many cases RSFT action may not be possible before the vehicle breaks up.

Table 6-2 is the counterpart of table 6-1, excluding the airframe and the thrust generation subsystems (RL10A-3 Rocket Engines). The predictions which appear in table 6-2 consider all the failure effect statements included in the Mathematical Model. Because of possible unknowns in the actual loads and environmental conditions to which the S-IV stage airframe will be exposed for the duration of its mission, a pessimistic point of view was assumed. For prediction purposes, all of the airframe unreliability was associated with vehicle loss. Since sufficient test data were not available to demonstrate the capability of the thrust generation subsystem to survive the critical ignition period (e.g., excessive thrust overshoots, adjacent engine igniting gasses from an unignited engine, etc.), it was necessary to determine the portion of single engine unreliability which contributes to such failures. Assuming the worst possible case, the prediction has indicated that approximately 5 percent of single engine failures may contribute to vehicle loss. For comparison purposes the predictions of the two subsystems are included in table 6-1 but not in table 6-2.

Item (1) in table 6-3 is the probability that the S-IV RSFT system will operate properly when called upon during S-I stage powered flight. This includes the probability that destruction of the S-IV stage will be initiated via shock propagation from the S-I stage command destruct subsystem or initiated by the S-IV stage should the S-I stage command destruct subsystem be unreliable. Item (2) indicates the success probability of the S-IV stage RSFT of the referenced Mathematical Model. Item (3) considers the extension of the S-IV stage RSFT to include all other S-IV stage components required for the destruct operation. This includes such items as parts of the S-IV stage sequencer, components of the electrical power subsystem, etc.

TABLE 6-1
PREDICTION--ALL S-IV STAGE SUBSYSTEMS

	One-Engine-Out Capability*	No-Engine-Out Capability**
(1) NO STAGE LOSS PROBABILITY	0.963	0.869
(2) STAGE LOSS PROBABILITY	0.037	0.131
(3) VEHICLE LOSS PROBABILITY	0.006	0.006
(4) MISSION LOSS PROBABILITY	0.031	0.125
(5) PERCENT STAGE LOSS EQUAL TO VEHICLE LOSS	16.8%	4.6%

*Analysis assumes that mission success can be achieved with one engine out.
**Analysis assumes that mission success cannot be achieved with one engine out.

TABLE 6-2
PREDICTION--EXCLUDING AIRFRAME AND THRUST GENERATION SUBSYSTEMS

(1) NO STAGE LOSS PROBABILITY	0.9763
(2) STAGE LOSS PROBABILITY	0.0237
(3) VEHICLE LOSS PROBABILITY	0.0008
(4) MISSION LOSS PROBABILITY	0.0229
(5) PERCENT STAGE LOSS EQUAL TO VEHICLE LOSS	3.3%

TABLE 6-3
PREDICTION--INHERENT RELIABILITY OF RSFT SYSTEM IN S-IV STAGE

	Inherent Reliability
(1) BEFORE S-I/S-IV SEPARATION	0.99950
(2) AFTER S-I/S-IV SEPARATION	0.99904
(3) AFTER S-I/S-IV SEPARATION (INCLUDING ALL OTHER S-IV STAGE COMPONENTS REQUIRED FOR COMMAND DESTRUCT OPERATION)	0.99586

T A B L E S

TABLE A
SA-10 (Standard)
IMPACT DATA FOR PREMATURE CUTOFF

T_{co} (sec)	Geodetic Latitude (deg)	Longitude (deg)	Remaining Flight Time (sec)	Range (n. mi)
0	28.53	80.56	0.0	0.0
20	28.53	80.56	23.42	1.51
40	28.53	80.55	54.32	1.78
60	28.52	80.44	90.60	6.98
80	28.49	80.10	133.34	24.95
100	28.40	79.20	192.21	72.71
120	28.18	77.21	272.25	178.86
140	27.58	72.94	393.91	408.62
160	27.10	70.15	450.98	560.43
180	26.92	69.25	455.78	610.01
200	26.72	68.31	463.38	661.51
220	26.50	67.33	470.81	716.24
240	26.27	66.27	478.30	774.61
260	26.01	65.16	485.87	836.93
280	25.73	63.97	493.51	903.50
300	25.41	62.70	501.33	974.84
320	25.06	61.34	509.46	1051.57
340	24.65	59.89	518.01	1134.39
360	24.21	58.33	527.05	1223.94
380	23.71	56.65	536.69	1320.98
400	23.14	54.84	547.12	1426.61
420	22.49	52.87	558.64	1542.31
440	21.74	50.73	571.61	1669.85
460	20.88	48.37	586.44	1811.45
480	19.87	45.76	603.88	1970.46
500	18.67	42.82	625.15	2152.16
520	17.20	39.44	652.20	2364.94
540	15.32	35.39	688.69	2623.65
560	12.81	30.31	741.31	2955.89
580	9.08	23.33	825.71	3424.16
600	2.43	11.79	990.51	4219.63
612	-5.69	-1.95	1210.97	5175.97
613	-6.70	-3.70	1239.86	5296.64
614	-7.80	-5.62	1271.55	5428.16
615	-8.98	-7.73	1306.54	5572.46
616	-10.28	-10.09	1345.44	5731.91
617	-11.70	-12.74	1389.05	5909.59
618	-13.27	-15.75	1438.41	6109.61
619	-15.00	-19.24	1494.98	6337.50

TABLE A
(CONT)

T co (sec)	Geodetic Latitude (deg)	Longitude (deg)	Remaining Flight Time (sec)	Range (n. mi)
620	-16.93	-23.35	1560.75	6601.07
621	-19.08	-28.30	1638.65	6911.78
622	-21.47	-34.47	1733.28	7287.55
623	-24.09	-42.50	1852.45	7759.25
624	-26.81	-53.71	2011.63	8388.15
625	-28.92	-71.46	2251.78	9338.41
626	ORBIT			

TABLE B
(SA-10 (3 σ Maximum)
IMPACT DATA FOR PREMATURE CUTOFF

T_{co} (sec)	Geodetic Latitude (deg)	Longitude (deg)	Remaining Flight Time (sec)	Range (n. mi)
0	28.53	80.56	0	0
20	28.53	80.56	25.14	1.51
40	28.53	80.54	57.35	2.10
60	28.52	80.41	95.01	8.49
80	28.48	80.02	140.63	29.01
100	28.38	79.02	204.20	82.36
120	28.13	76.80	291.07	200.87
140	27.42	71.97	426.73	461.35
160	26.96	69.41	476.61	600.88
180	26.76	68.44	483.35	654.47
200	26.53	67.41	490.54	710.95
220	26.29	66.34	497.50	770.90
240	26.02	65.19	504.43	834.78
260	25.73	63.98	511.35	902.85
280	25.41	62.69	518.29	975.40
300	25.05	61.32	525.35	1052.97
320	24.66	59.85	532.70	1136.23
340	24.21	58.29	540.47	1225.92
360	23.71	56.62	548.78	1322.76
380	23.14	54.82	557.76	1427.62
400	22.50	52.87	567.71	1541.86
420	21.77	50.76	579.05	1677.33
440	20.93	48.45	592.24	1806.33
460	19.94	45.89	607.98	1961.98
480	18.77	43.02	627.38	2139.13
500	17.35	39.73	652.37	2345.83
520	15.55	35.81	686.30	2595.88
540	13.14	30.91	735.59	2915.43
560	9.61	24.23	814.73	3362.38
580	3.42	13.40	966.94	4106.64
594	-5.70	-2.03	1213.81	5180.37
595	-6.72	-3.81	1243.16	5302.67
596	-7.83	-5.75	1275.42	5436.22
597	-9.04	-7.90	1311.09	5582.99
598	-10.36	-10.30	1350.82	5745.46
599	-11.81	-13.01	1395.43	5926.86
600	-13.41	-16.09	1446.04	6131.47
601	-15.18	-19.68	1504.15	6365.14
602	-17.15	-23.91	1571.89	6636.13
603	-19.35	-29.04	1652.39	6956.72
604	-21.80	-35.46	1750.62	7346.34
605	-24,47	-43.90	1875.17	7838.92
606	-27.19	-55.84	2043.78	8504.80
607	ORBIT			

TABLE C

SA-10 (3 σ Minimum)
IMPACT DATA FOR PREMATURE CUTOFF

T_{co} (sec)	Geodetic Latitude (deg)	Longitude (deg)	Remaining Flight Time (sec)	Range (n. mi)
0	28.53	80.56	0	0
20	28.53	80.56	21.97	1.51
40	28.53	80.55	51.33	1.51
60	28.52	80.45	86.12	5.99
80	28.50	80.16	125.94	21.71
100	28.42	79.36	180.85	64.01
120	28.23	77.59	255.44	158.65
140	27.73	73.81	366.67	361.26
160	27.25	70.88	430.47	520.64
180	27.08	70.04	434.00	566.34
200	26.90	69.22	442.03	611.94
220	26.70	68.33	449.52	660.97
240	26.50	67.38	456.76	713.53
260	26.28	66.37	464.07	769.66
280	26.03	65.29	471.50	829.63
300	25.76	64.14	479.13	893.93
320	25.45	62.91	487.09	963.14
340	25.11	61.59	495.47	1037.89
360	24.73	60.16	504.33	1118.80
380	24.29	58.63	513.72	1206.51
400	23.80	56.98	523.80	1301.93
420	23.24	55.19	534.78	1406.27
440	22.59	53.24	546.89	1520.92
460	21.86	51.11	560.42	1647.49
480	21.01	48.76	575.82	1788.34
500	20.00	46.15	593.87	1946.98
520	18.80	43.21	615.78	2128.79
540	17.33	39.80	643.52	2342.22
560	15.46	35.74	680.54	2601.74
580	12.94	30.64	733.57	2934.91
600	9.21	23.63	818.33	3404.82
620	2.51	11.99	984.38	4206.34
632	-5.81	-2.07	1210.44	5185.67
633	-6.86	-3.90	1240.58	5311.24
634	-8.00	-5.90	1273.78	5448.72
635	-9.24	-8.13	1310.60	5600.23
636	-10.61	-10.61	1351.74	5768.45
637	-12.11	-13.43	1398.13	5957.00
638	-13.77	-16.67	1450.99	6170.65

TABLE C
(CONT)

T_{co} (sec)	Geodetic Latitude (deg)	Longitude (deg)	Remaining Flight Time (sec)	Range (n. mi)
639	-15.62	-20.44	1512.06	6416.05
640	-17.68	-24.94	1583.76	6702.71
641	-19.98	-30.45	1669.80	7045.11
642	-22.54	-37.47	1776.14	7466.59
643	-25.30	-46.86	1913.11	8007.90
644	-27.95	-60.57	2103.65	8764.44
645	ORBIT			

ILLUSTRATIONS

50

FIGURE 1

WIND SPEED VS ALTITUDE
(Month of August)

FIGURE   1-A

WIND SPEED VS. ALTITUDE
FROM 67.5 DEGREES EAST
OF NORTH
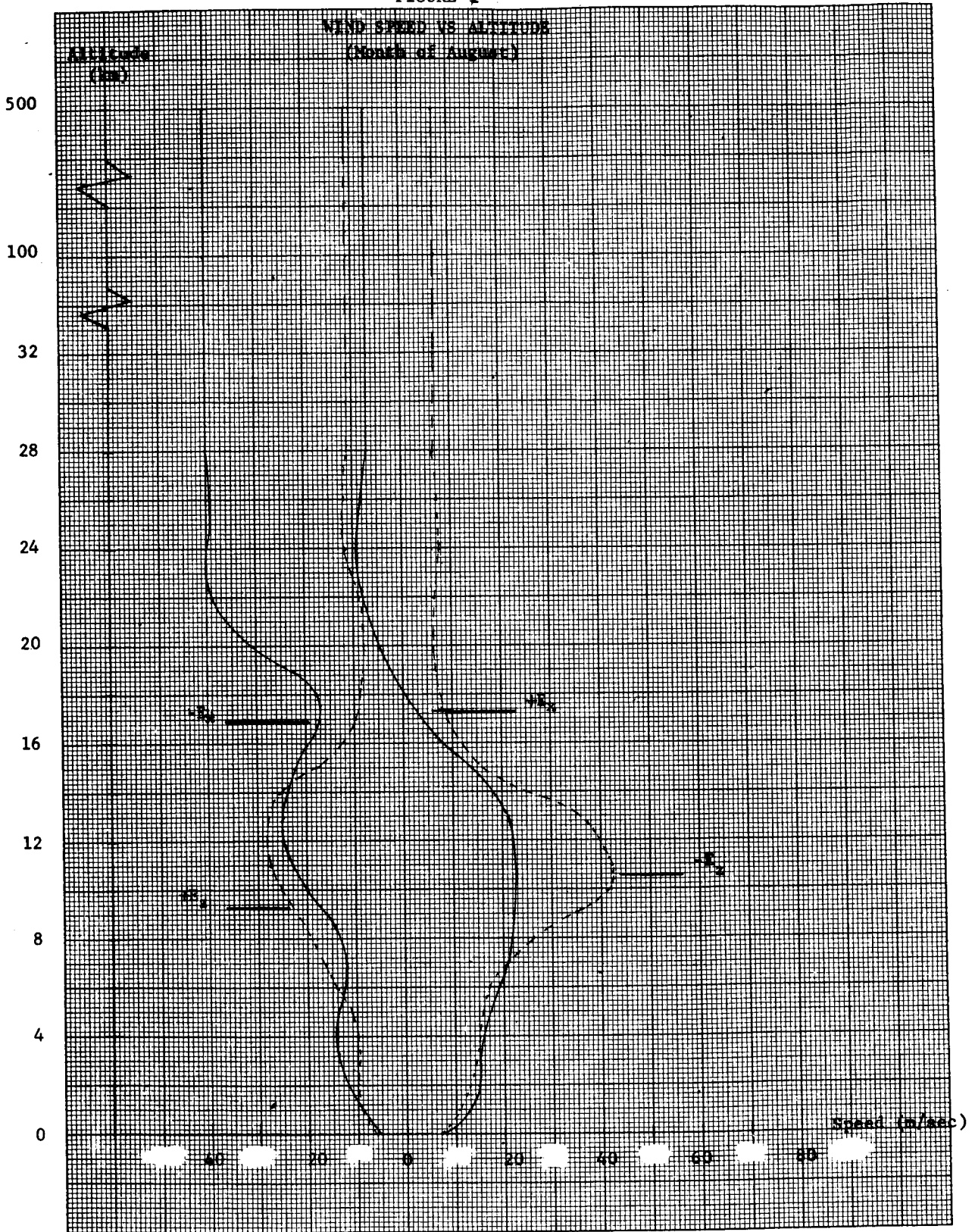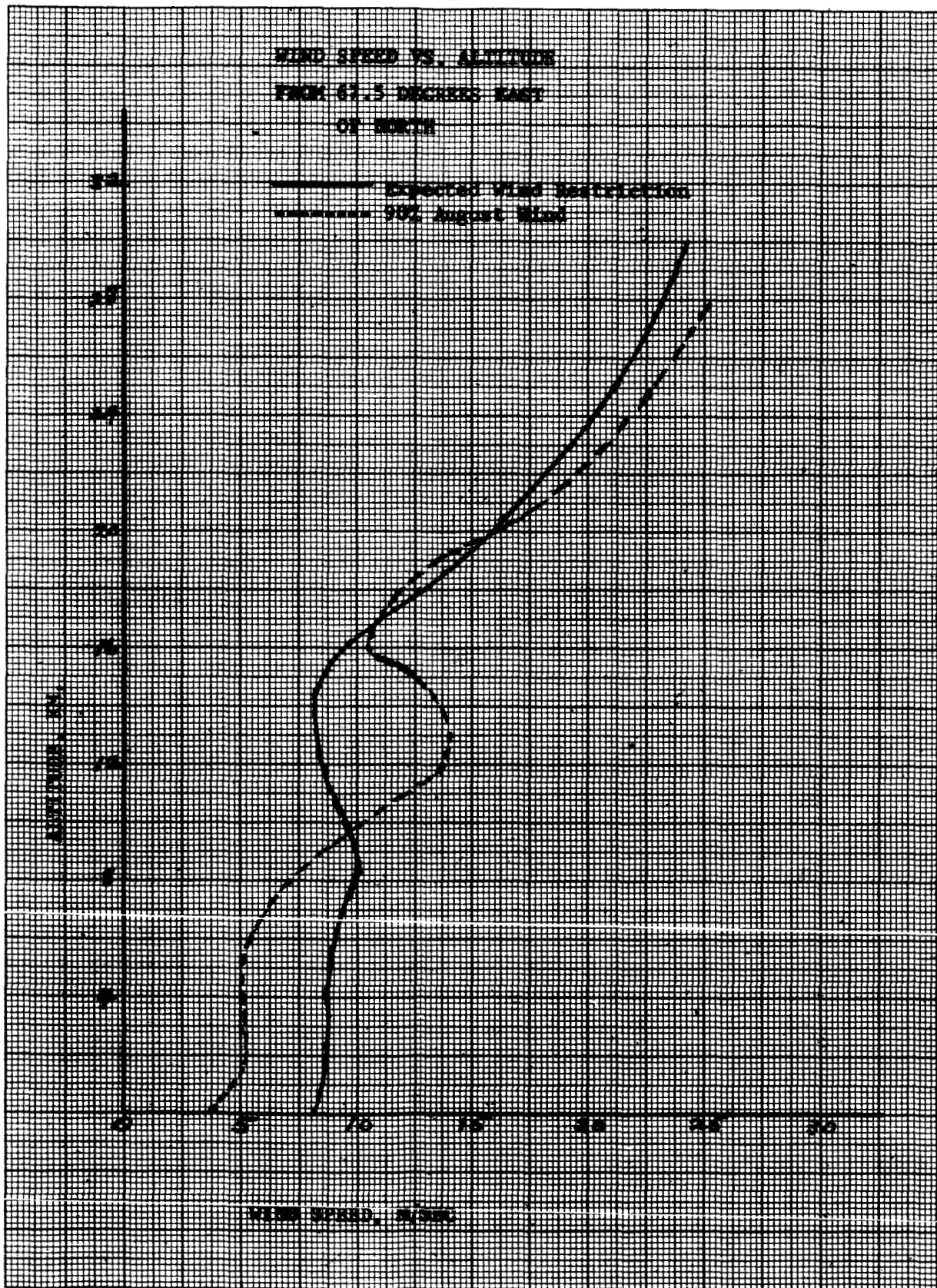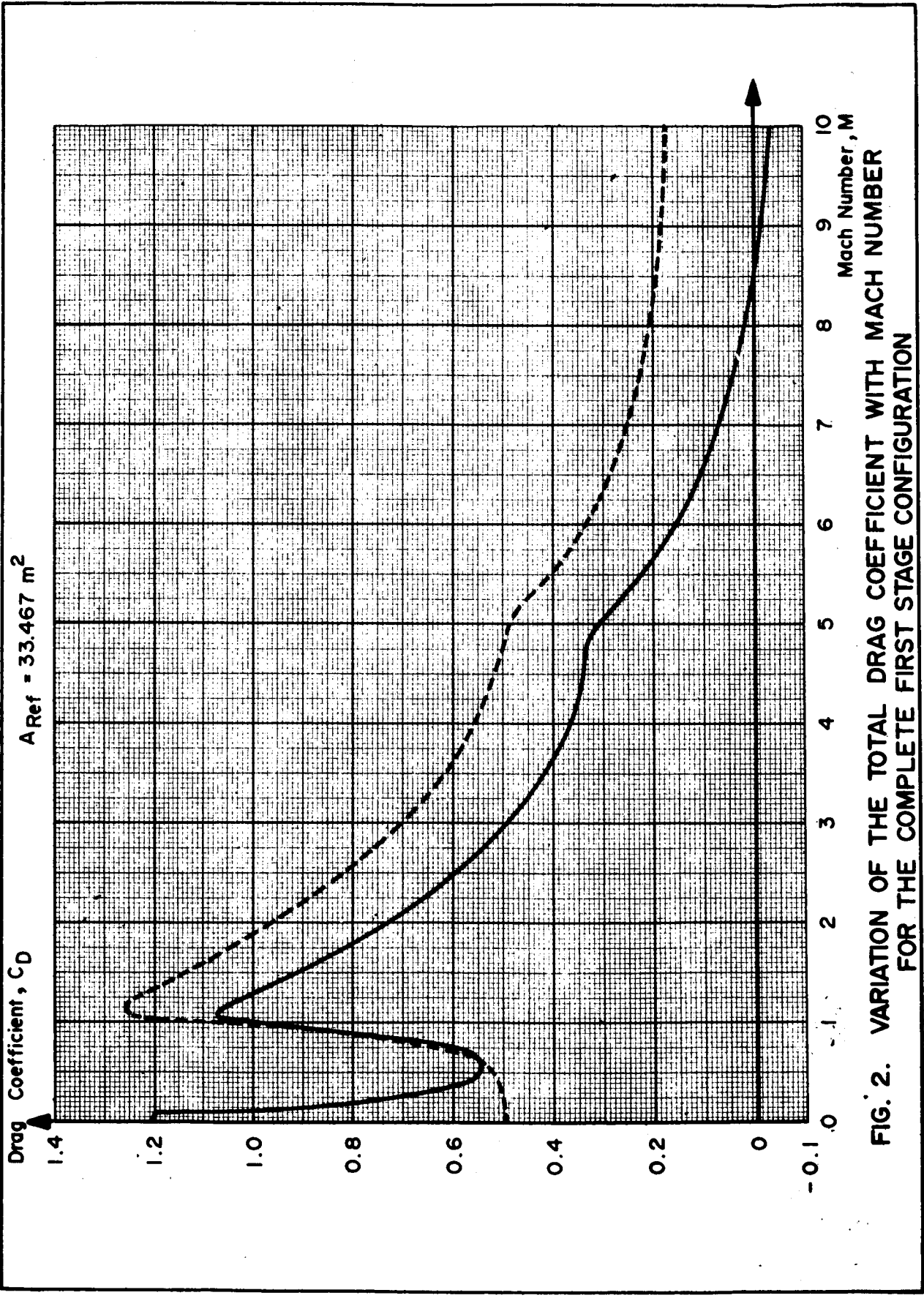
FIG. 2. VARIATION OF THE TOTAL DRAG COEFFICIENT WITH MACH NUMBER FOR THE COMPLETE FIRST STAGE CONFIGURATION
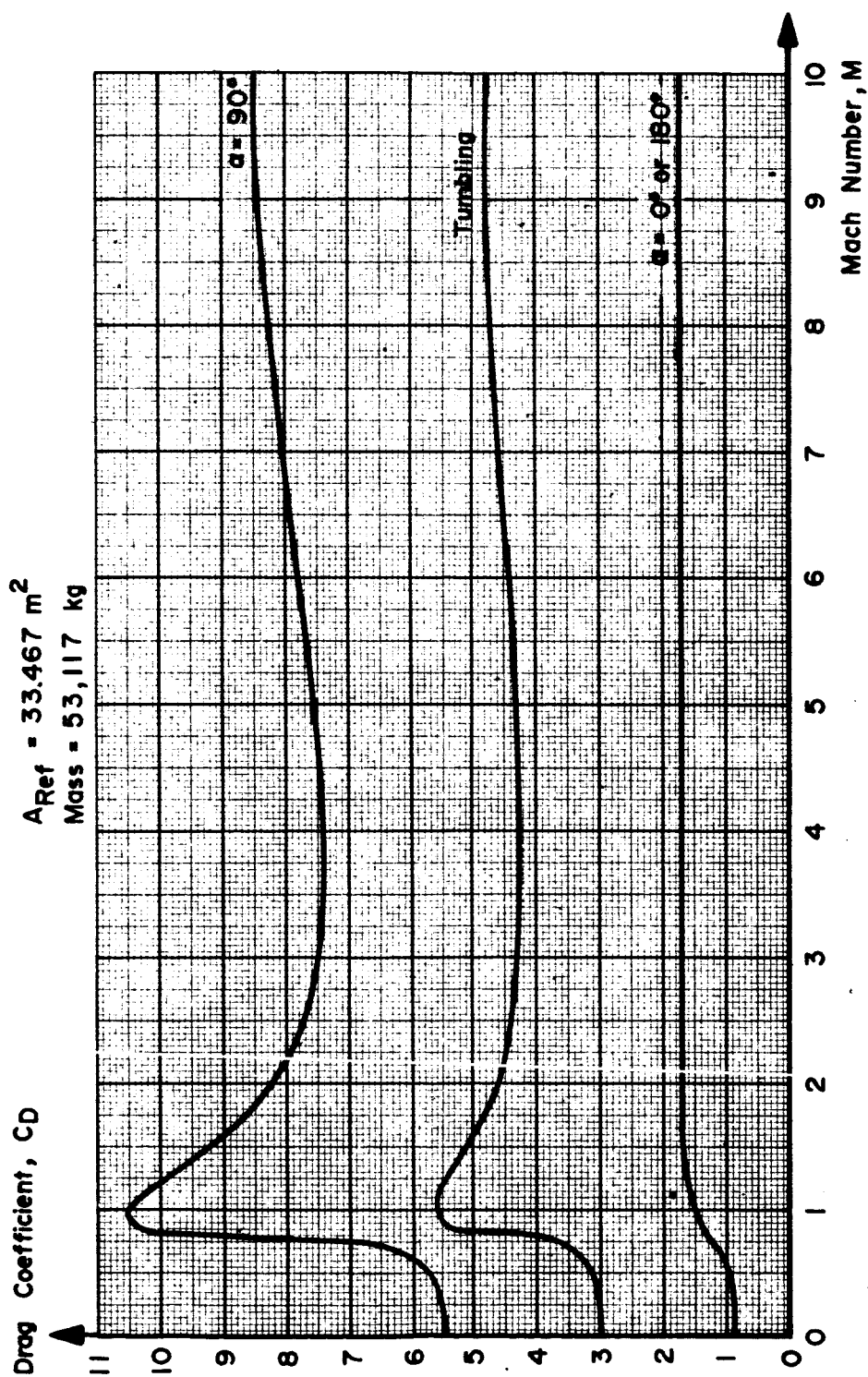
FIG. 3. SATURN I, BLOCK II BOOSTER
VARIATION OF TOTAL DRAG COEFFICIENT WITH MACH NUMBER
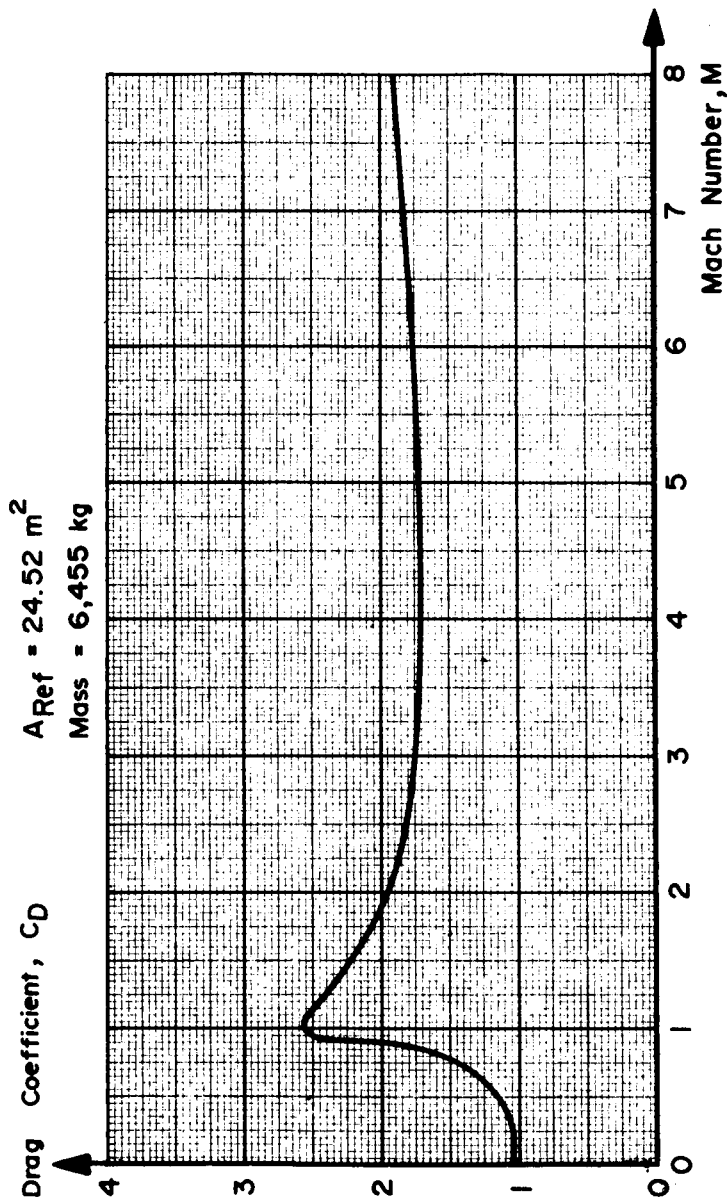
FIG. 4. S–IV STAGE (DRY)

VARIATION OF TOTAL DRAG COEFFICIENT WITH MACH NUMBER TUMBLING CASE
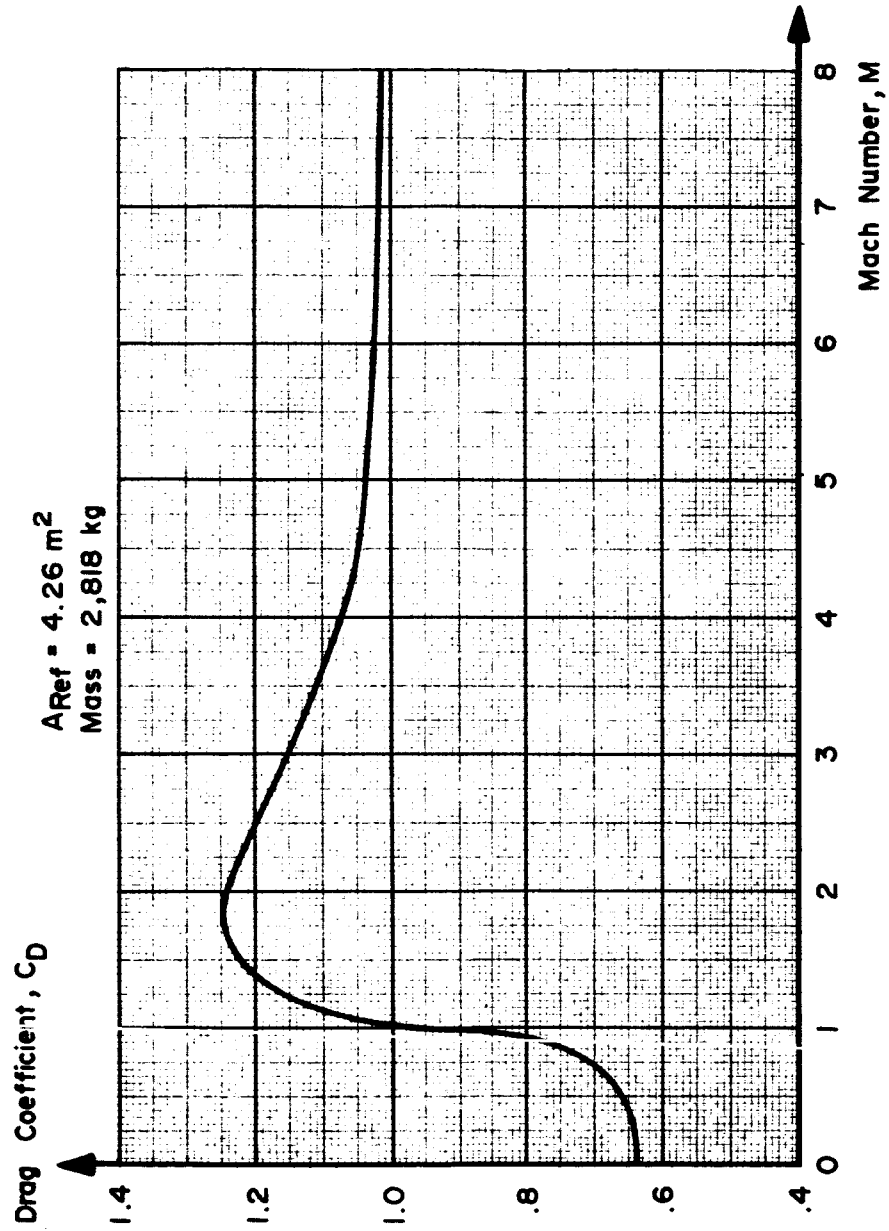
FIG. 5. 4 ENGINE CLUSTER
VARIATION OF TOTAL DRAG COEFFICIENT WITH MACH NUMBER
$\alpha = 0°$

56
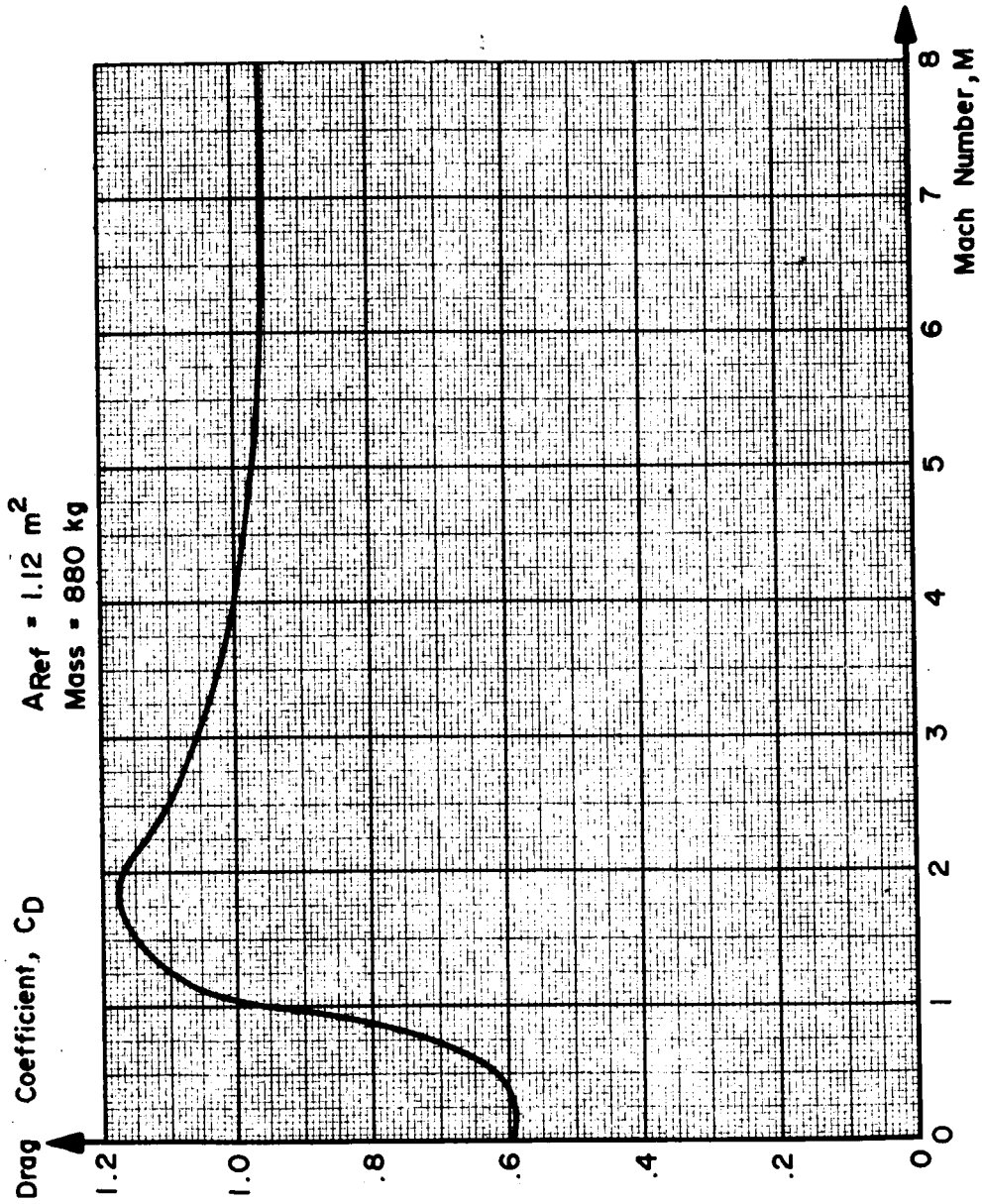
FIG. 6. SINGLE ENGINE
VARIATION OF TOTAL DRAG COEFFICIENT WITH MACH NUMBER
$\alpha = 0°$
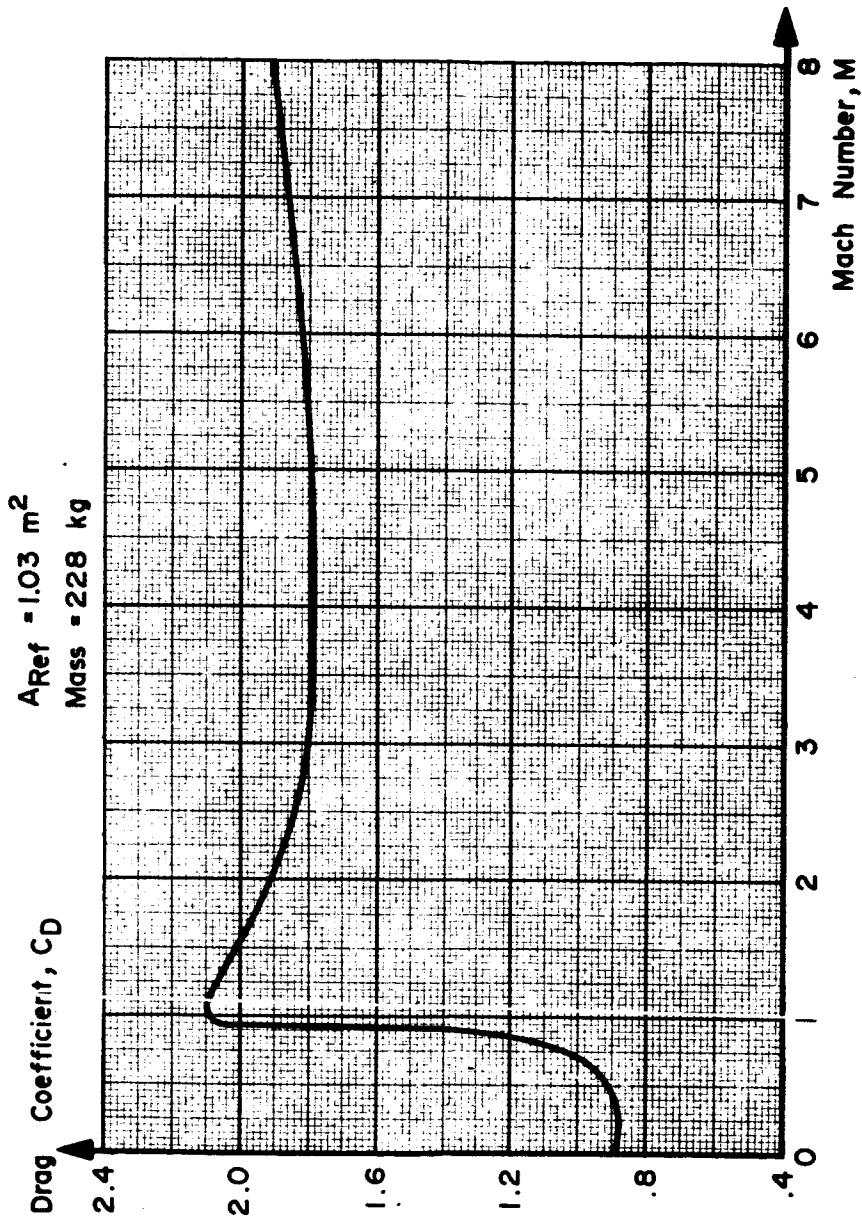
FIG. 7. INSTRUMENT CANNISTER
VARIATION OF TOTAL DRAG COEFFICIENT WITH MACH NUMBER
TUMBLING CASE

Fragment of S-I Barrel A_{Ref} = 3.68 m^2,   Mass = 227 kg

Fragment of S-I Tail Shroud A_{Ref} = .677 m^2,   Mass = 136 kg

Fragment of S-I Head Shield A_{Ref} = .178 m^2,   Mass = 34 kg
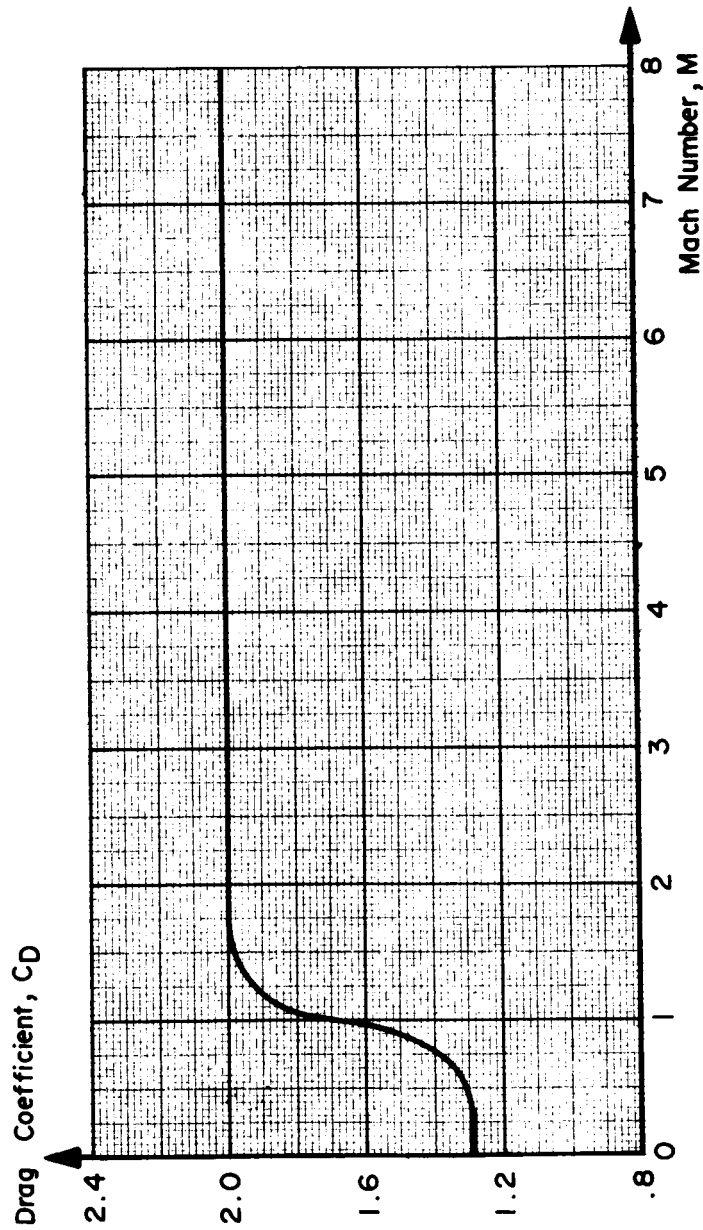
FIG. 8. SECTIONS

VARIATION OF TOTAL DRAG COEFFICIENT WITH MACH NUMBER

α = 90°
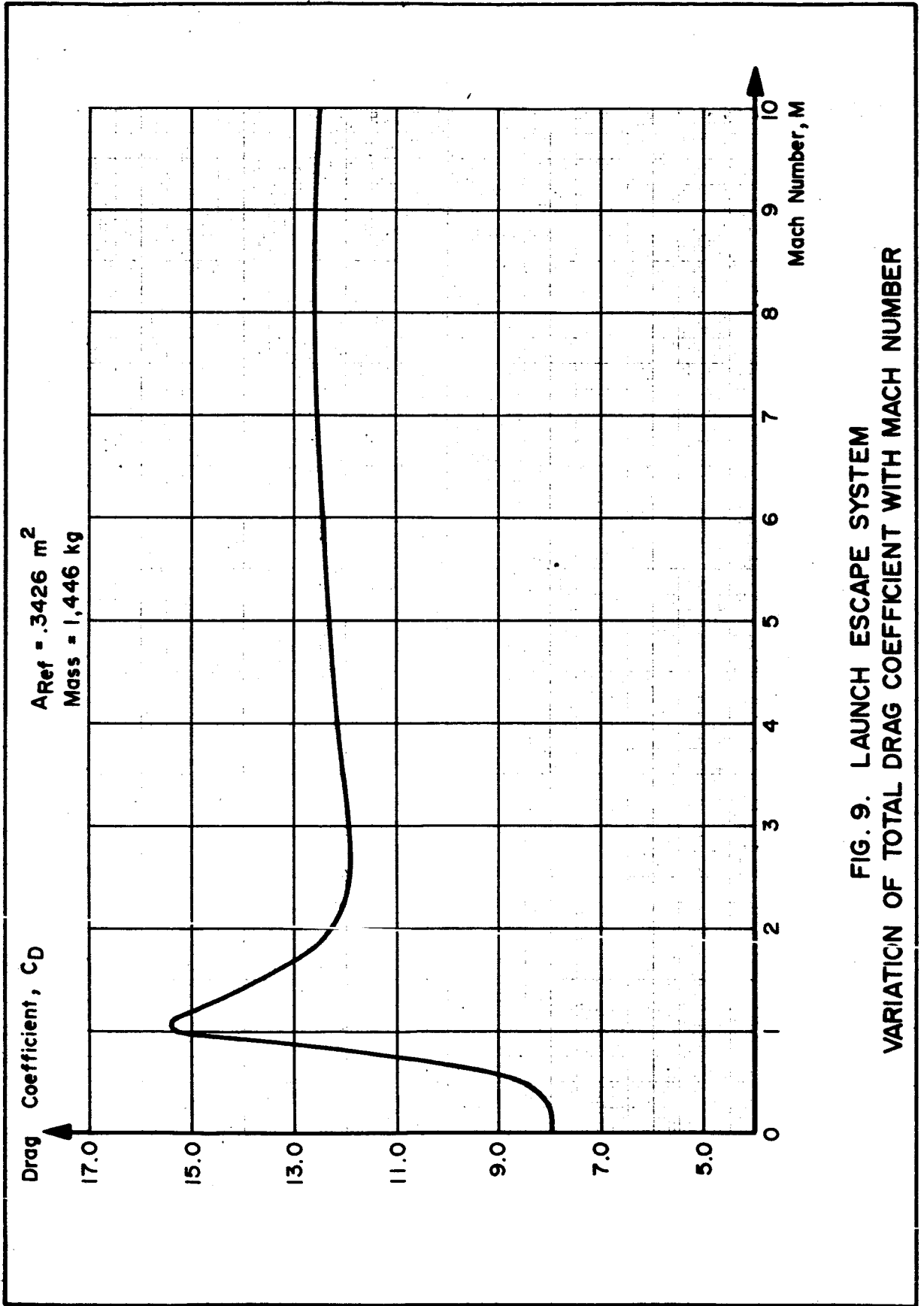
FIG. 9. LAUNCH ESCAPE SYSTEM

VARIATION OF TOTAL DRAG COEFFICIENT WITH MACH NUMBER

60
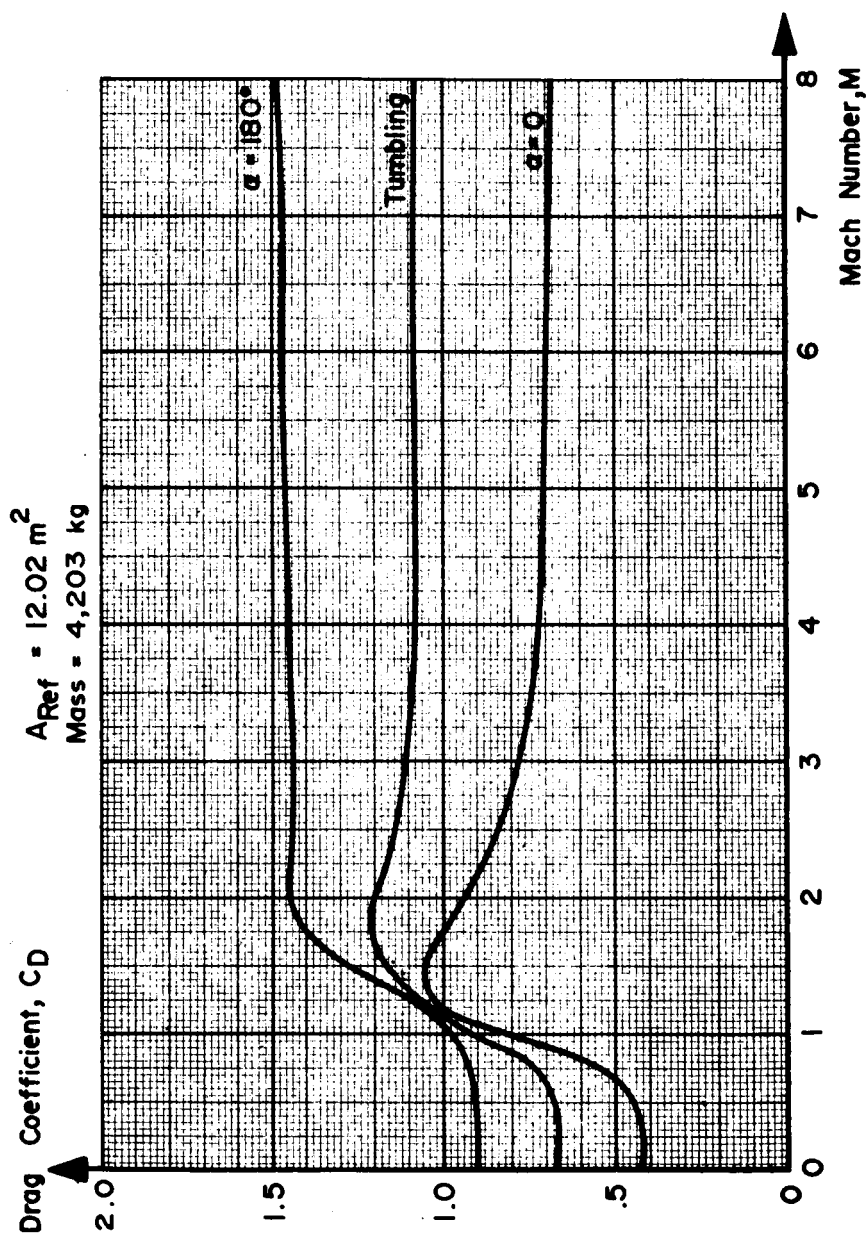
FIG. 10. COMMAND MODULE WITHOUT LES VARIATION OF ESTIMATED
TOTAL DRAG COEFFICIENT WITH MACH NUMBER
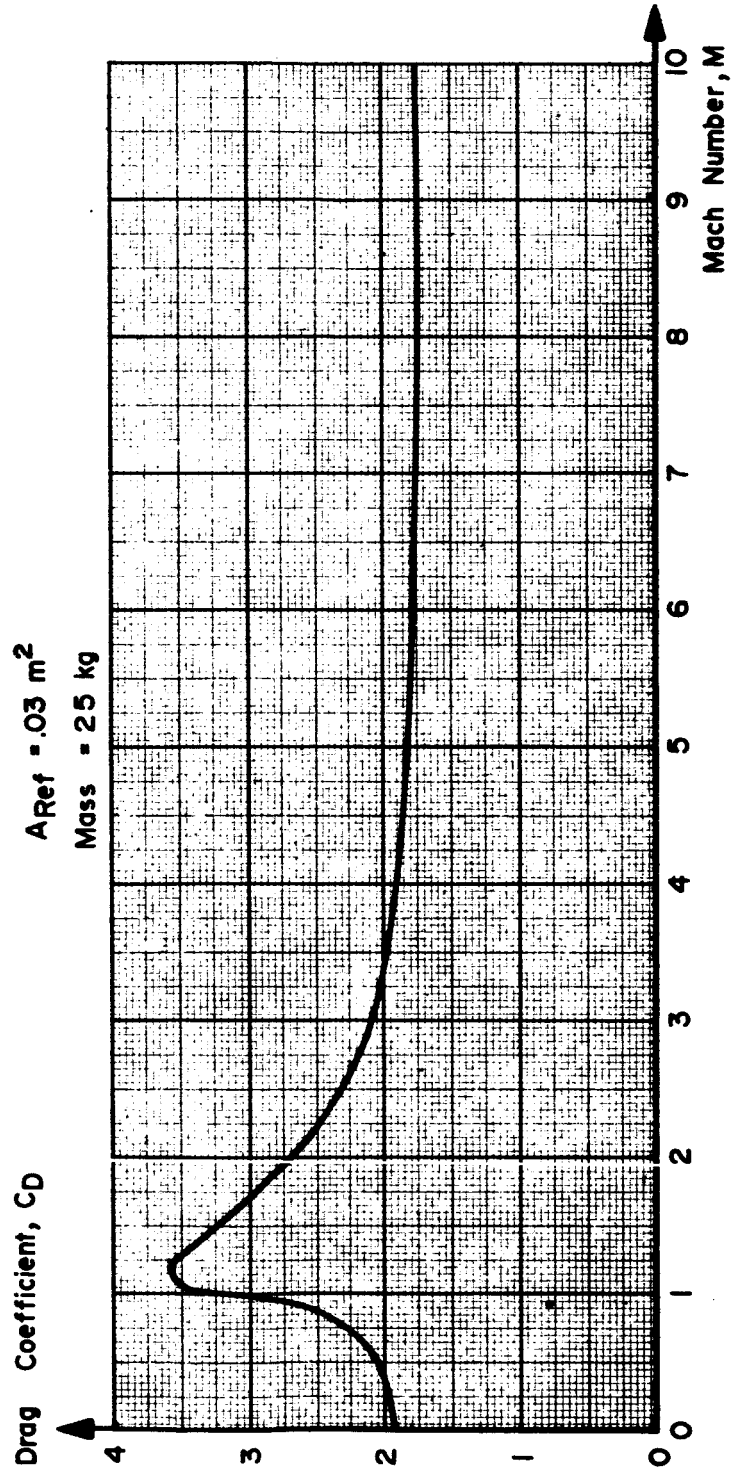
FIG. II. RECOVERABLE CAMERA CAPSULE
VARIATION OF TOTAL DRAG COEFFICIENT WITH MACH NUMBER

62
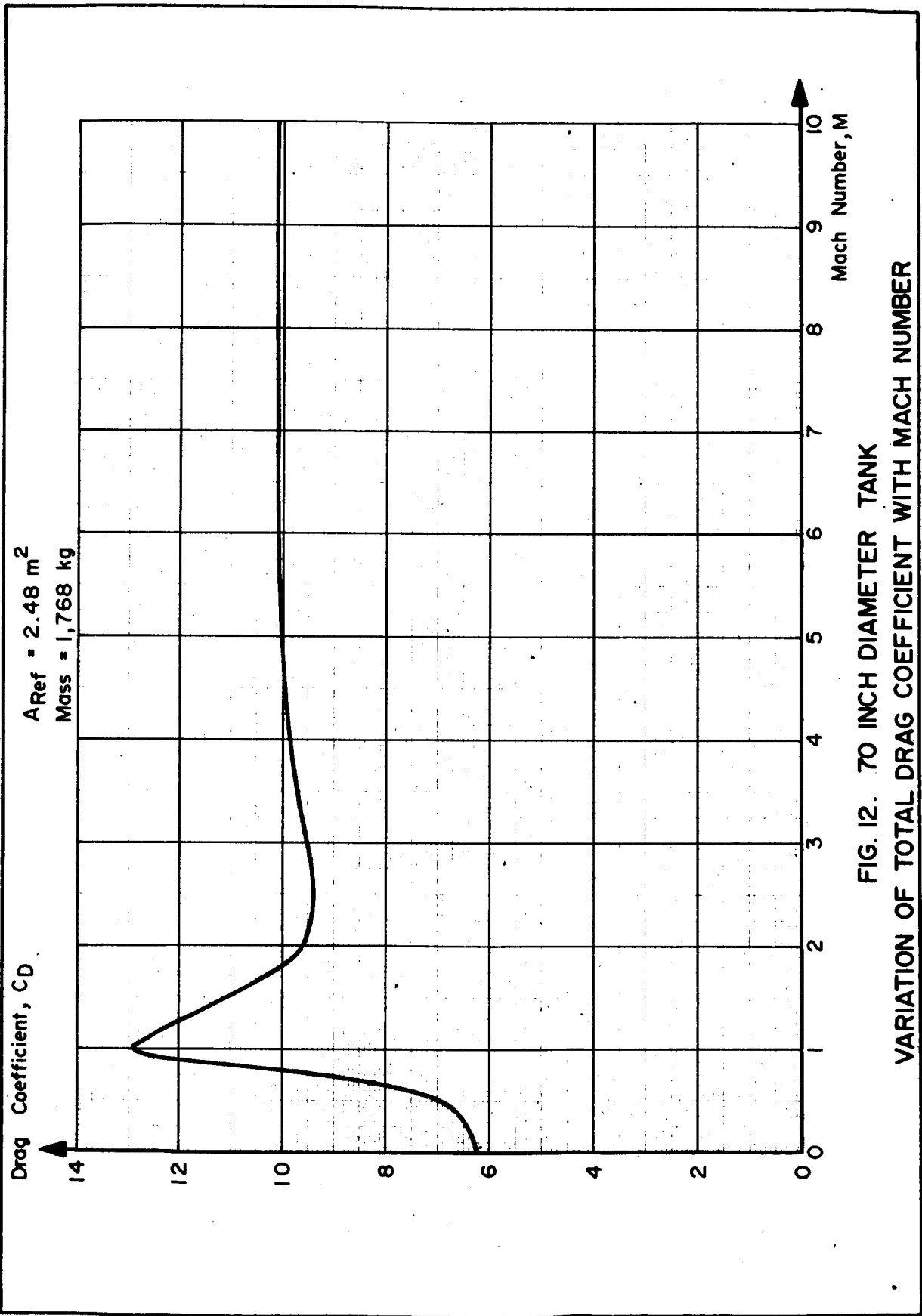
FIG. 12. 70 INCH DIAMETER TANK
VARIATION OF TOTAL DRAG COEFFICIENT WITH MACH NUMBER
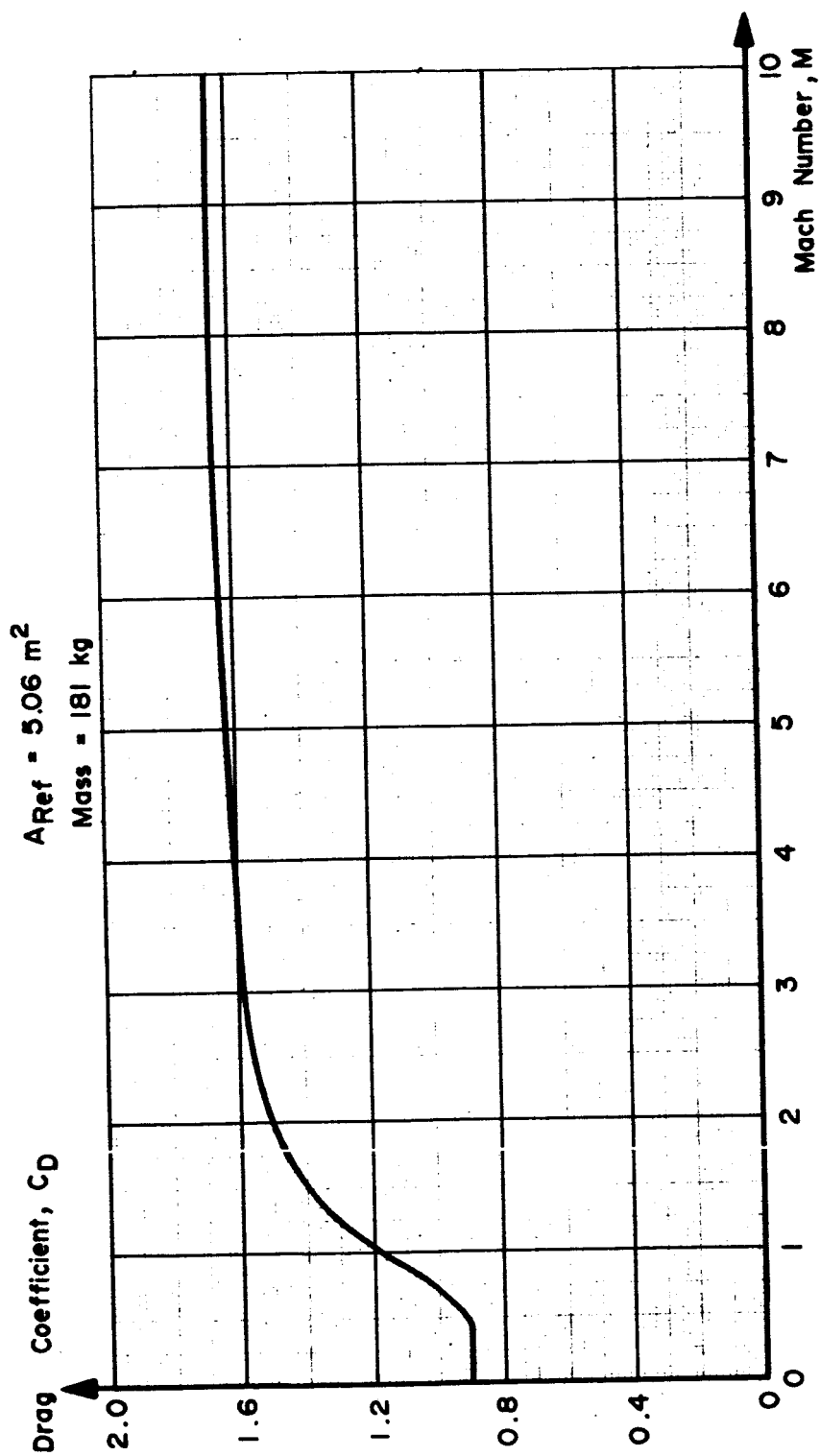
FIG. 13. RL IOA-3 TURBOPUMP ASSEMBLY
VARIATION OF TOTAL DRAG COEFFICIENT WITH MACH NUMBER

64
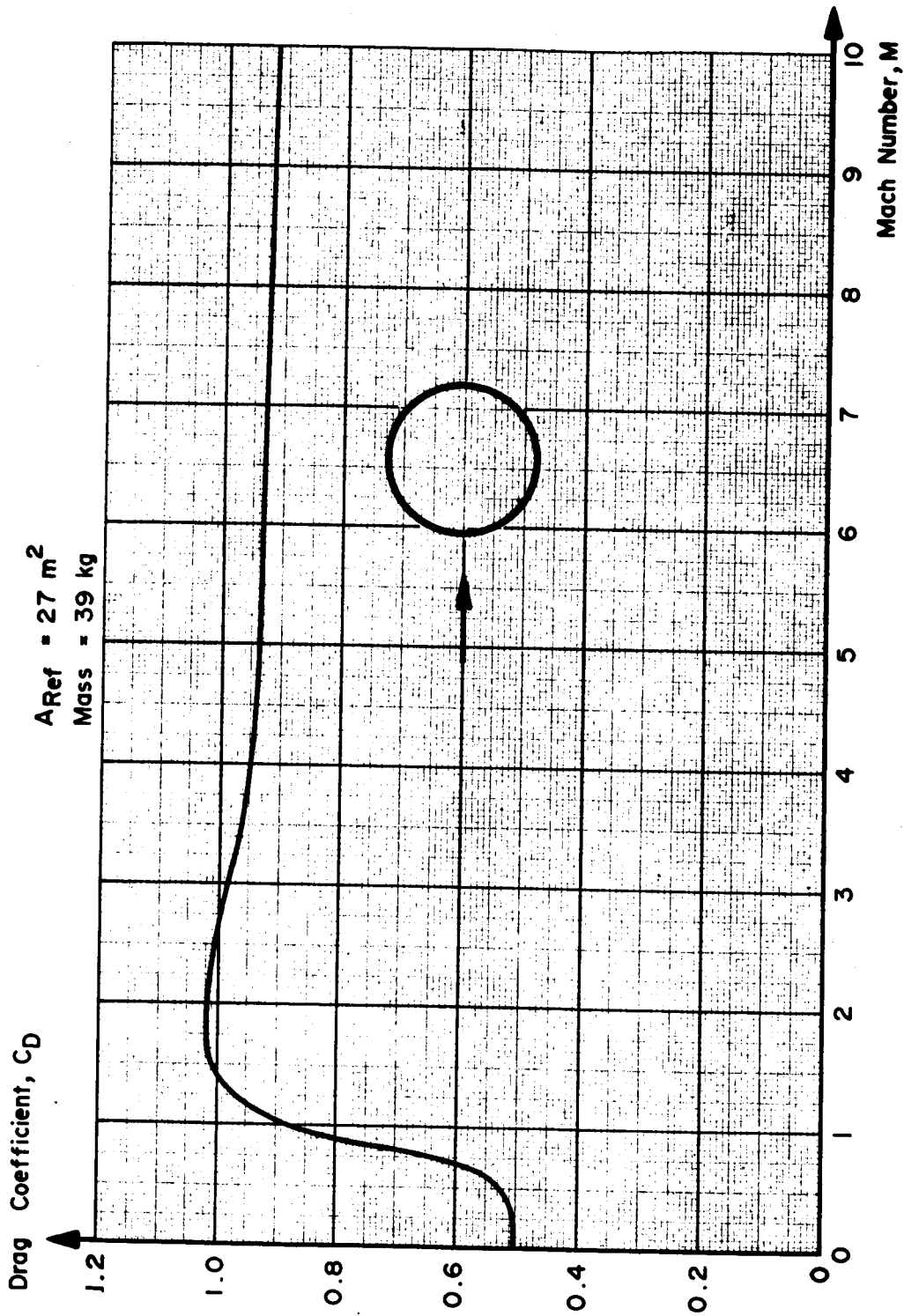
FIG. 14. SPHERE

VARIATION OF TOTAL DRAG COEFFICIENT WITH MACH NUMBER

FIG. 15. S–IV STAGE (DRY)

VARIATION OF TOTAL DRAG COEFFICIENT WITH MACH NUMBER

$\alpha = 180°$ (NOT TUMBLING)
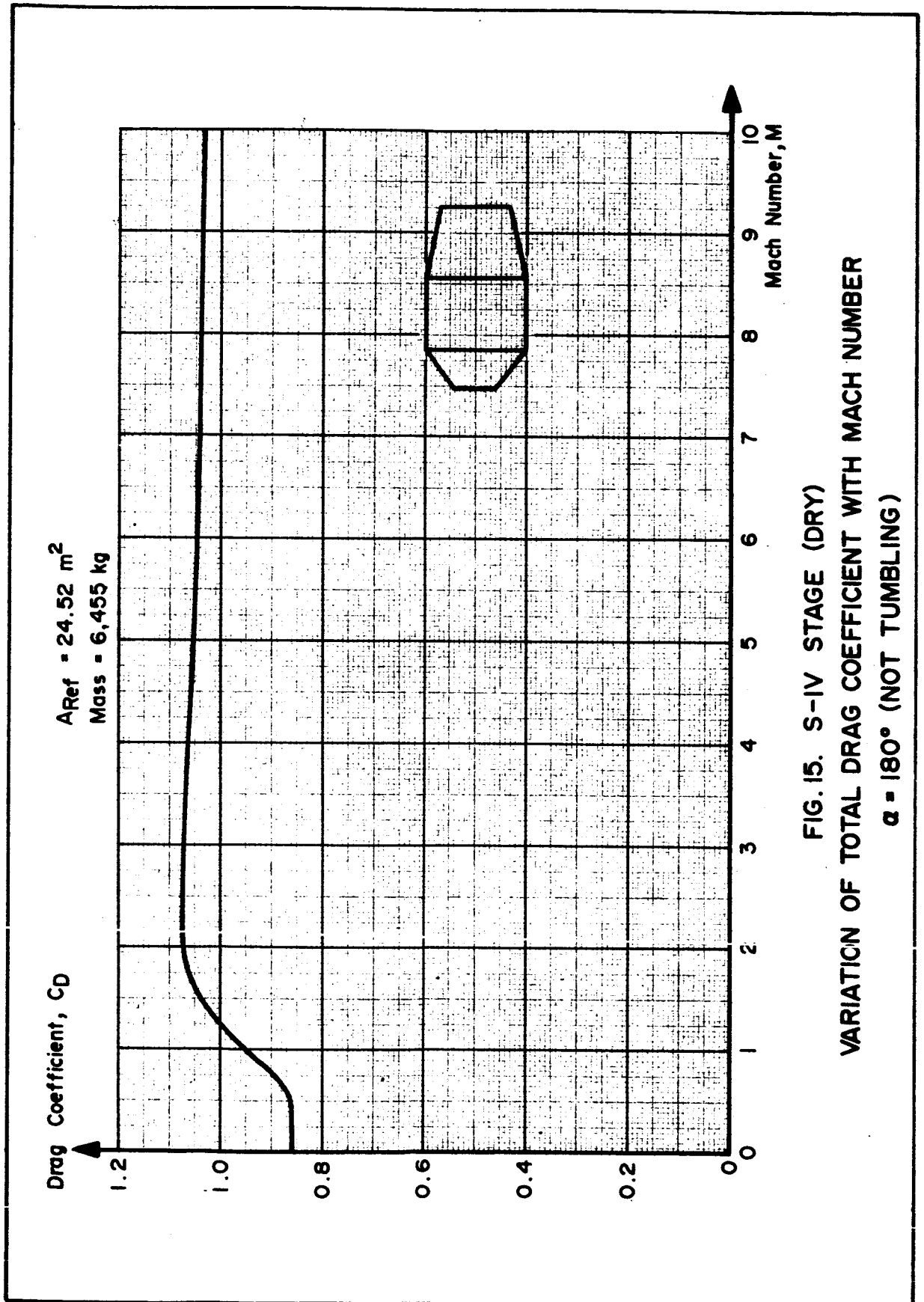
FIGURE 16

IMPACT TRACE AND CORRIDORS
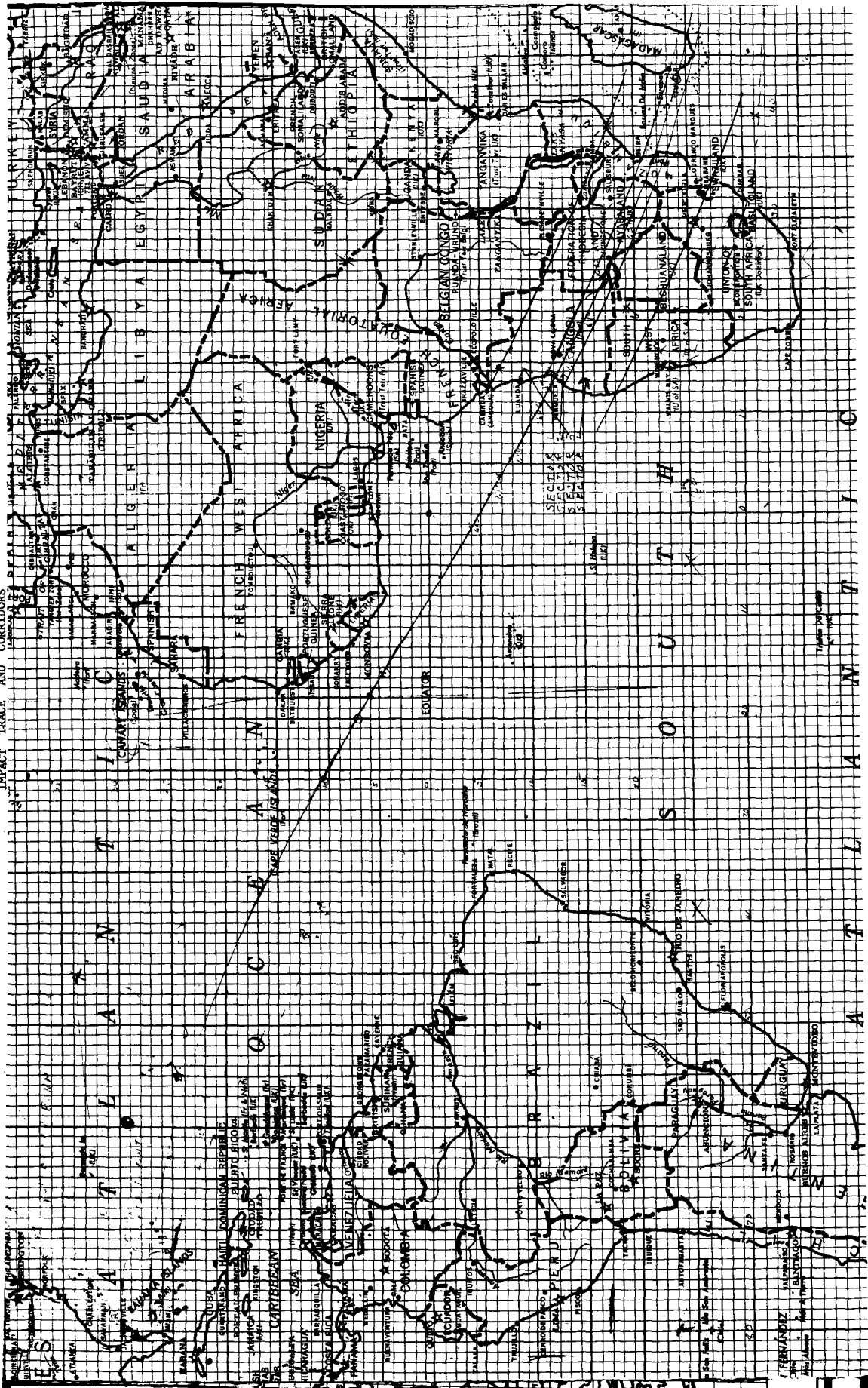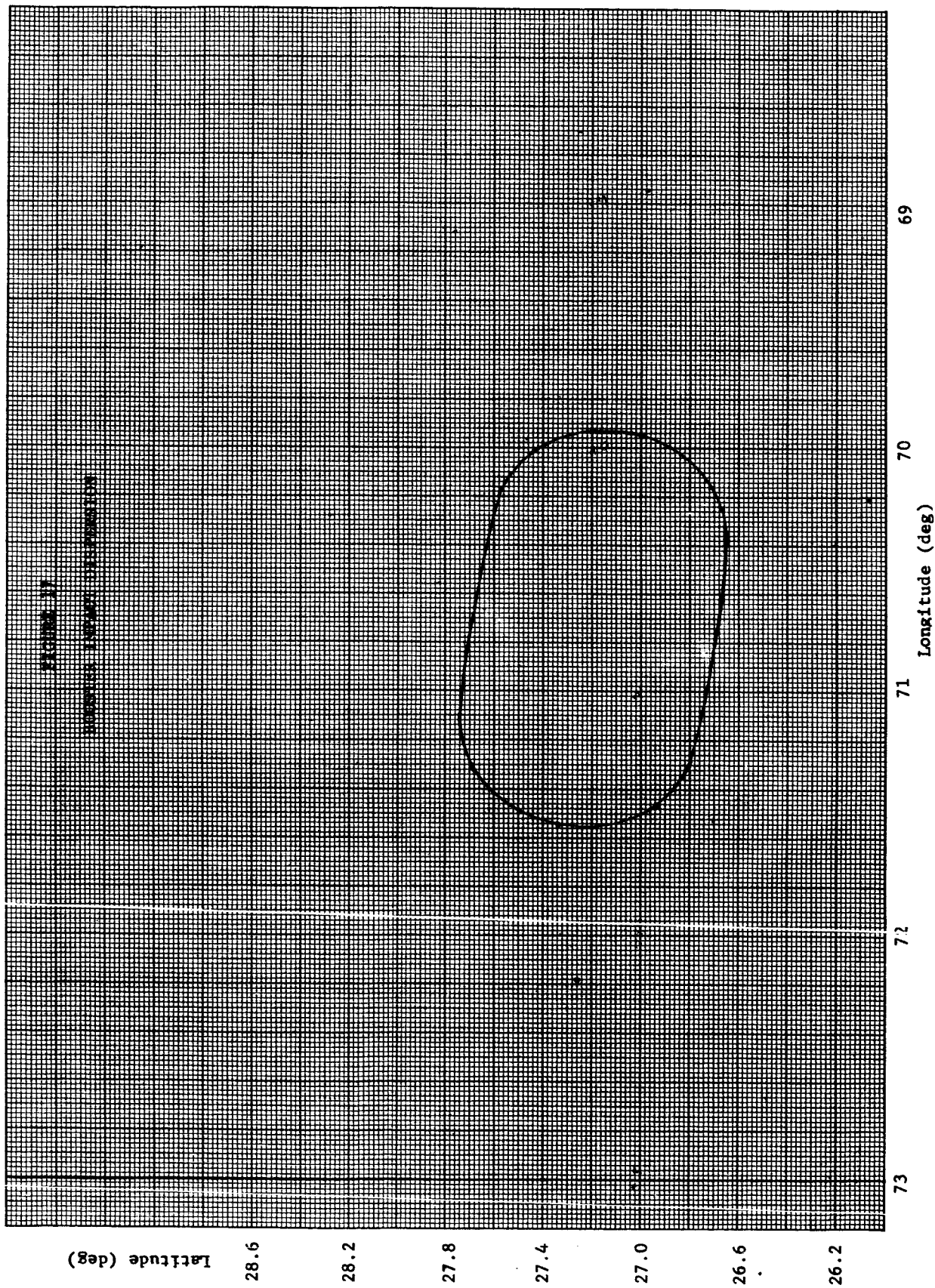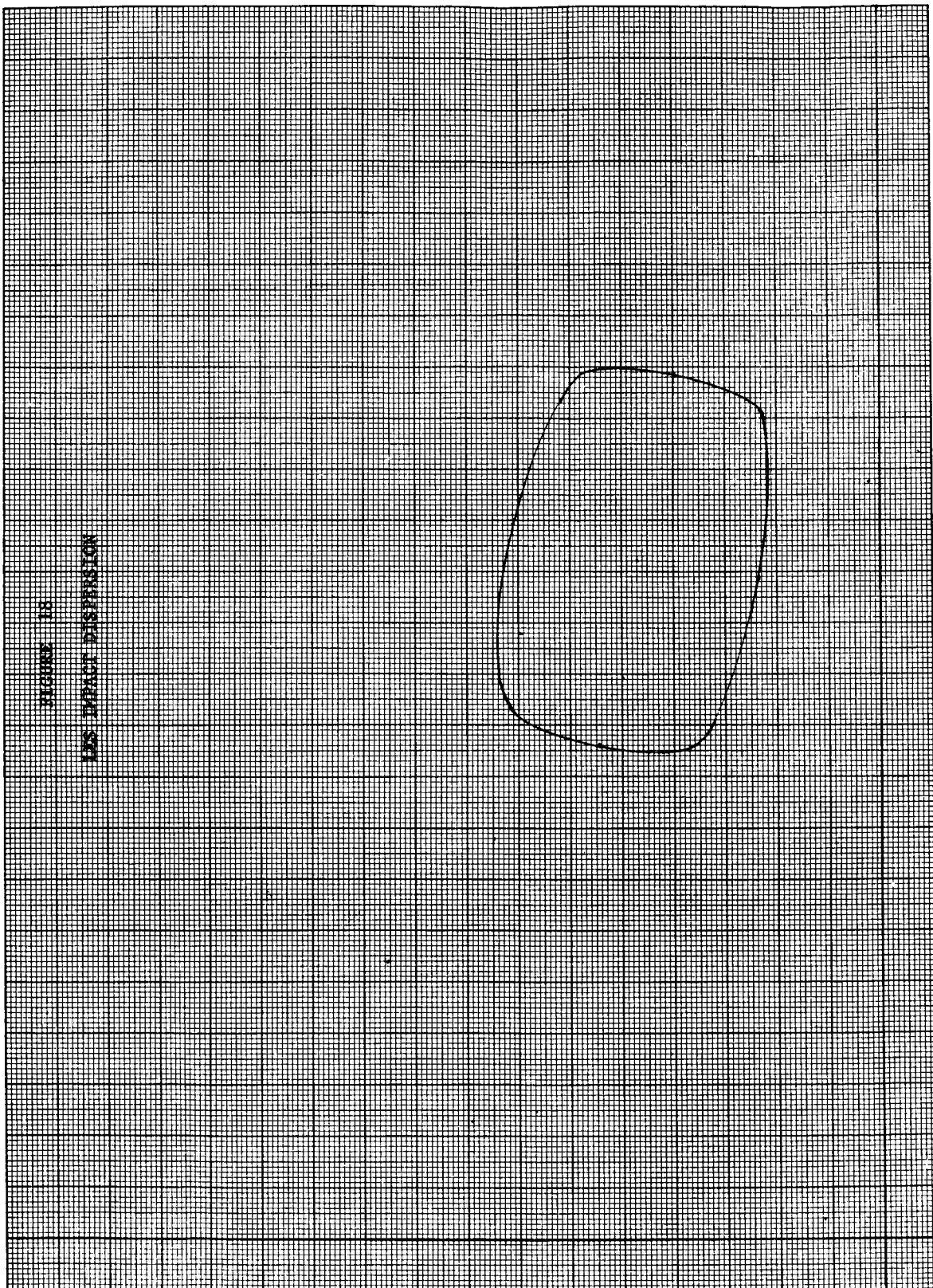
FIGURE 17

HORIZONTAL IMPACT DISPERSION

Longitude (deg)

Latitude (deg)

FIGURE 18

LES IMPACT DISPERSION

CHANGE IN TOTAL VELOCITY VECTOR ORIENTATION IN
THE LATERAL DIRECTION VERSUS TIME FOR MALFUNCTION   FIGURE 19
$(-\beta_y$ of 11.5, 10, 7, 3, 1, .5) at $T_o = 16$

TIME SEC.
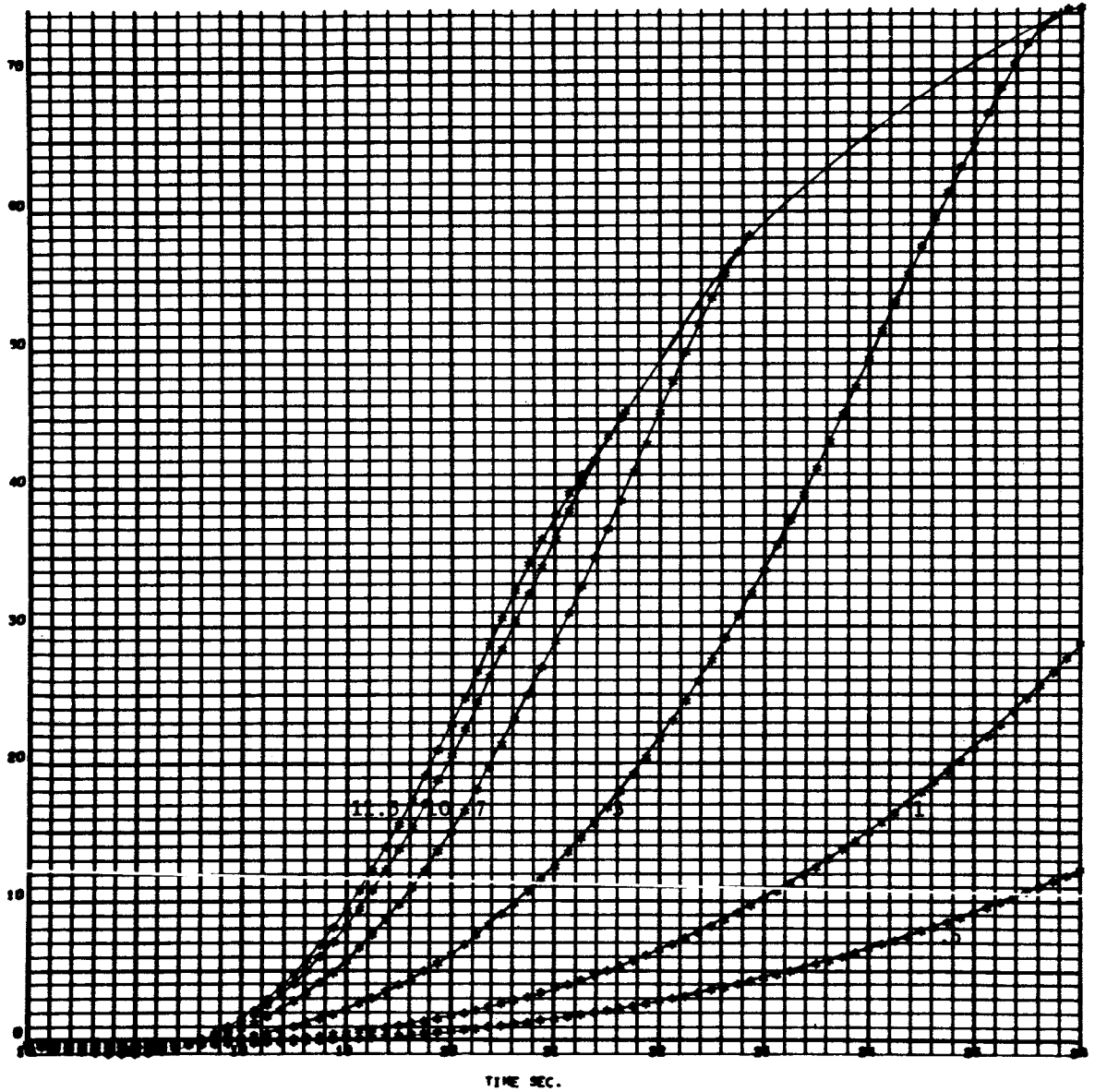
CHANGE IN TOTAL VELOCITY VECTOR ORIENTATION IN
THE LATERAL DIRECTION VERSUS TIME FOR MALFUNCTION   FIGURE 20
$(-\beta_y$ of 11.5, 10, 7, 3, 1, .5) at $T_o = 20$
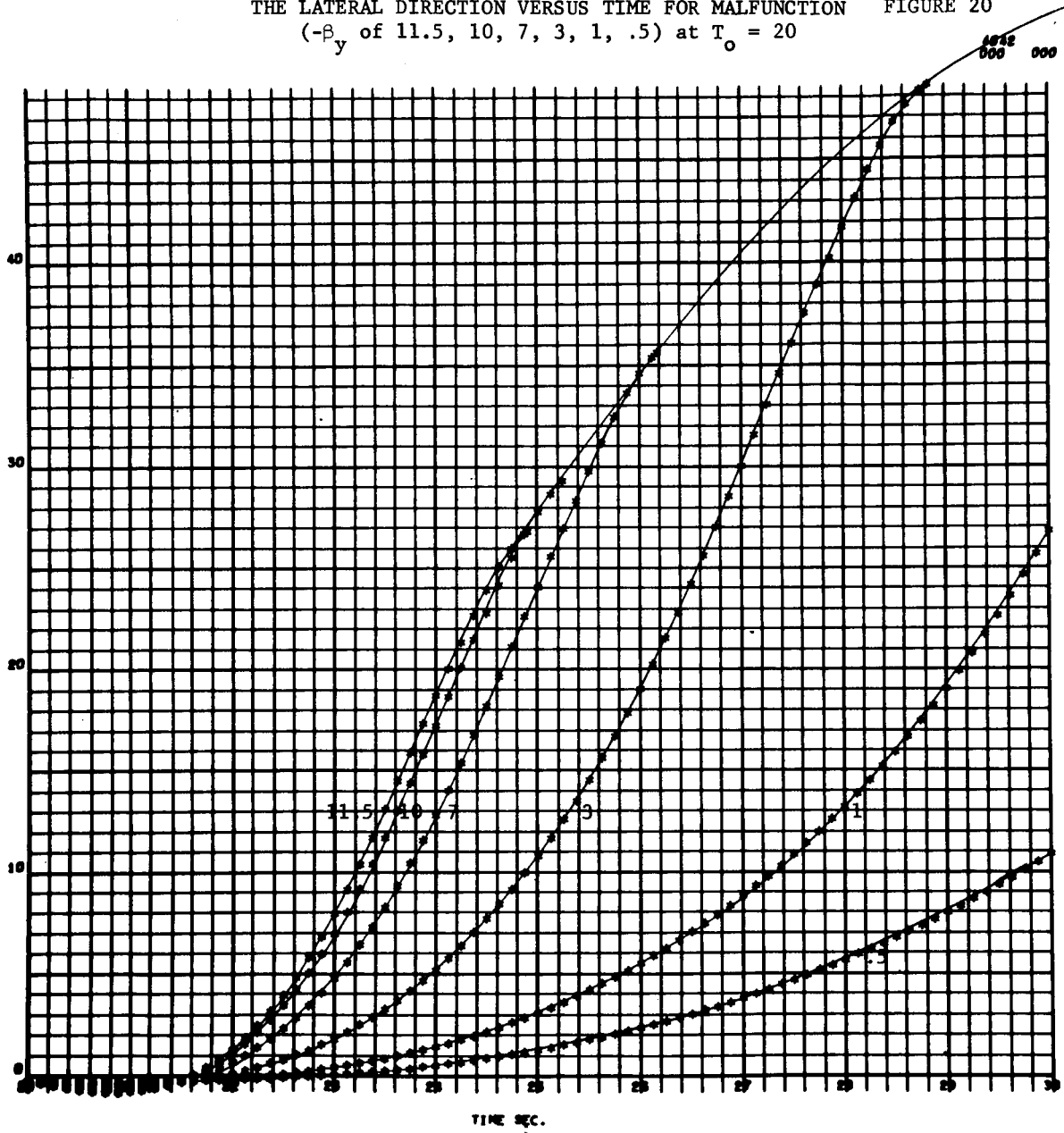
TIME SEC.

CHANGE IN TOTAL VELOCITY VECTOR ORIENTATION IN
THE LATERAL DIRECTION VERSUS TIME FOR MALFUNCTION   FIGURE 21
$(-\beta_y$ of 11.5, 10, 7, 3, 1, .5) at $T_o = 24$
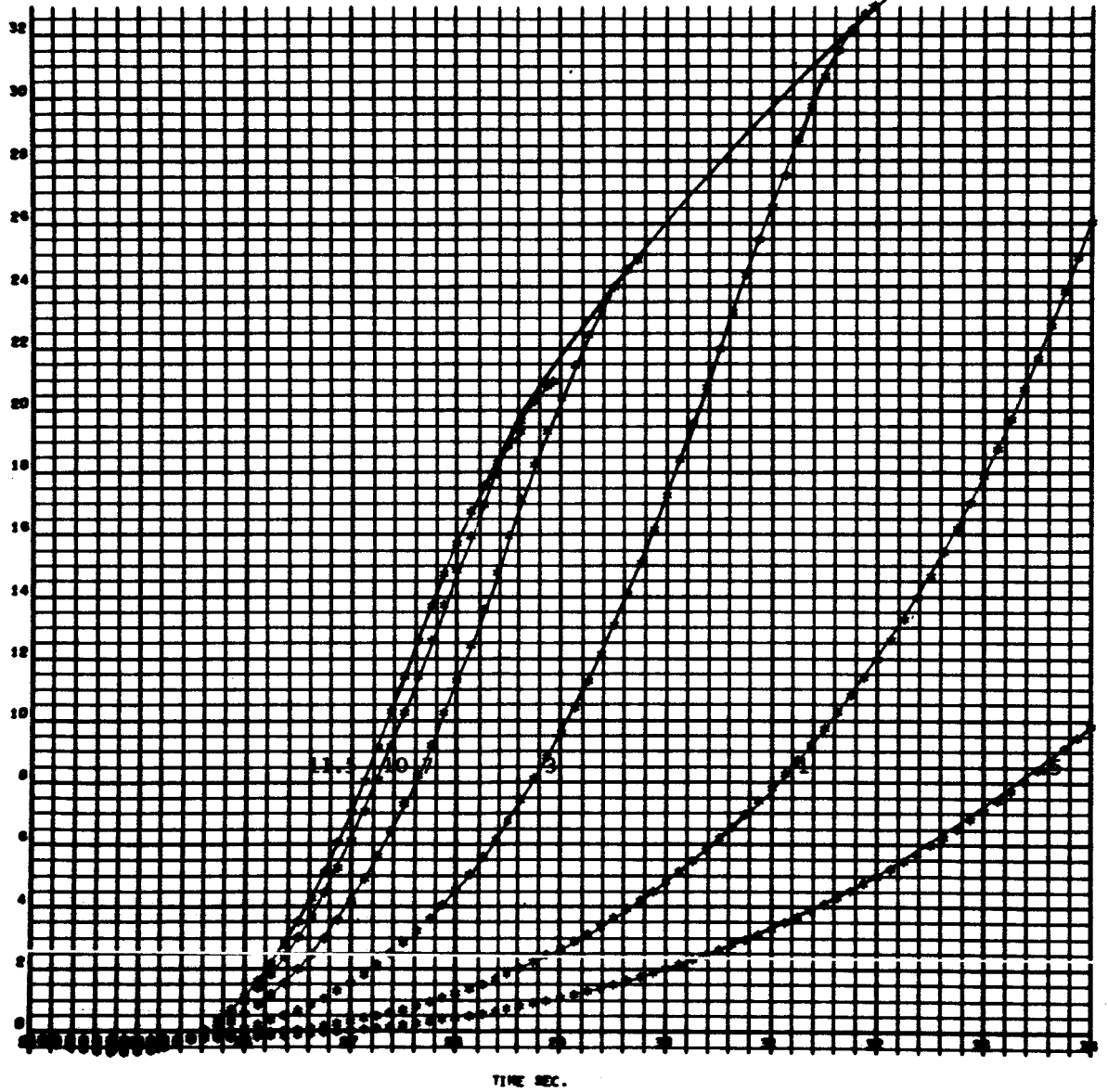
TIME SEC.

72

CHANGE IN TOTAL VELOCITY VECTOR ORIENTATION IN
THE LATERAL DIRECTION VERSUS TIME FOR MALFUNCTION   FIGURE 22
$(-\beta_y$ of 11.5, 10, 7, 3, 1, .5) at $T_o = 28$

TIME SEC.
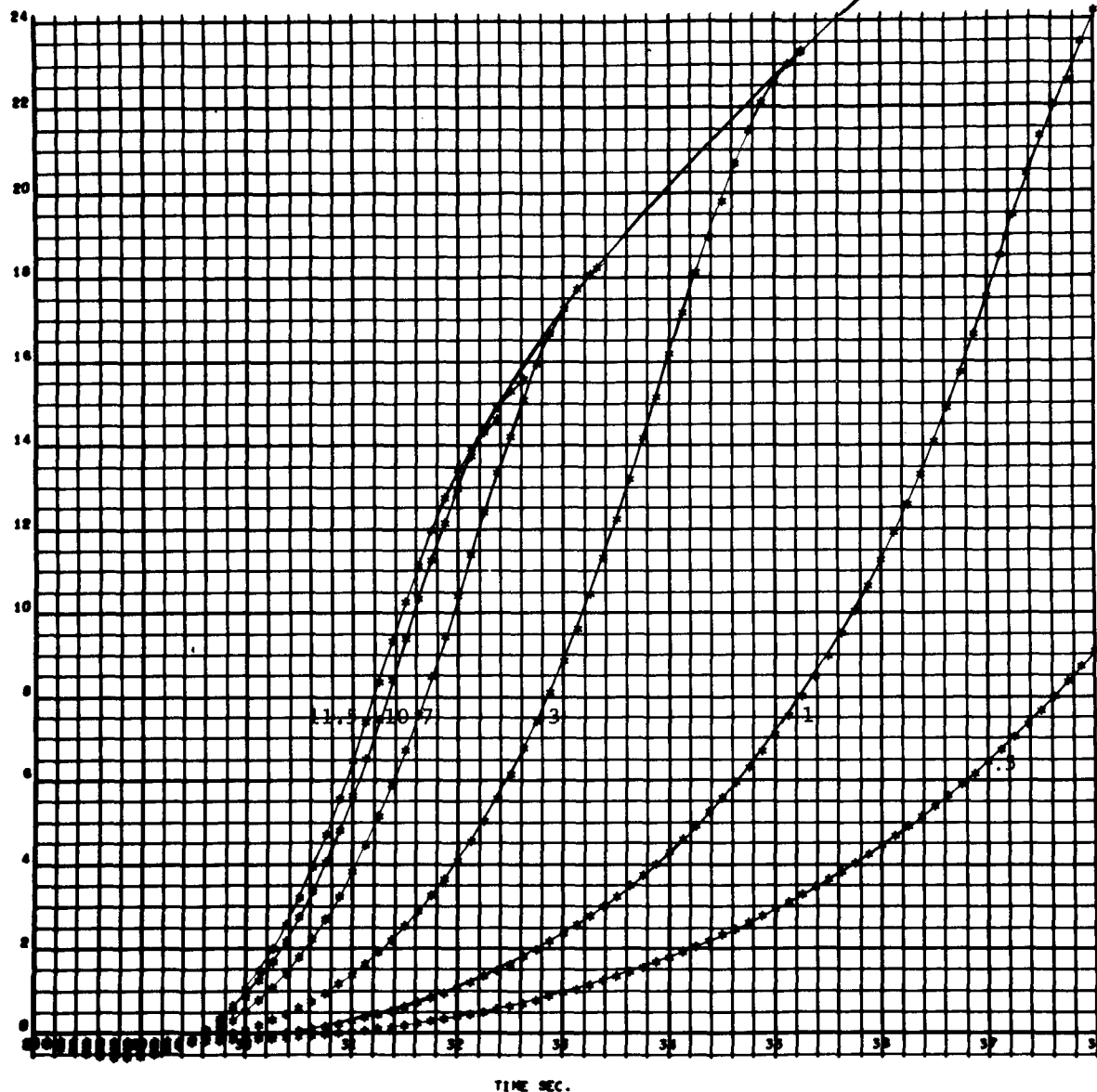
CHANGE IN TOTAL VELOCITY VECTOR ORIENTATION IN
THE LATERAL DIRECTION VERSUS TIME FOR MALFUNCTION   FIGURE 23
$(-\beta_y$ of 11.5, 10, 7, 3, 1, .5) at $T_o = 32$
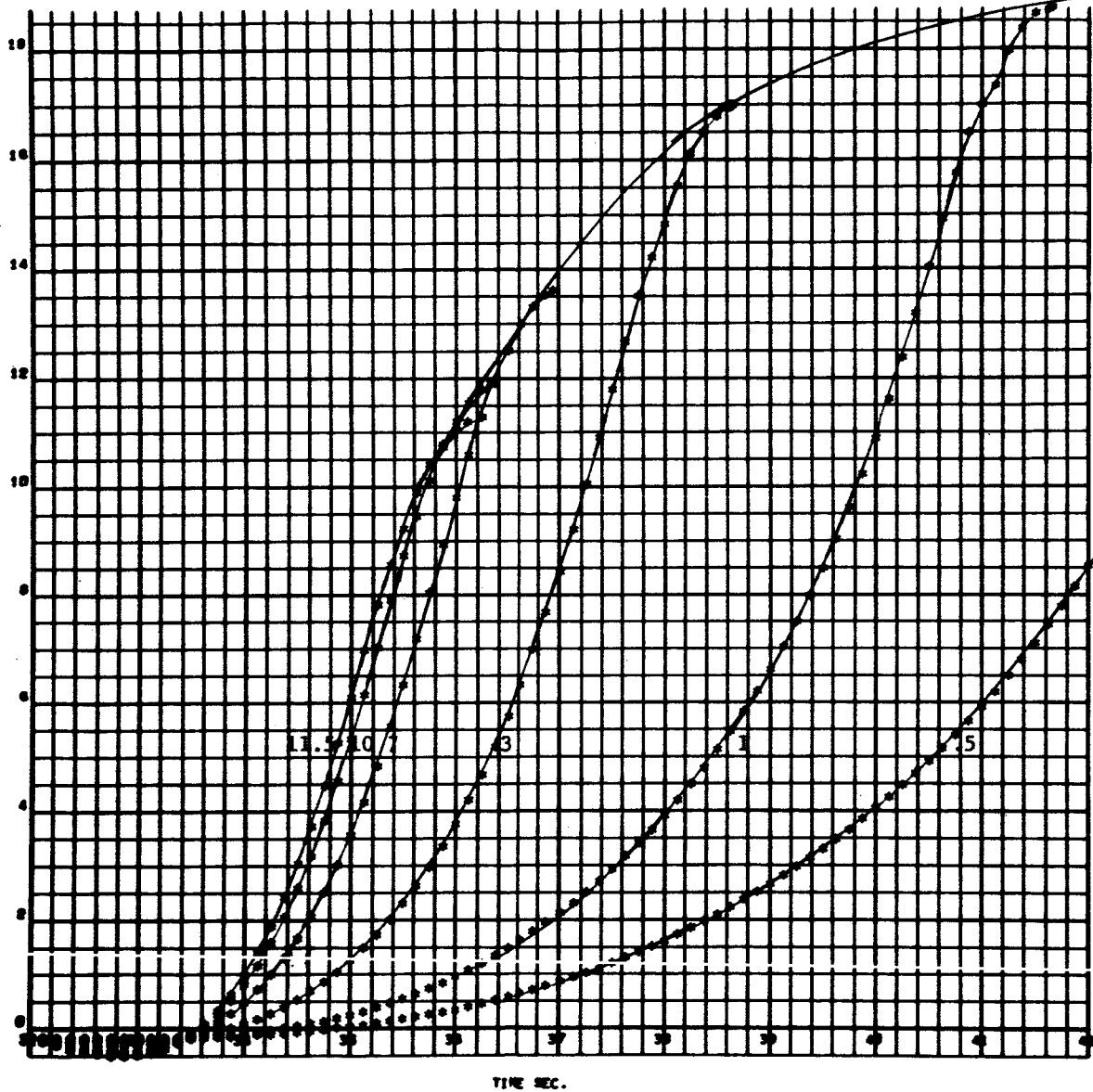
TIME SEC.

74

TIME SEC.

CHANGE IN TOTAL VELOCITY VECTOR ORIENTATION IN
THE LATERAL DIRECTION VERSUS TIME FOR MALFUNCTION   FIGURE 25
$(-\beta_y$ of 11.5, 10, 7, 3, 1, .5) at $T_o = 40$

TIME SEC.
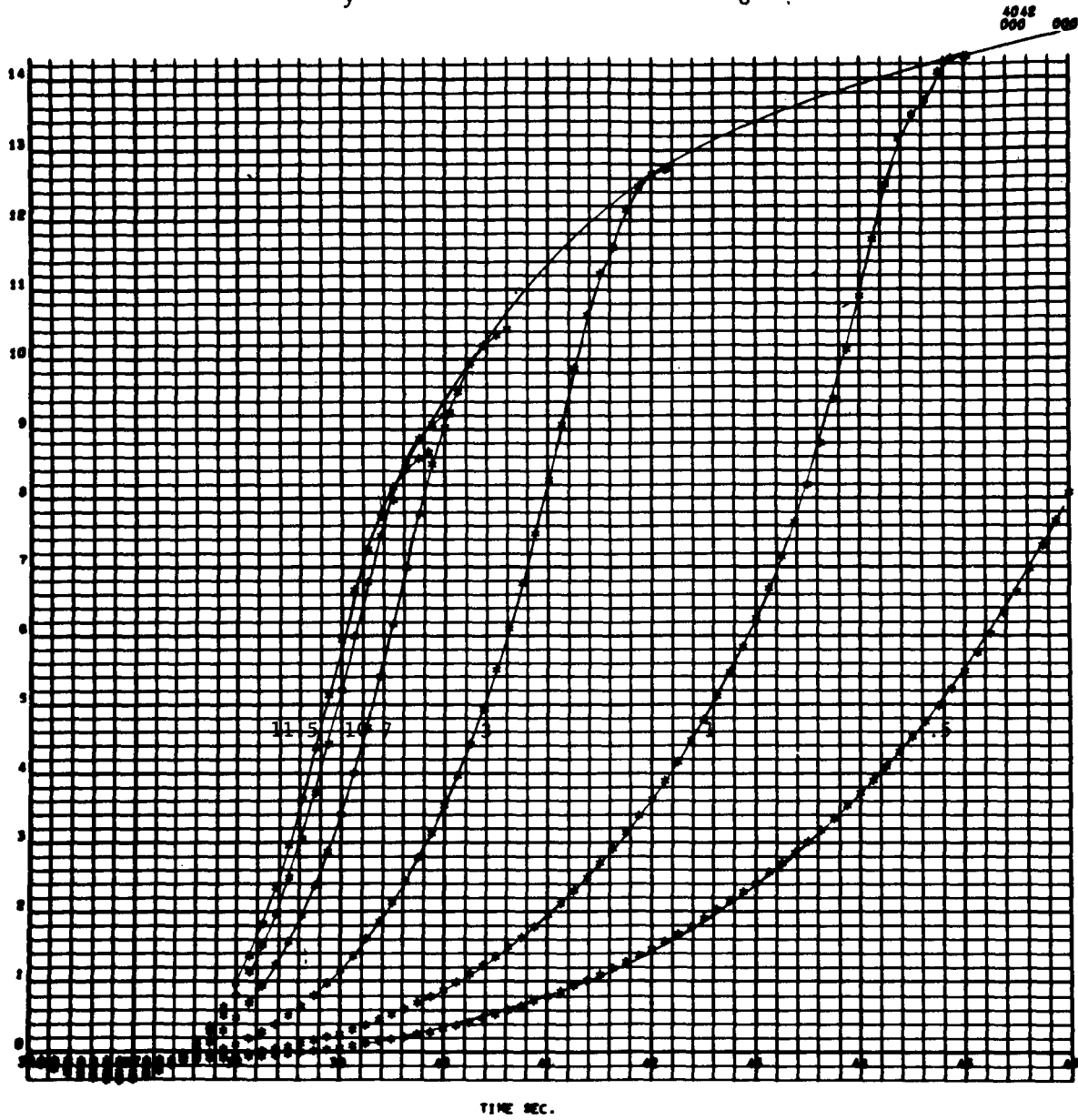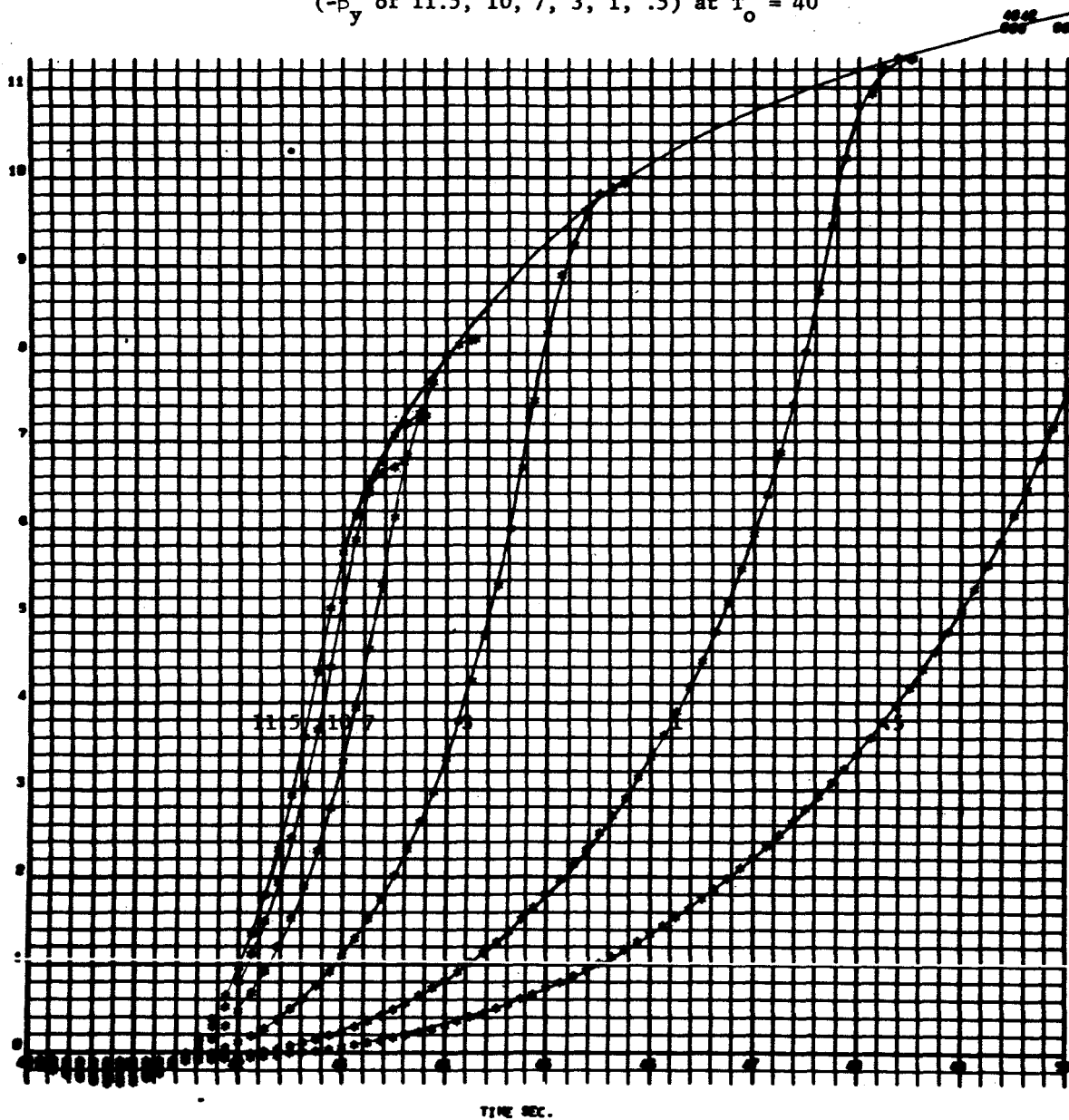
CHANGE IN TOTAL VELOCITY VECTOR ORIENTATION IN
THE LATERAL DIRECTION VERSUS TIME FOR MALFUNCTION   FIGURE 26
$(-\beta_y$ of 11.5, 10, 7, 3, 1, .5) at T_o = 44
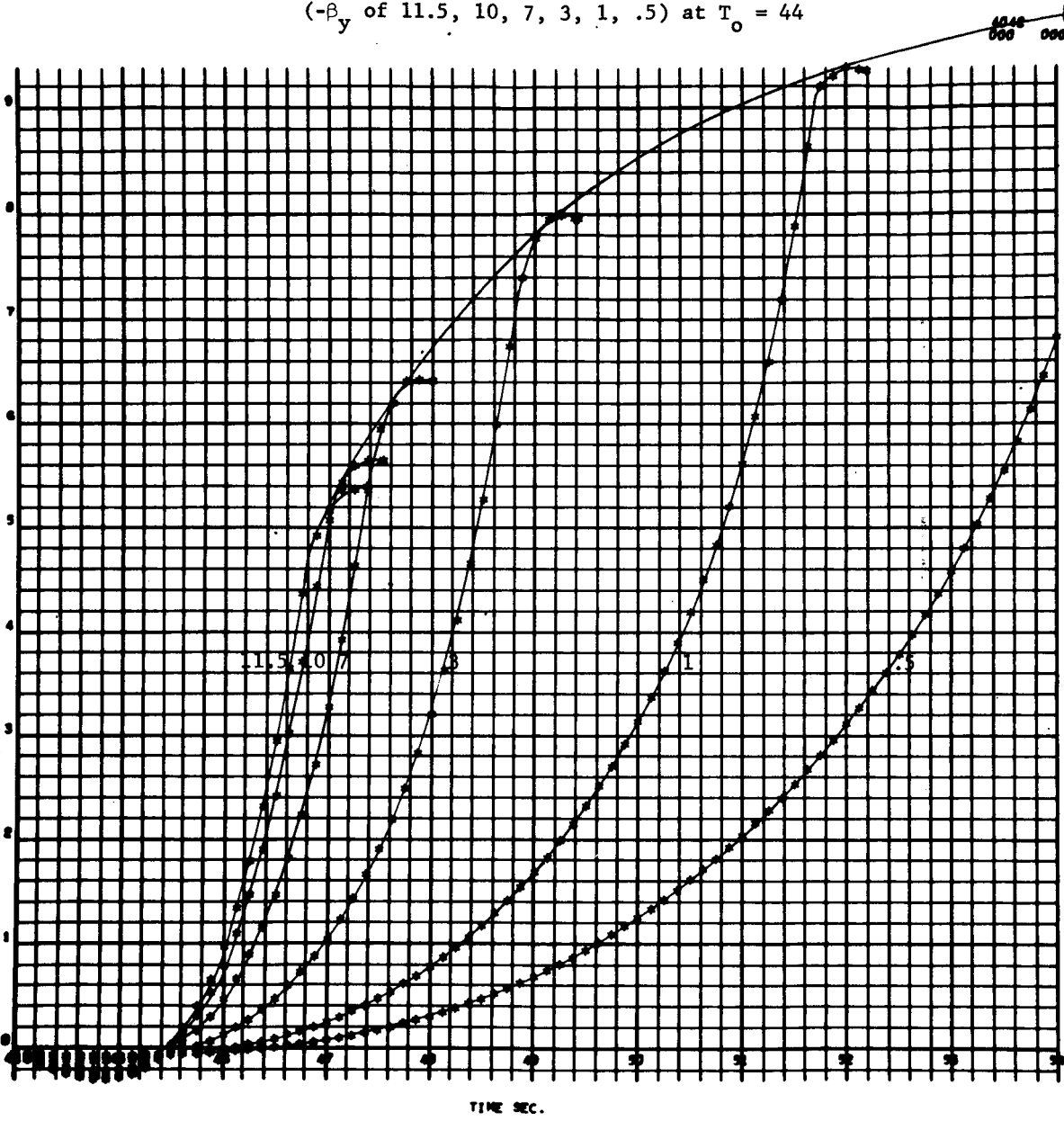
CHANGE IN TOTAL VELOCITY VECTOR ORIENTATION IN
THE LATERAL DIRECTION VERSUS TIME FOR MALFUNCTION   FIGURE 27
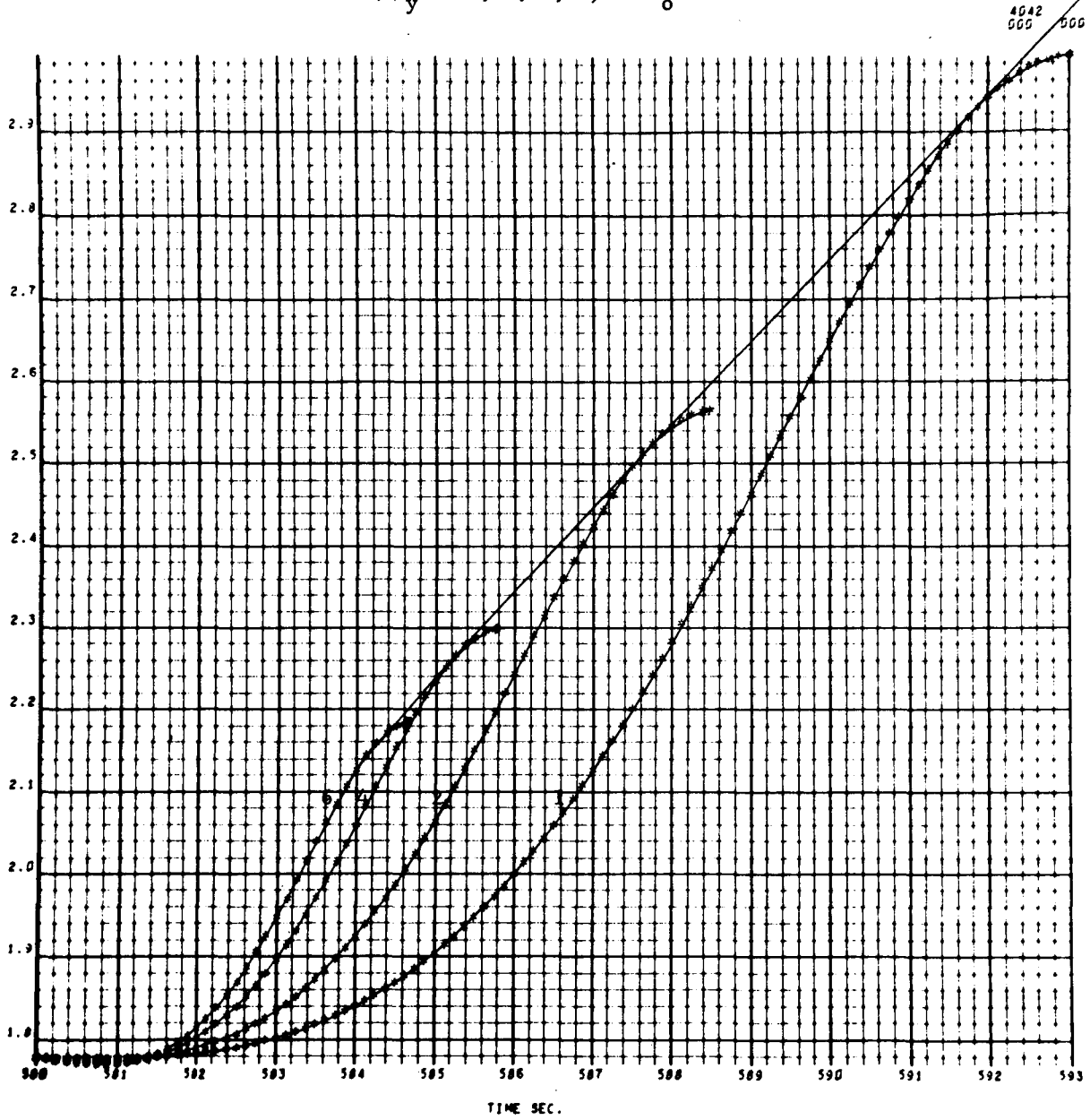($-\beta_y$ of 11.5, 10, 7, 3, 1, .5) at T_o = 48

TIME SEC.

78
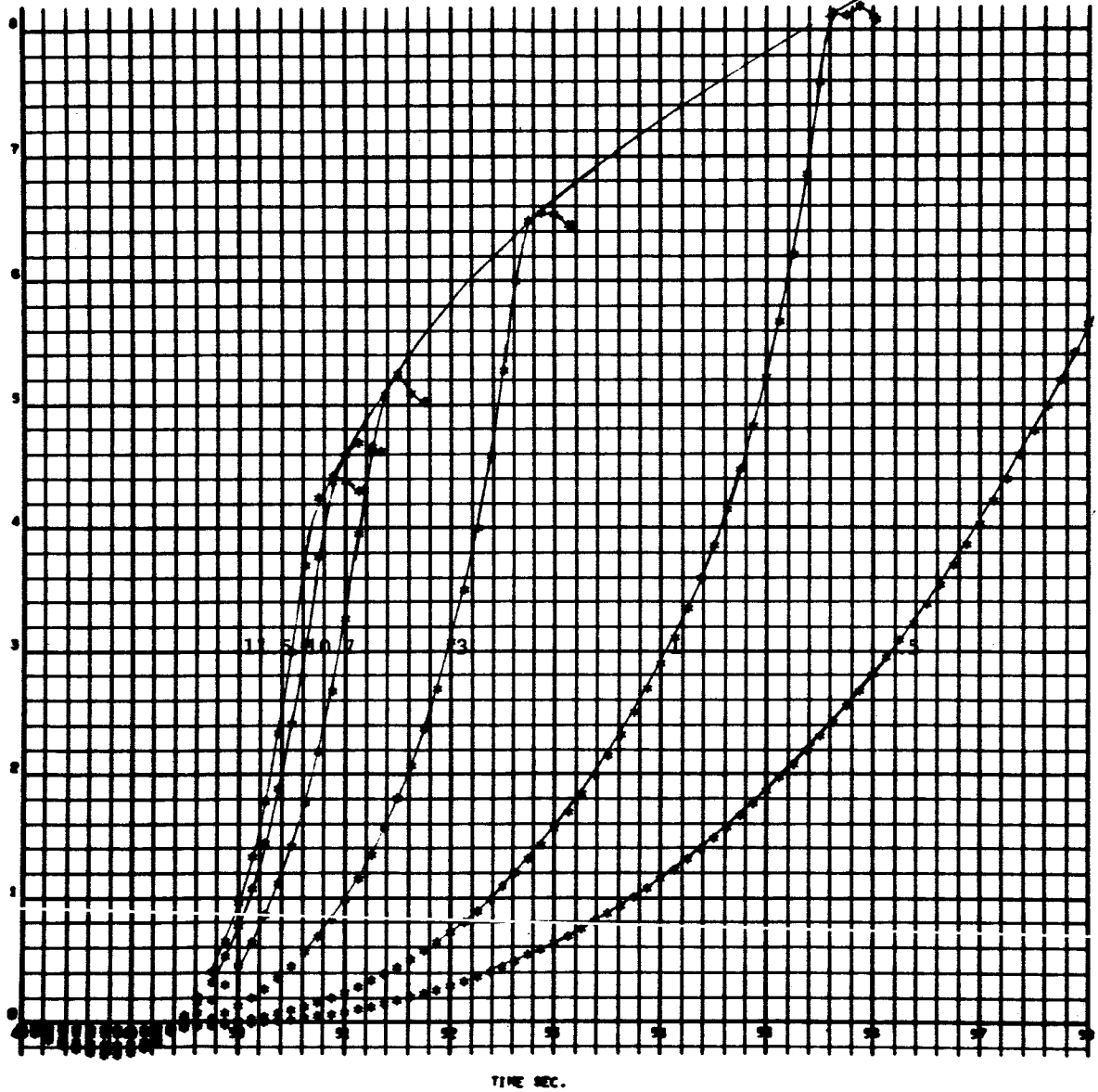
CHANGE IN TOTAL VELOCITY VECTOR ORIENTATION IN
THE LATERAL DIRECTION VERSUS TIME FOR MALFUNCTION
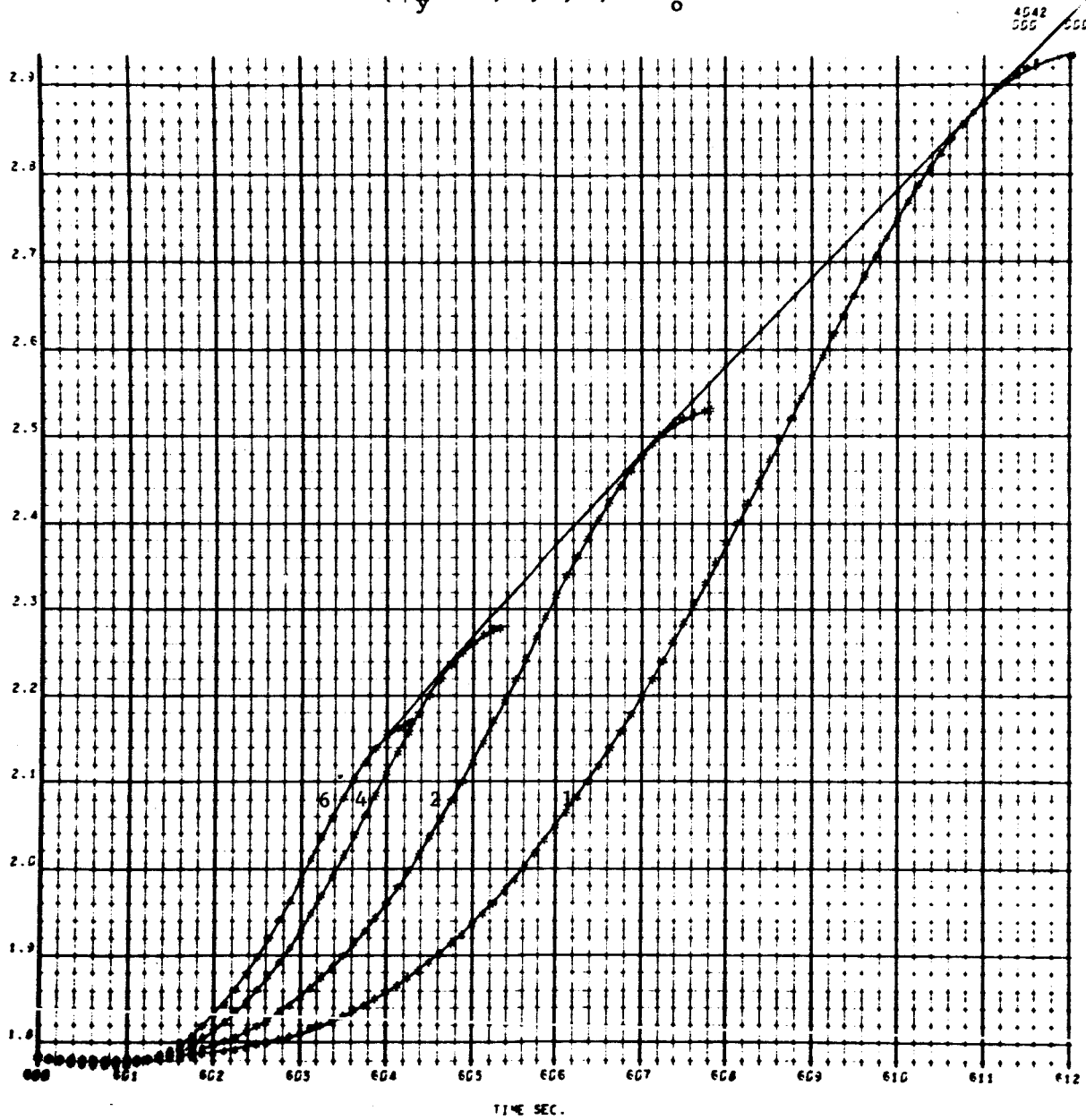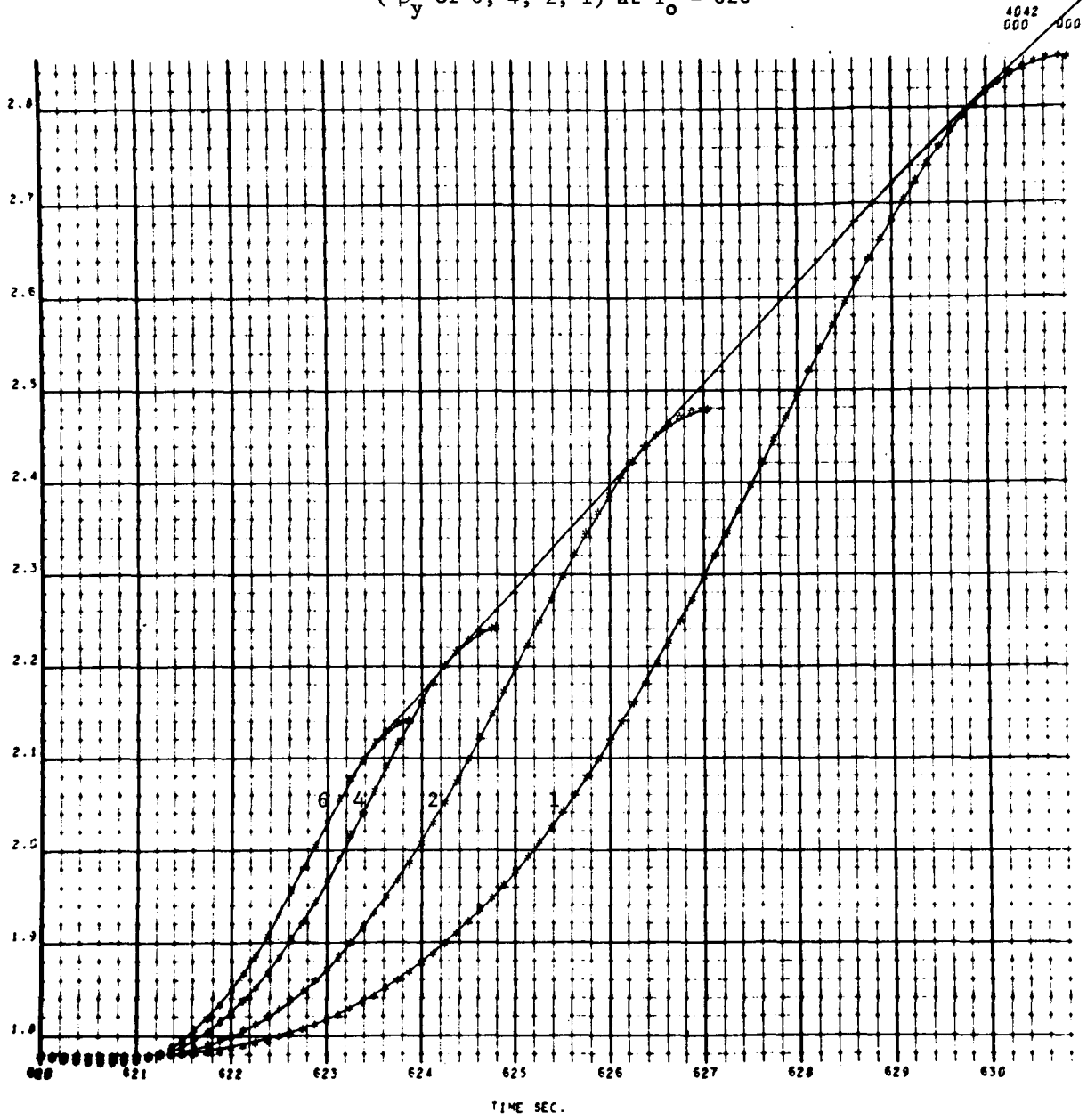$(-\beta_y$ of 11.5, 10, 7, 3, 1, .5) at $T_o = 52$

FIGURE 28
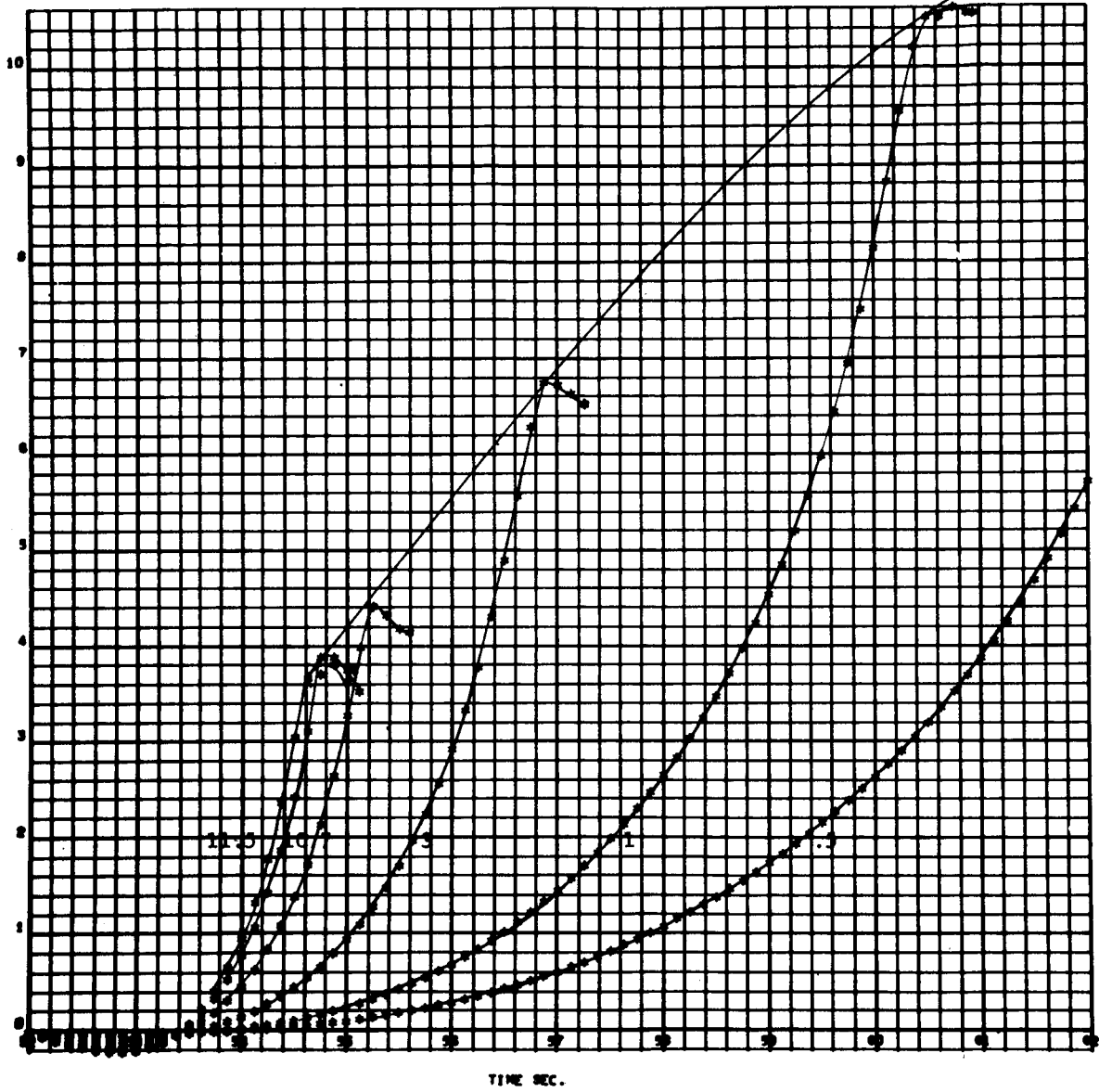
TIME SEC.

CHANGE IN TOTAL VELOCITY VECTOR ORIENTATION IN
THE LATERAL DIRECTION VERSUS TIME FOR MALFUNCTION   FIGURE 29
$(-\beta_y$ of 11.5, 10, 7, 3, 1, .5) at T_o = 56
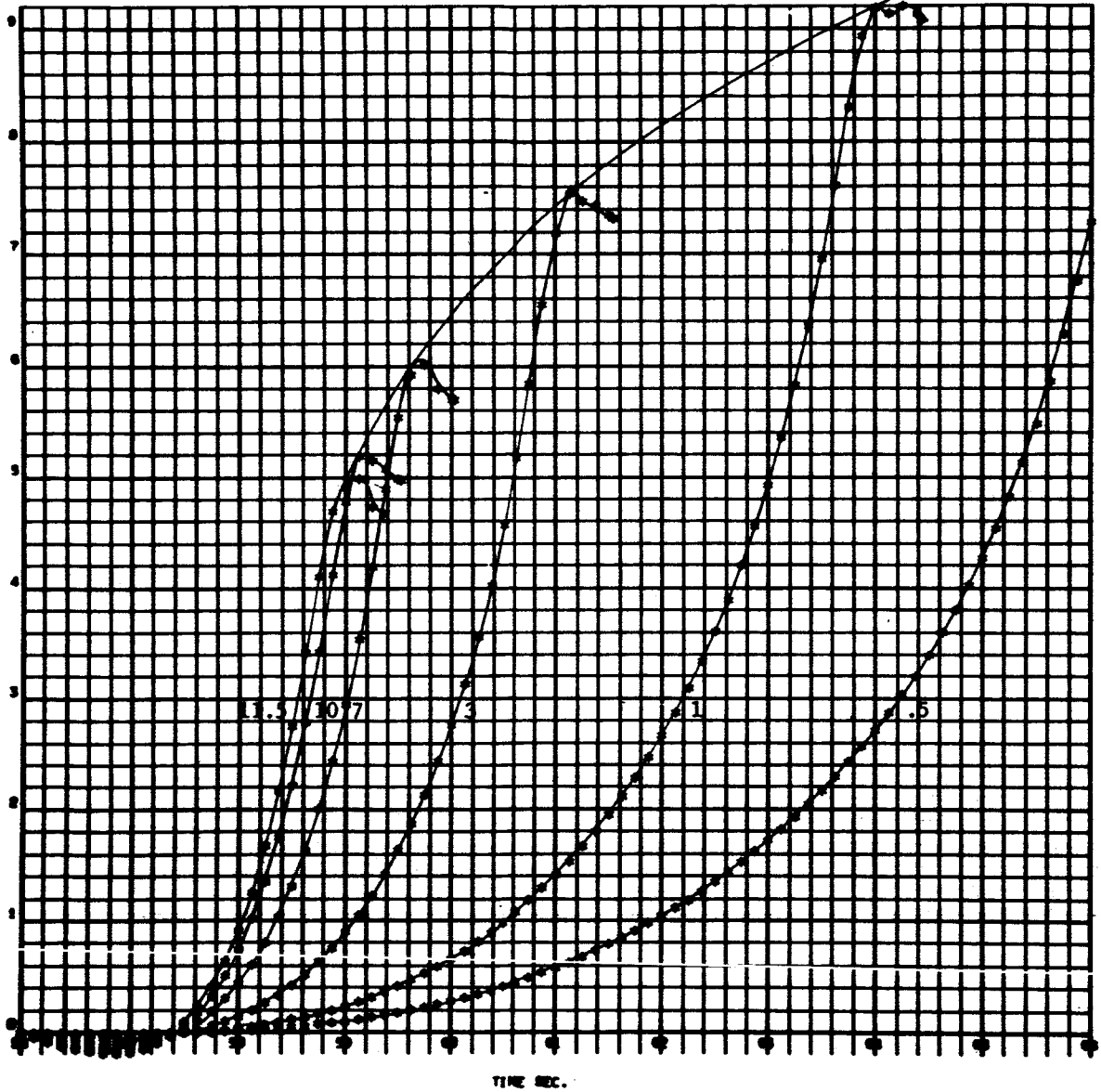
CHANGE IN TOTAL VELOCITY VECTOR ORIENTATION IN
THE LATERAL DIRECTION VERSUS TIME FOR MALFUNCTION   FIGURE 30
$(-\beta_y$ of 11.5, 10, 7, 3, 1, .5) at $T_o = 60$

CHANGE IN TOTAL VELOCITY VECTOR ORIENTATION IN
THE LATERAL DIRECTION VERSUS TIME FOR MALFUNCTION
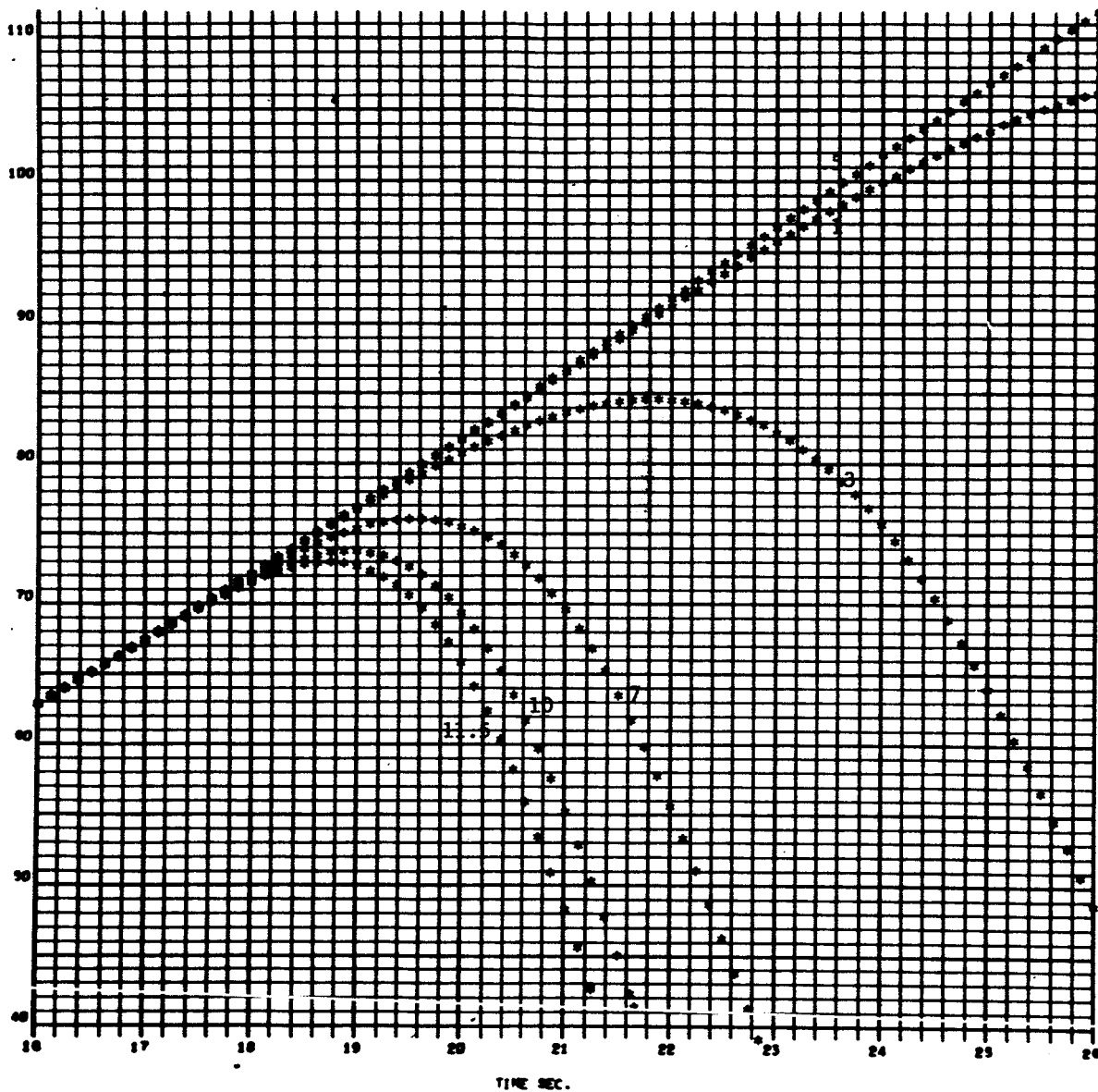$(-\beta_y$ of 11.5, 10, 7, 3, 1, .5) at $T_o = 64$

FIGURE 31

TIME SEC.

CHANGE IN TOTAL VELOCITY VECTOR ORIENTATION IN
THE LATERAL DIRECTION VERSUS TIME FOR MALFUNCTION   FIGURE 32
$(-\beta_y$ of 11.5, 10, 7, 3, 1, .5) at T_o = 68

TIME SEC.

CHANGE IN TOTAL VELOCITY VECTOR ORIENTATION IN
THE LATERAL DIRECTION VERSUS TIME FOR MALFUNCTION   FIGURE 33
(-β$_y$ of 11.5, 10, 7, 3, 1, .5) at T$_o$ = 72

TIME SEC.

CHANGE IN TOTAL VELOCITY VECTOR ORIENTATION IN
THE LATERAL DIRECTION VERSUS TIME FOR MALFUNCTION   FIGURE 34
$(-\beta_y$ of 11.5, 10, 7, 3, 1, .5) at $T_o = 76$

TIME SEC.

CHANGE IN TOTAL VELOCITY VECTOR ORIENTATION IN
THE LATERAL DIRECTION VERSUS TIME FOR MALFUNCTION   FIGURE 35
$(-\beta_y$ of 11.5, 10, 7, 3, 1, .5) at T_o = 80

TIME SEC.

CHANGE IN TOTAL VELOCITY VECTOR ORIENTATION IN
THE LATERAL DIRECTION VERSUS TIME FOR MALFUNCTION   FIGURE 36
$(-\beta_y$ of 11.5, 10, 7, 3, 1, .5) at $T_o = 84$

TIME SEC.

CHANGE IN TOTAL VELOCITY VECTOR ORIENTATION IN
THE LATERAL DIRECTION VERSUS TIME FOR MALFUNCTION
$(-\beta_y$ of 11.5, 10, 7, 3, 1, .5) at $T_o = 88$

FIGURE 37

TIME SEC.

CHANGE IN TOTAL VELOCITY VECTOR ORIENTATION IN
THE LATERAL DIRECTION VERSUS TIME FOR MALFUNCTION   FIGURE 38
$(-\beta_y$ of 11.5, 10, 7, 3, 1, .5) at T_o = 92

CHANGE IN TOTAL VELOCITY VECTOR ORIENTATION IN
THE LATERAL DIRECTION VERSUS TIME FOR MALFUNCTION   FIGURE 39
$(-\beta_y$ of 11.5, 10, 7, 3, 1, .5) at T_o = 96

TIME SEC.

90

CHANGE IN TOTAL VELOCITY VECTOR ORIENTATION IN
THE LATERAL DIRECTION VERSUS TIME FOR MALFUNCTION   FIGURE 40
$(-\beta_y$ of 11.5, 10, 7, 3, 1, .5) at $T_o = 100$

TIME SEC.

CHANGE IN TOTAL VELOCITY VECTOR ORIENTATION IN
THE LATERAL DIRECTION VERSUS TIME FOR MALFUNCTION   FIGURE 41
$(-\beta_y$ of 11.5, 10, 7, 3, 1, .5) at $T_o = 104$

TIME SEC.

CHANGE IN TOTAL VELOCITY VECTOR ORIENTATION IN
THE LATERAL DIRECTION VERSUS TIME FOR MALFUNCTION
$(-\beta_y$ of 11.5, 10, 7, 3, 1, .5) at T_o = 108

FIGURE 42

TIME SEC.

CHANGE IN TOTAL VELOCITY VECTOR ORIENTATION IN
THE LATERAL DIRECTION VERSUS TIME FOR MALFUNCTION
$(-\beta_y$ of 11.5, 10, 7, 3, 1, .5) at T_o = 112

FIGURE 43

TIME SEC.

CHANGE IN TOTAL VELOCITY VECTOR ORIENTATION IN
THE LATERAL DIRECTION VERSUS TIME FOR MALFUNCTION
$(-\beta_y$ of 11.5, 10, 7, 3, 1, .5) at $T_o = 116$

FIGURE 44

CHANGE IN TOTAL VELOCITY VECTOR ORIENTATION IN
THE LATERAL DIRECTION VERSUS TIME FOR MALFUNCTION
$(-\beta_y$ of 11.5, 10, 7, 3, 1, .5) at T_o = 120   FIGURE 45

TIME SEC.

CHANGE IN TOTAL VELOCITY VECTOR ORIENTATION IN
THE LATERAL DIRECTION VERSUS TIME FOR MALFUNCTION   FIGURE 46
$(-\beta_y$ of 11.5, 10, 7, 3, 1, .5) at T_o = 124

TIME SEC.

CHANGE IN TOTAL VELOCITY VECTOR ORIENTATION IN
THE LATERAL DIRECTION VERSUS TIME FOR MALFUNCTION
$(-\beta_y$ of 11.5, 10, 7, 3, 1, .5) at $T_0 = 128$

FIGURE 47
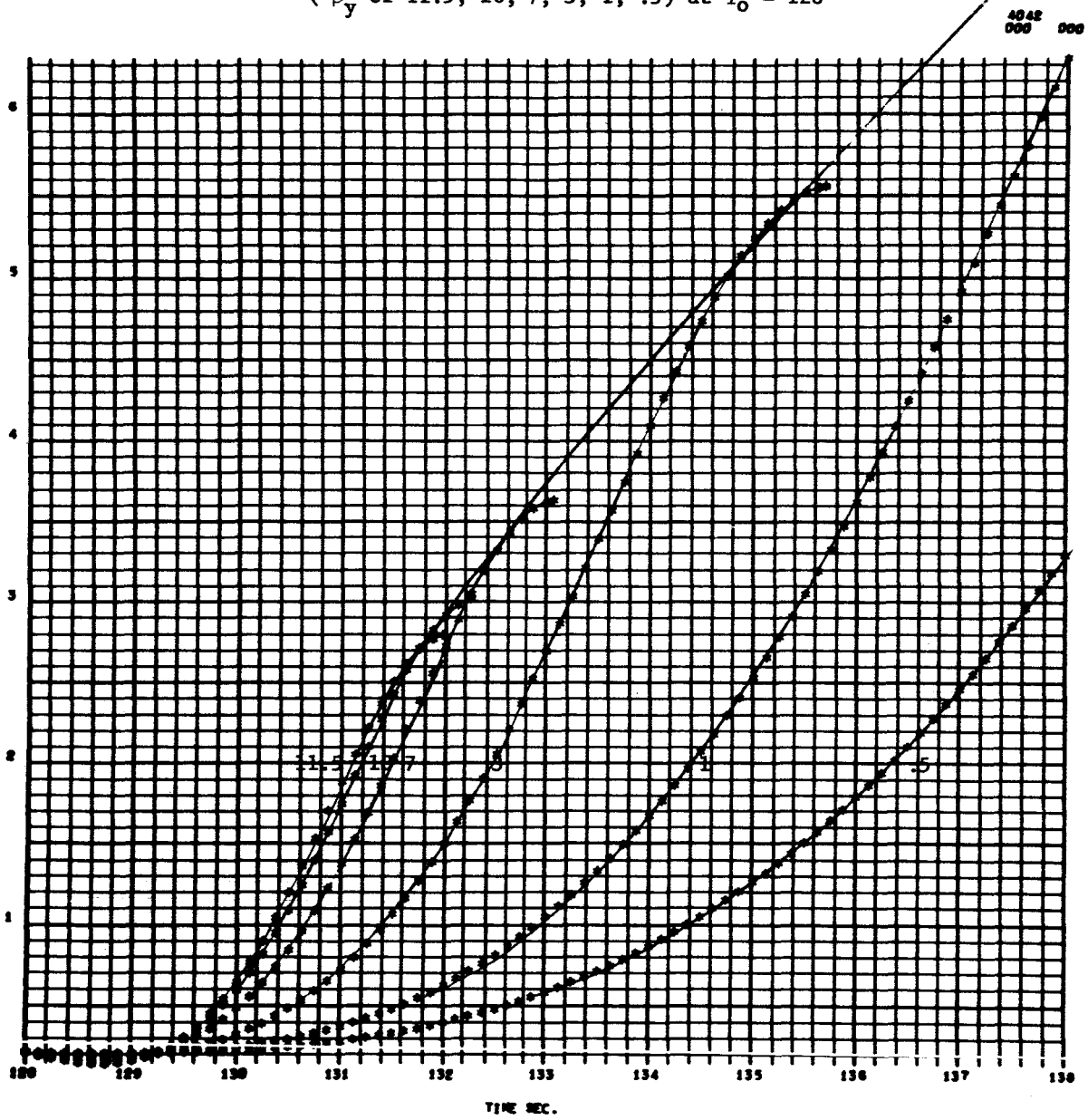
TIME SEC.

CHANGE IN TOTAL VELOCITY VECTOR ORIENTATION IN
THE LATERAL DIRECTION VERSUS TIME FOR MALFUNCTION   FIGURE 48
$(-\beta_y$ of 11.5, 10, 7, 3, 1, .5) at $T_o = 132$

TIME SEC.

CHANGE IN TOTAL VELOCITY VECTOR ORIENTATION IN
THE LATERAL DIRECTION VERSUS TIME FOR MALFUNCTION   FIGURE 49
$(-\beta_y$ of 11.5, 10, 7, 3, 1, .5) at T_o = 136

TIME SEC.
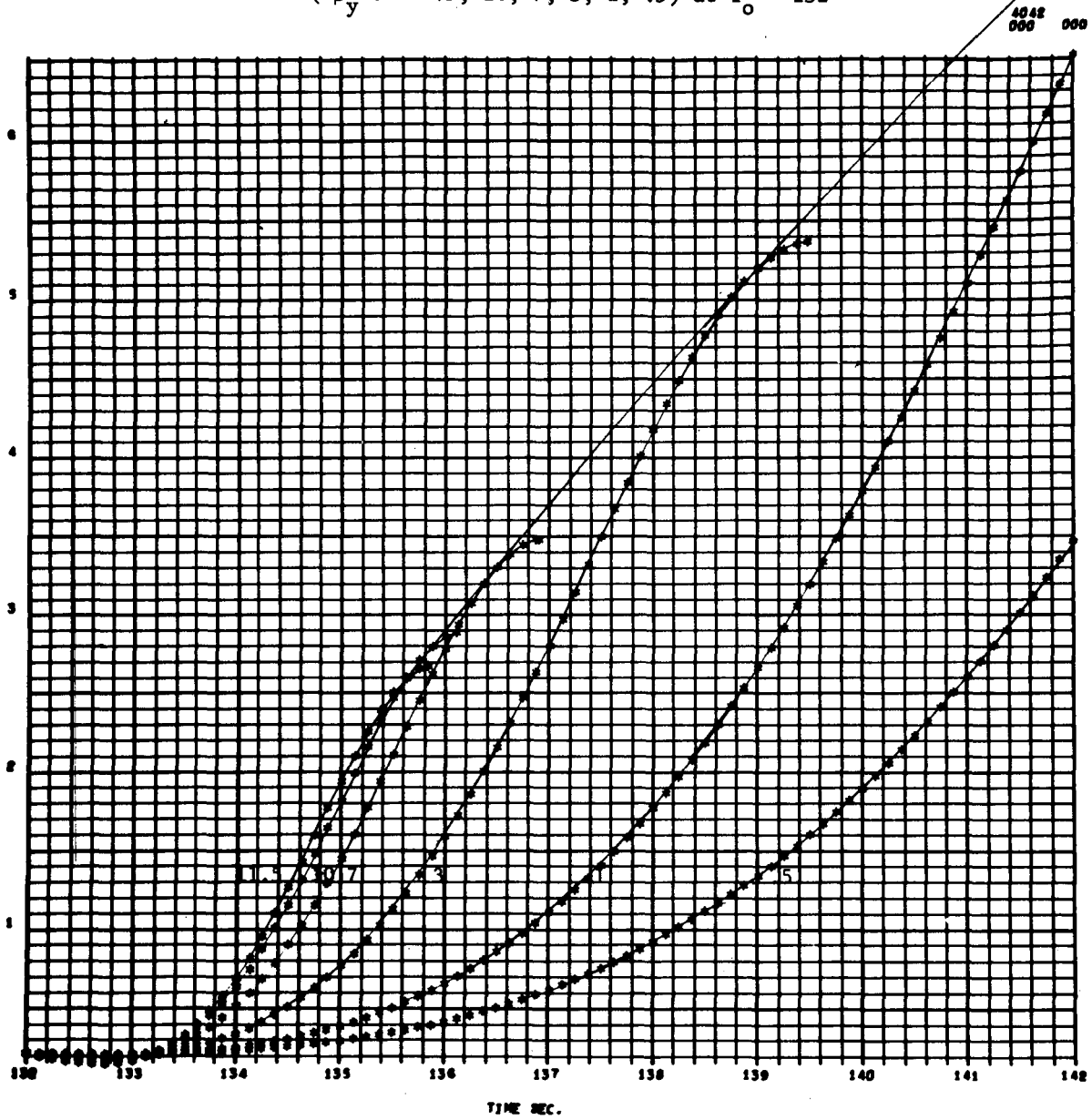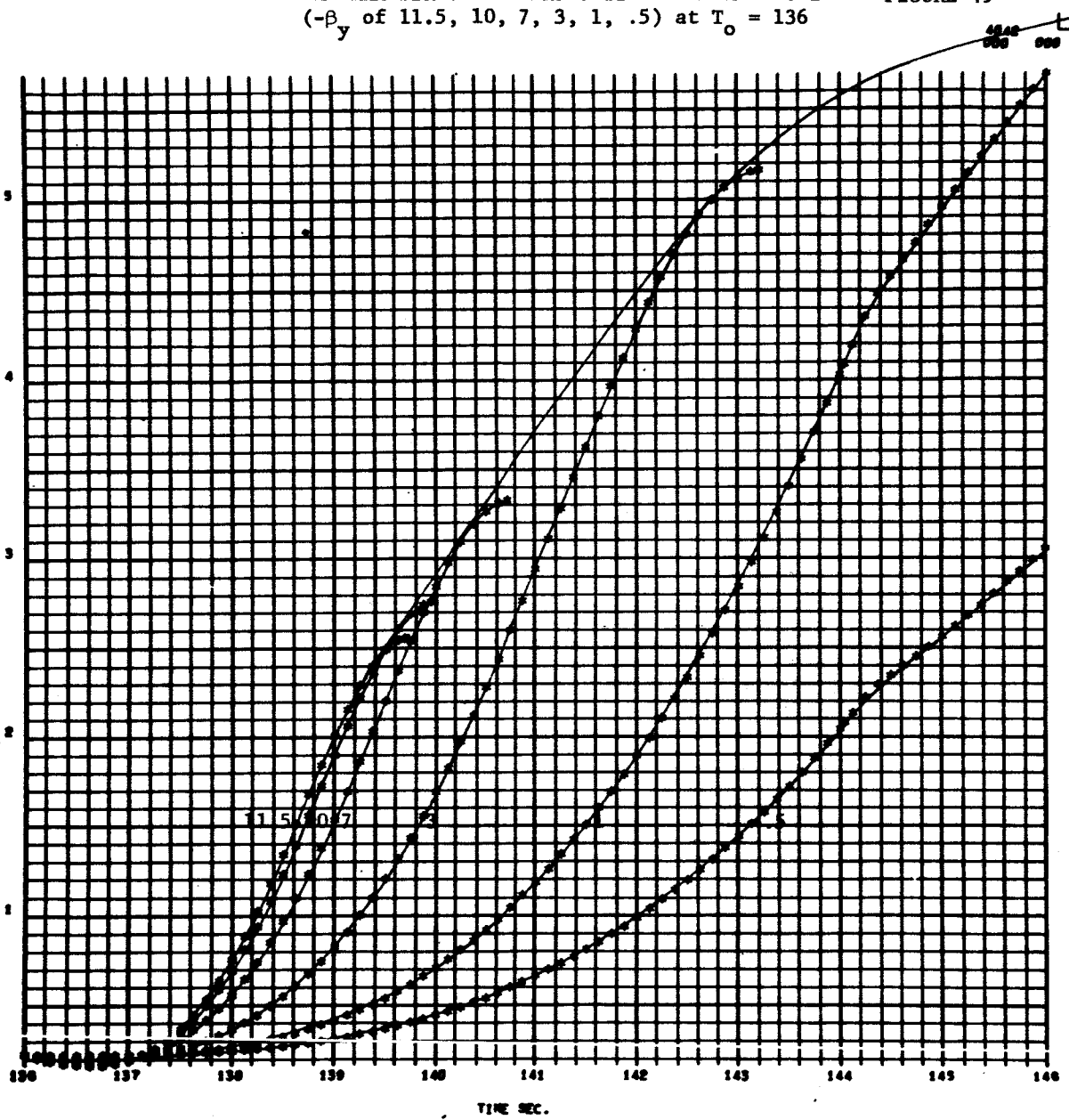
CHANGE IN TOTAL VELOCITY VECTOR ORIENTATION IN
THE LATERAL DIRECTION VERSUS TIME FOR MALFUNCTION   FIGURE 50
$(-\beta_y$ of 6, 4, 2, 1) at $T_o = 180$
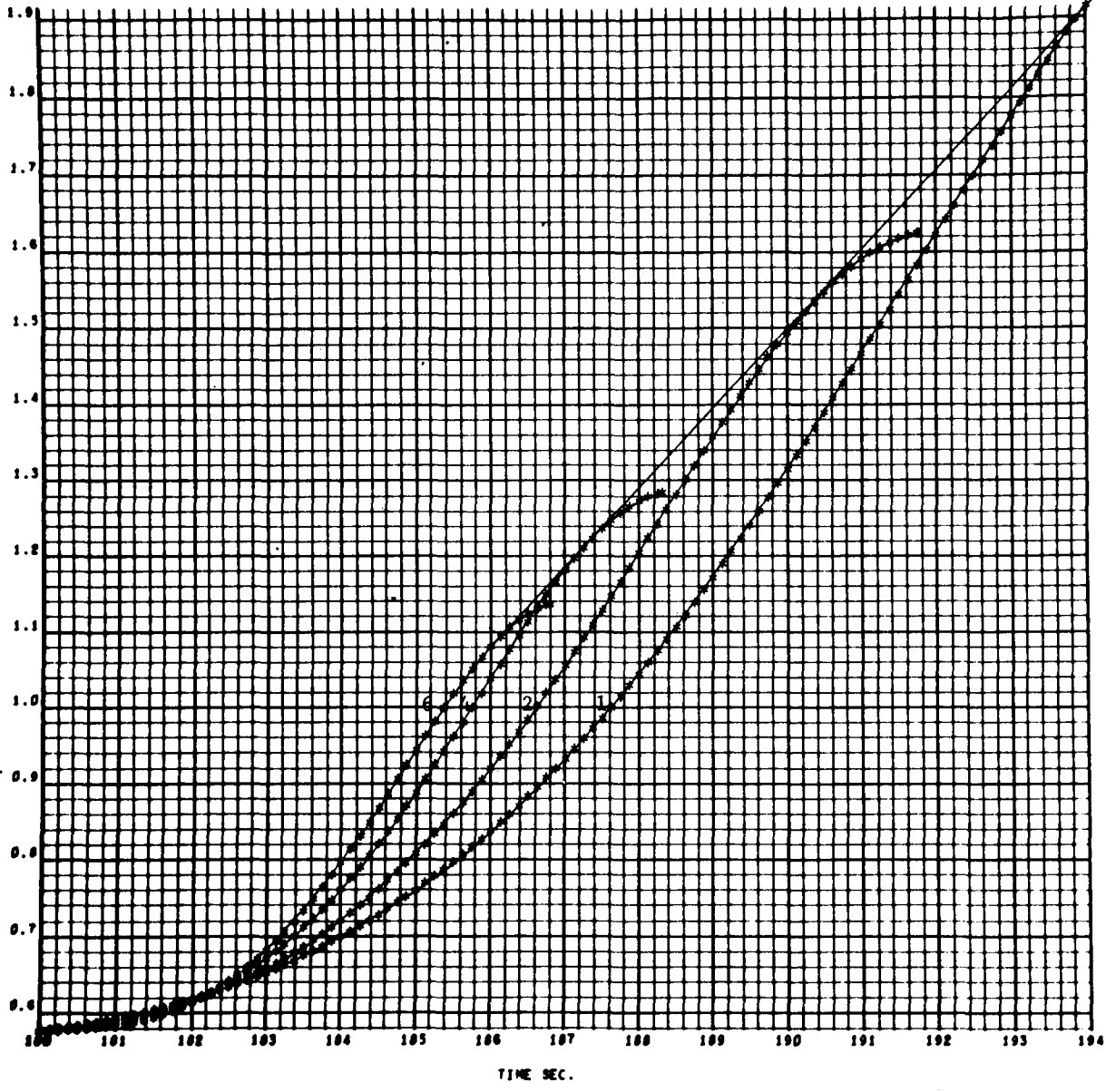
TIME SEC.

CHANGE IN TOTAL VELOCITY VECTOR ORIENTATION IN
THE LATERAL DIRECTION VERSUS TIME FOR MALFUNCTION   FIGURE 51
$(-\beta_y$ of 6, 4, 2, 1) at T_o = 200
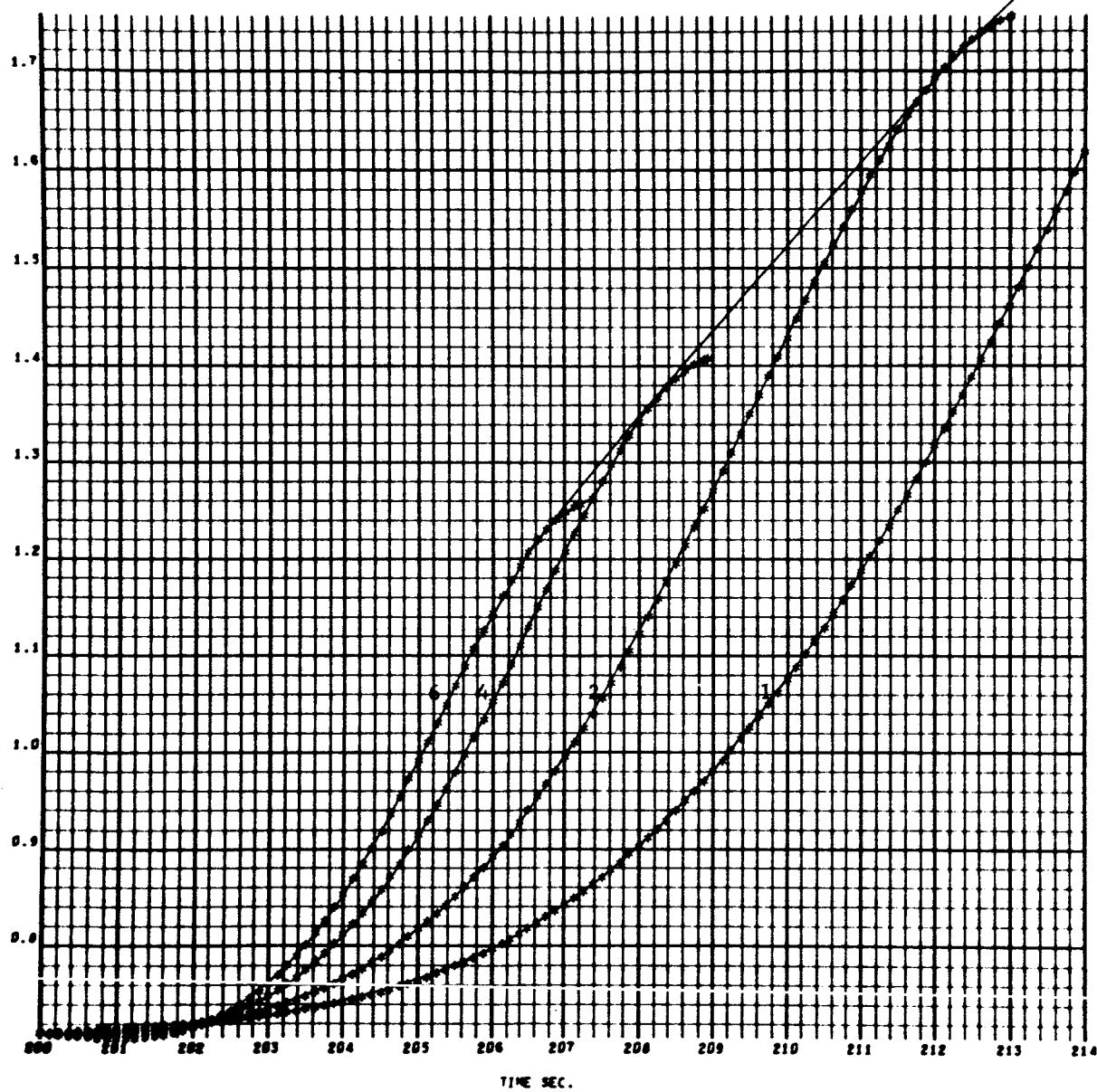
TIME SEC.

102

CHANGE IN TOTAL VELOCITY VECTOR ORIENTATION IN
THE LATERAL DIRECTION VERSUS TIME FOR MALFUNCTION   FIGURE 52
$(-\beta_y$ of 6, 4, 2, 1) at $T_o = 220$

TIME SEC.

104
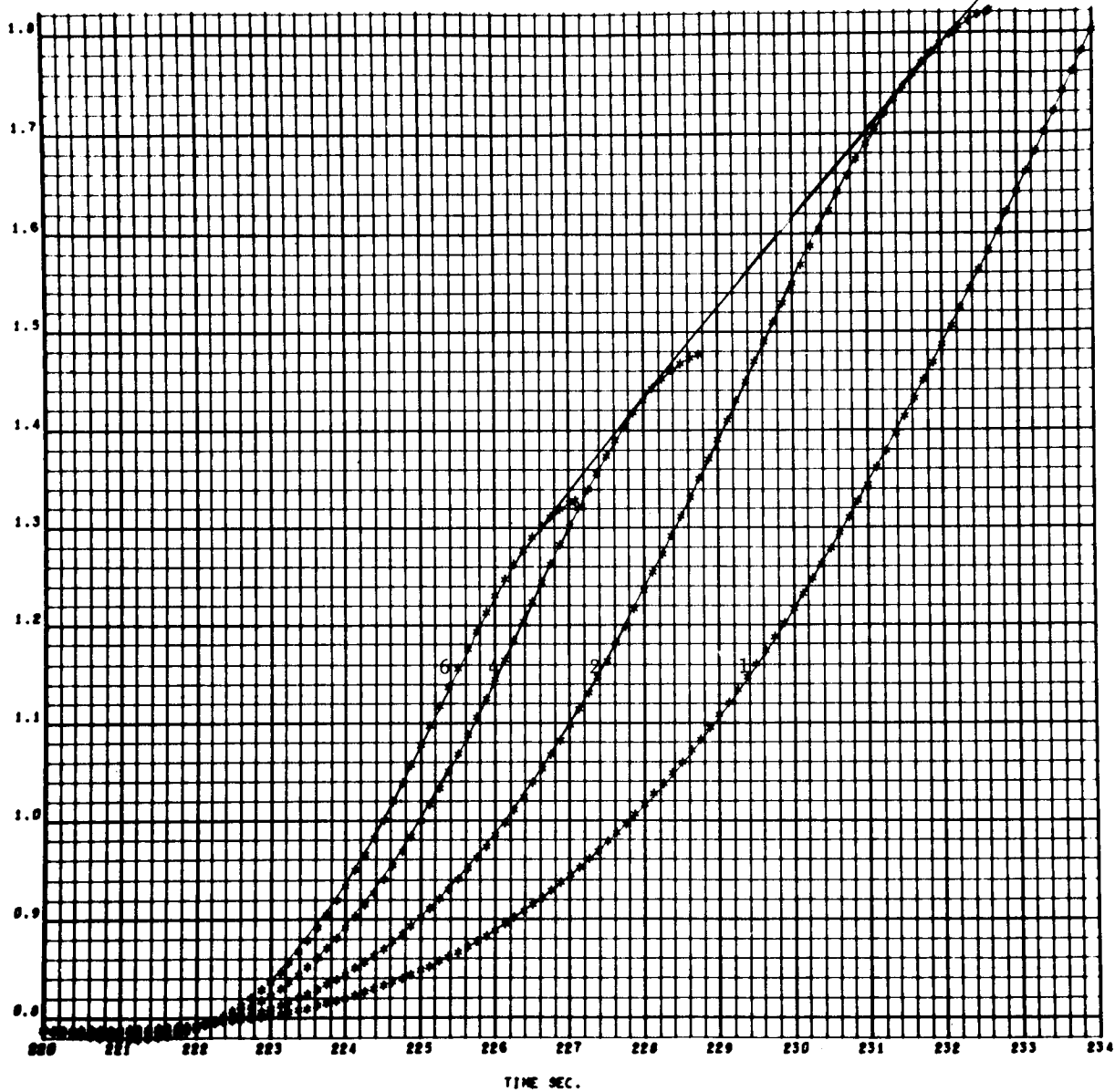
CHANGE IN TOTAL VELOCITY VECTOR ORIENTATION IN
THE LATERAL DIRECTION VERSUS TIME FOR MALFUNCTION   FIGURE 54
$(-\beta_y$ of 6, 4, 2, 1) at T_o = 260
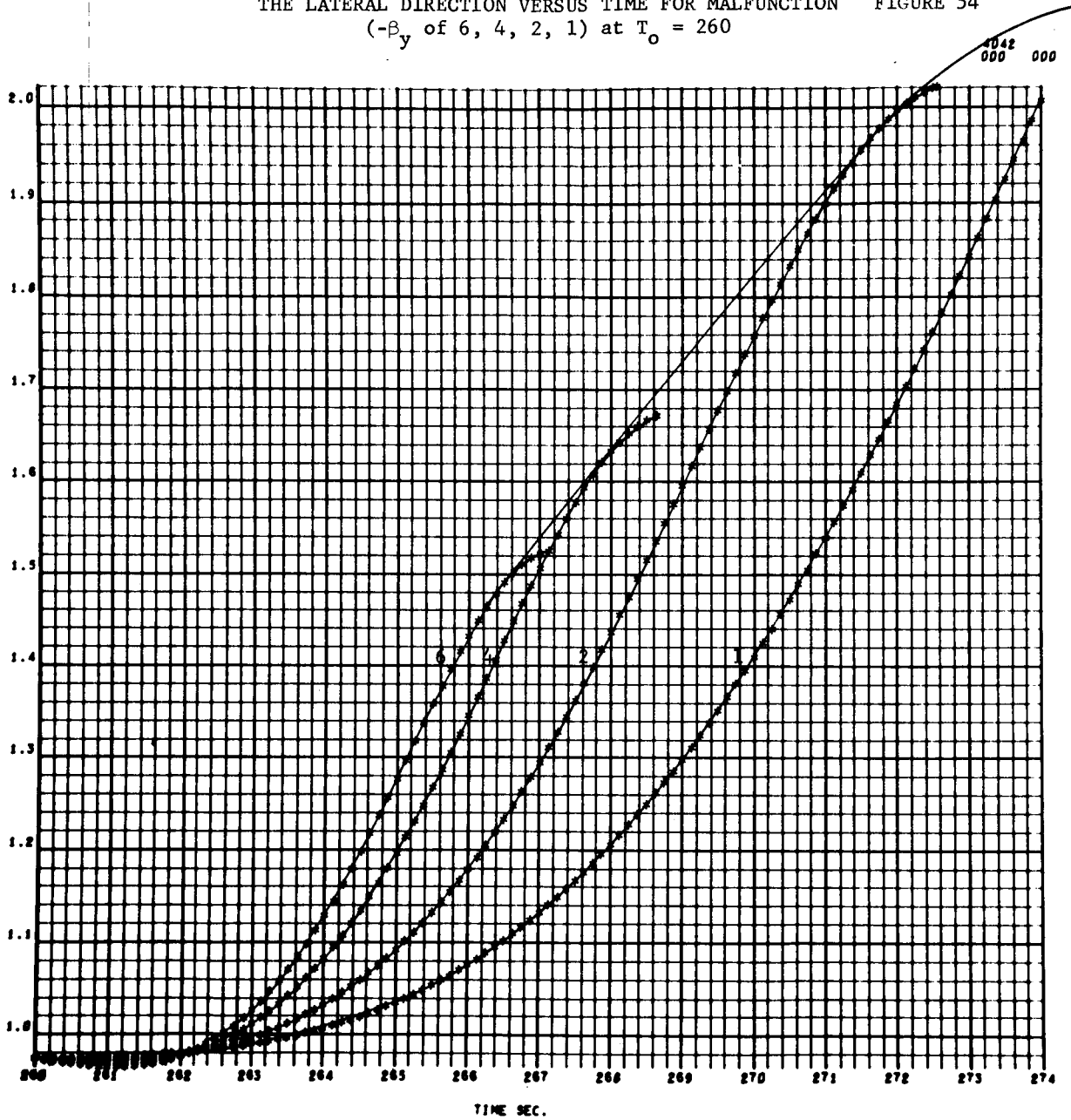
TIME SEC.

CHANGE IN TOTAL VELOCITY VECTOR ORIENTATION IN
THE LATERAL DIRECTION VERSUS TIME FOR MALFUNCTION   FIGURE 55
$(-\beta_y$ of 6, 4, 2, 1) at T_o = 280
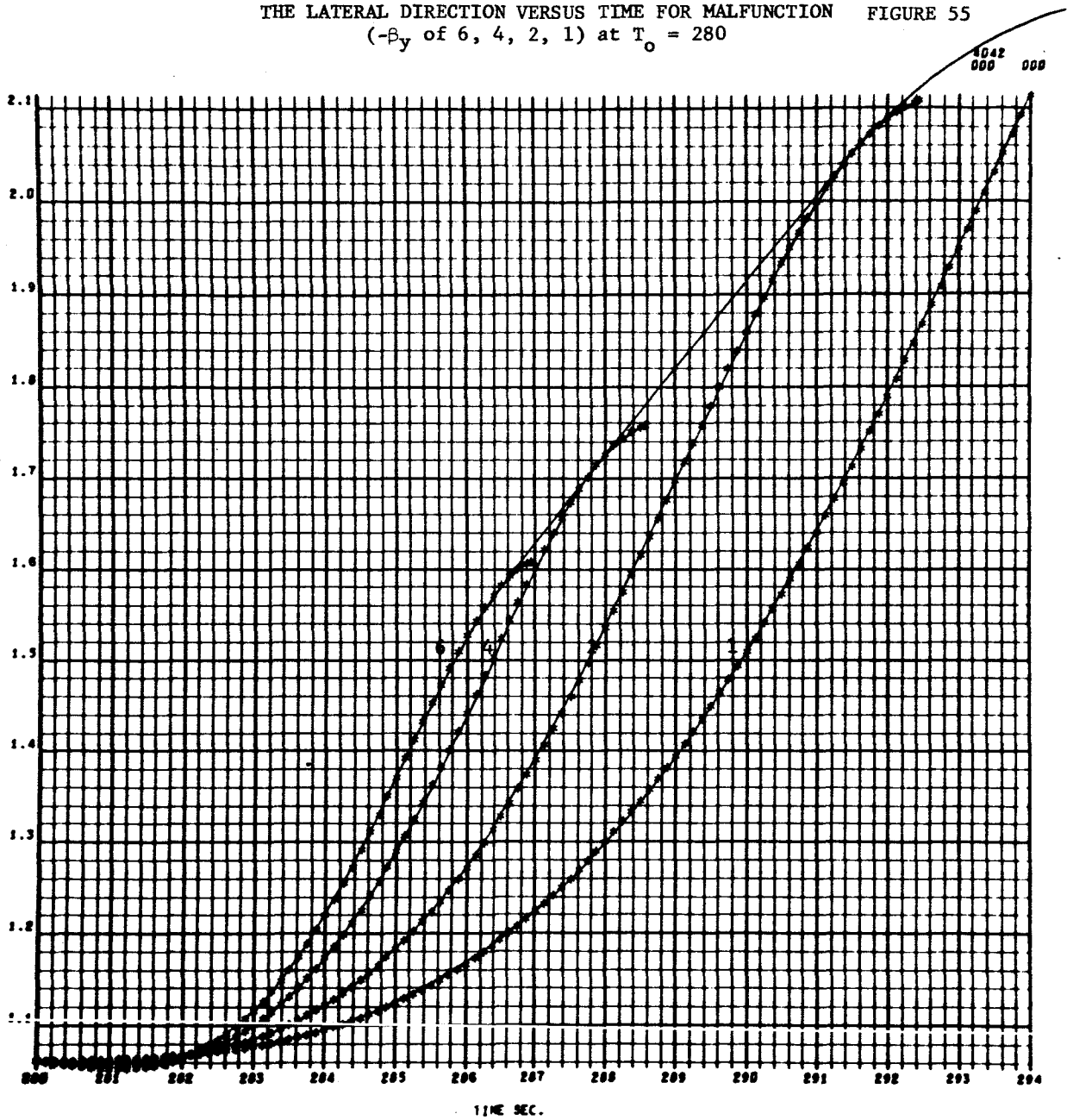
TIME SEC.

CHANGE IN TOTAL VELOCITY VECTOR ORIENTATION IN
THE LATERAL DIRECTION VERSUS TIME FOR MALFUNCTION   FIGURE 56
$(-\beta_y$ of 6, 4, 2, 1) at T_o = 300

TIME SEC.

CHANGE IN TOTAL VELOCITY VECTOR ORIENTATION IN
THE LATERAL DIRECTION VERSUS TIME FOR MALFUNCTION   FIGURE 57
$(-\beta_y$ of 6, 4, 2, 1) at $T_o = 320$

TIME SEC.

CHANGE IN TOTAL VELOCITY VECTOR ORIENTATION IN
THE LATERAL DIRECTION VERSUS TIME FOR MALFUNCTION   FIGURE 58
$(-\beta_y$ of 6, 4, 2, 1) at T_o = 340

TIME SEC.

CHANGE IN TOTAL VELOCITY VECTOR ORIENTATION IN
THE LATERAL DIRECTION VERSUS TIME FOR MALFUNCTION
$(-\beta_y$ of 6, 4, 2, 1) at $T_o = 360$

FIGURE 59

TIME SEC.

CHANGE IN TOTAL VELOCITY VECTOR ORIENTATION IN
THE LATERAL DIRECTION VERSUS TIME FOR MALFUNCTION   FIGURE 60
$(-\beta_y$ of 6, 4, 2, 1) at T_o = 380

TIME SEC.

CHANGE IN TOTAL VELOCITY VECTOR ORIENTATION IN
THE LATERAL DIRECTION VERSUS TIME FOR MALFUNCTION   FIGURE 61
$(-\beta_y$ of 6, 4, 2, 1) at T_o = 400

CHANGE IN TOTAL VELOCITY VECTOR ORIENTATION IN
THE LATERAL DIRECTION VERSUS TIME FOR MALFUNCTION   FIGURE 62
$(-\beta_y$ of 6, 4, 2, 1) at $T_o = 420$

TIME SEC.

CHANGE IN TOTAL VELOCITY VECTOR ORIENTATION IN
THE LATERAL DIRECTION VERSUS TIME FOR MALFUNCTION   FIGURE 63
$(-\beta_y$ of 6, 4, 2, 1) at T_o = 440

TIME SEC.

CHANGE IN TOTAL VELOCITY VECTOR ORIENTATION IN
THE LATERAL DIRECTION VERSUS TIME FOR MALFUNCTION
$(-\beta_y$ of 6, 4, 2, 1) at $T_o = 460$

FIGURE 64

TIME SEC.

CHANGE IN TOTAL VELOCITY VECTOR ORIENTATION IN
THE LATERAL DIRECTION VERSUS TIME FOR MALFUNCTION FIGURE 65
$(-\beta_y$ of 6, 4, 2, 1) at $T_o = 480$

TIME SEC.

CHANGE IN TOTAL VELOCITY VECTOR ORIENTATION IN
THE LATERAL DIRECTION VERSUS TIME FOR MALFUNCTION   FIGURE 66
$(-\beta_y$ of 6, 4, 2, 1) at $T_o = 500$

TIME SEC.

CHANGE IN TOTAL VELOCITY VECTOR ORIENTATION IN
THE LATERAL DIRECTION VERSUS TIME FOR MALFUNCTION   FIGURE 67
$(-\beta_y$ of 6, 4, 2, 1) at $T_o = 520$

TIME SEC.

118

CHANGE IN TOTAL VELOCITY VECTOR ORIENTATION IN
THE LATERAL DIRECTION VERSUS TIME FOR MALFUNCTION   FIGURE 68
$(-\beta_y$ of 6, 4, 2, 1) at $T_o = 540$

TIME SEC.

CHANGE IN TOTAL VELOCITY VECTOR ORIENTATION IN
THE LATERAL DIRECTION VERSUS TIME FOR MALFUNCTION
$(-\beta_y$ of 6, 4, 2, 1) at $T_o = 560$

FIGURE 69

TIME SEC.

CHANGE IN TOTAL VELOCITY VECTOR ORIENTATION IN
THE LATERAL DIRECTION VERSUS TIME FOR MALFUNCTION   FIGURE 70
$(-\beta_y$ of 6, 4, 2, 1) at T_o = 580

TIME SEC.

CHANGE IN TOTAL VELOCITY VECTOR ORIENTATION IN
THE LATERAL DIRECTION VERSUS TIME FOR MALFUNCTION   FIGURE 71
$(-\beta_y$ of 6, 4, 2, 1) at $T_o = 600$

TIME SEC.

122

CHANGE IN TOTAL VELOCITY VECTOR ORIENTATION IN
THE LATERAL DIRECTION VERSUS TIME FOR MALFUNCTION   FIGURE 72
$(-\beta_y$ of 6, 4, 2, 1) at $T_o = 620$

TIME SEC.

EARTH-FIXED VELOCITY AS A FUNCTION OF TIME FOR MALFUNCTION
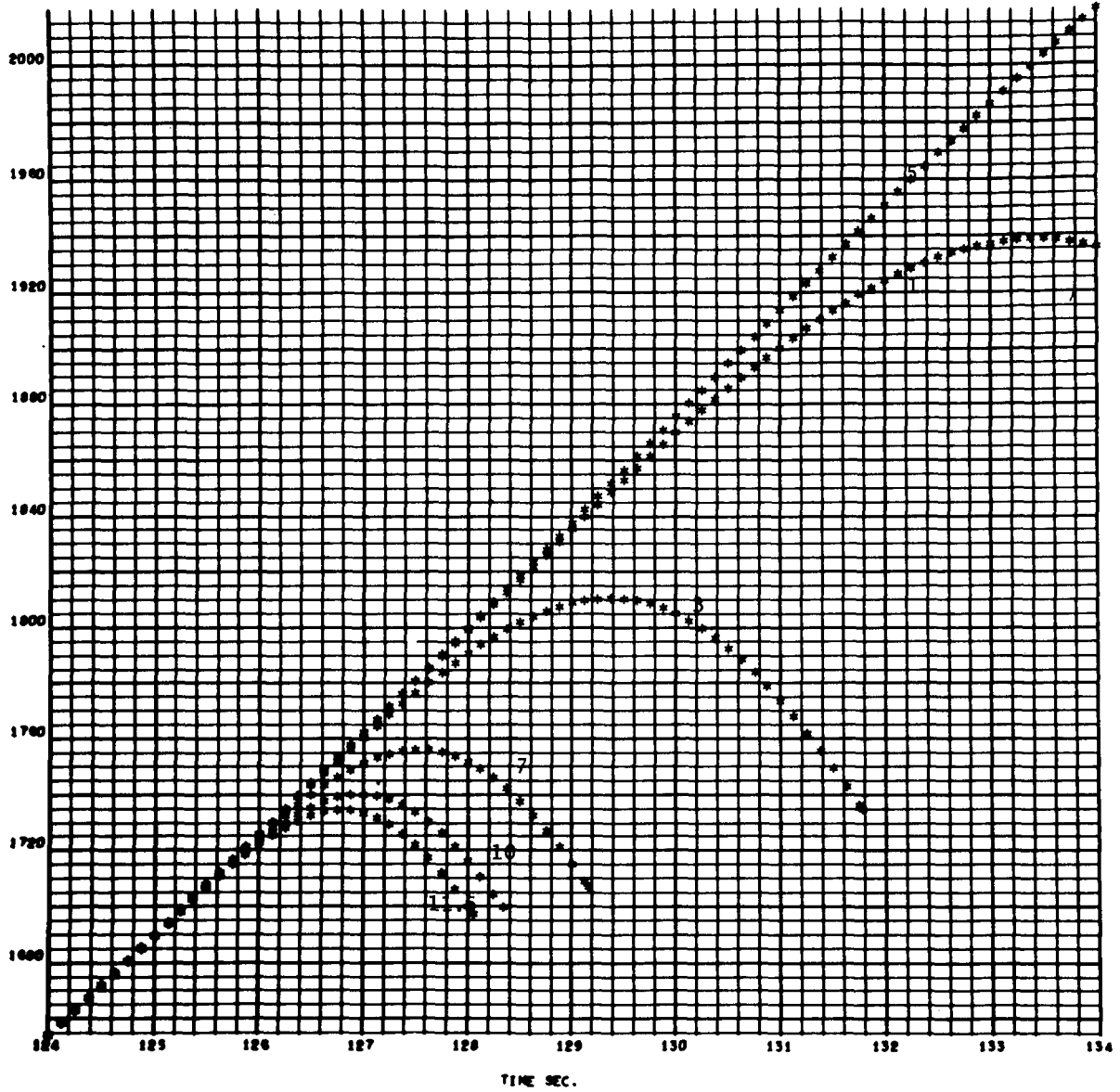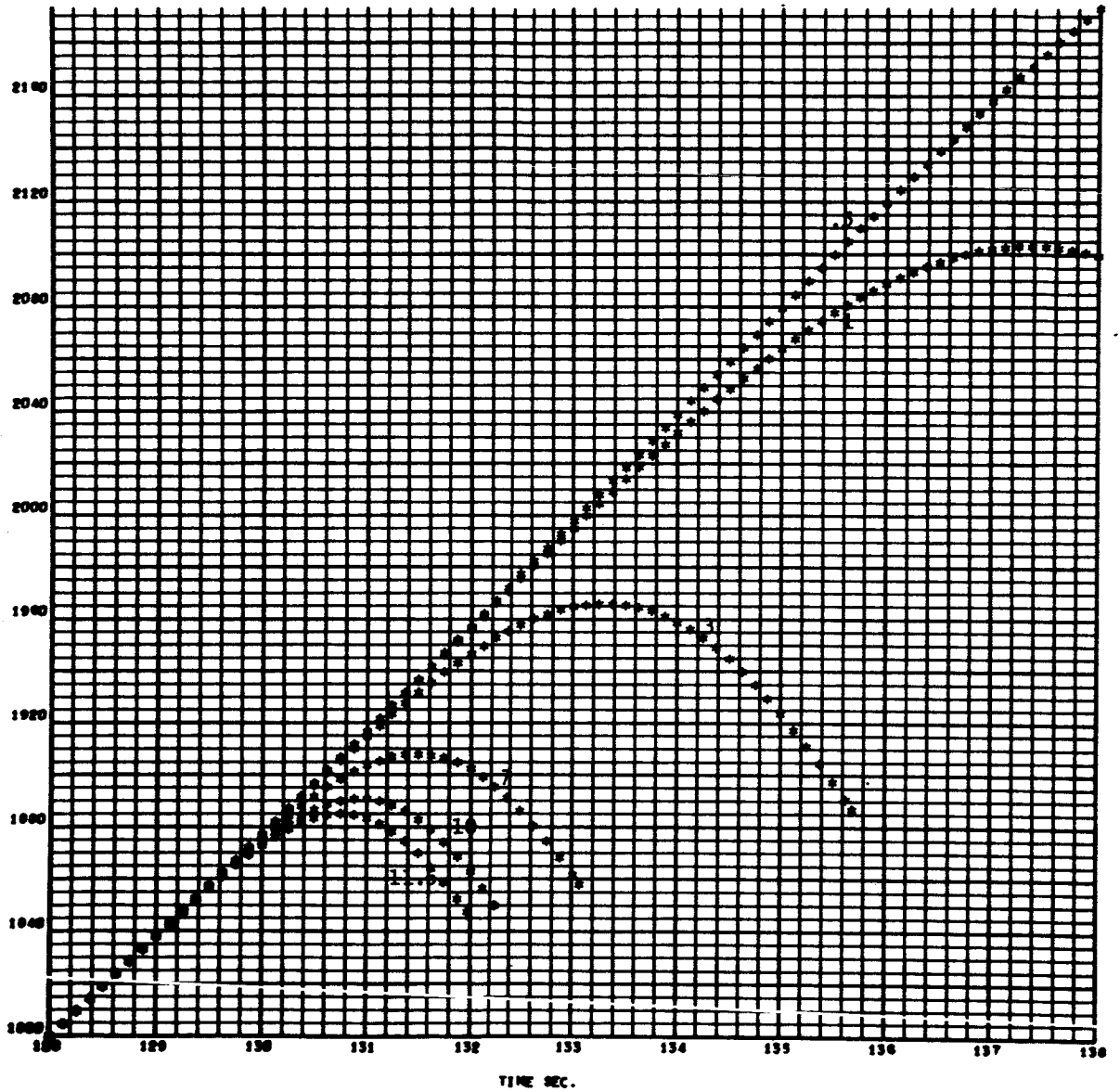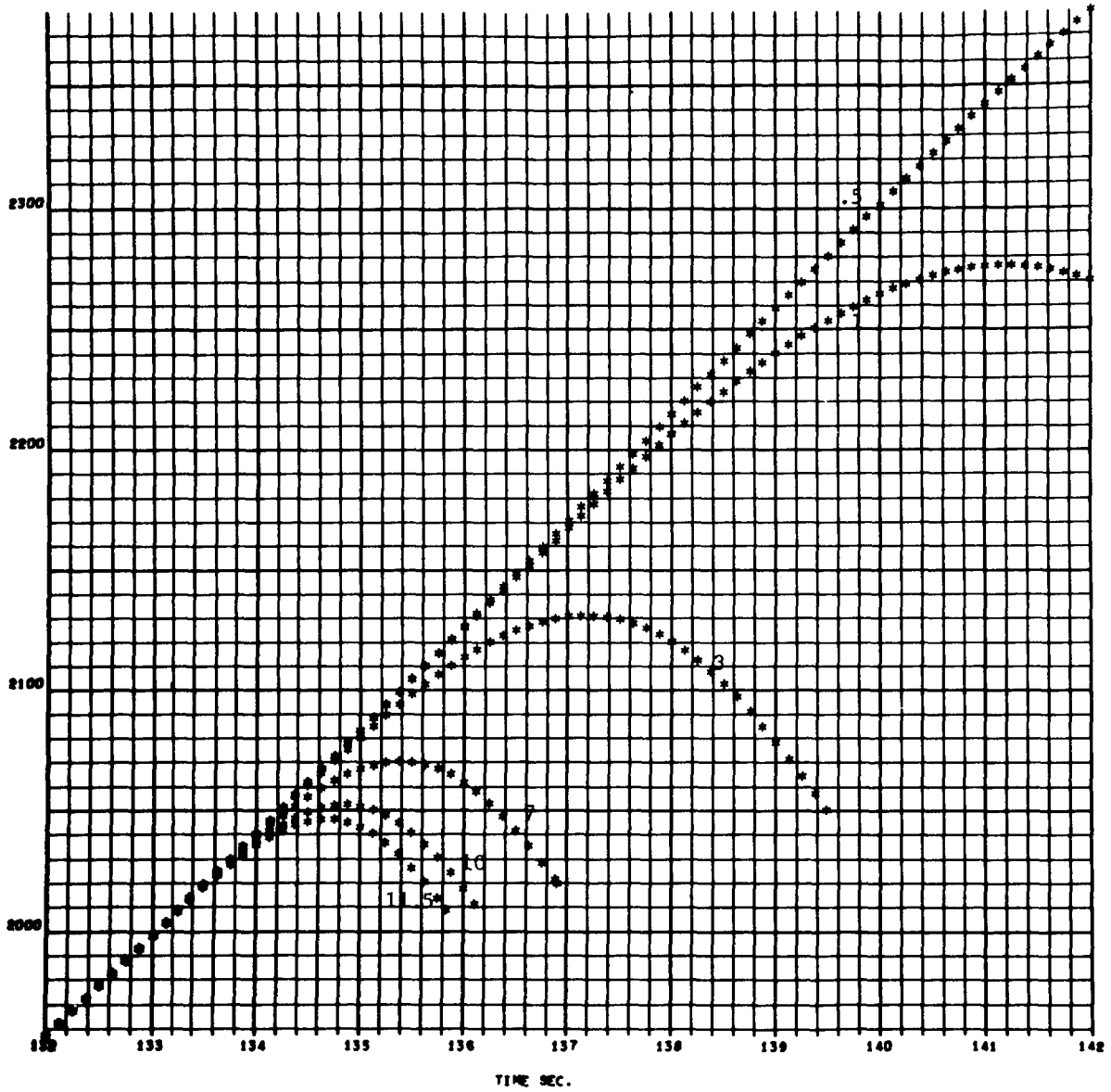$(-\beta_y$ of 11.5, 10, 7, 3, 1, .5) at $T_o = 20$ FIGURE 74

TIME SEC.

EARTH-FIXED VELOCITY AS A FUNCTION OF TIME FOR MALFUNCTION
$(-\beta_y$ of 11.5, 10, 7, 3, 1, .5) at $T_o = 24$ FIGURE 75

TIME SEC.

EARTH-FIXED VELOCITY AS A FUNCTION OF TIME FOR MALFUNCTION
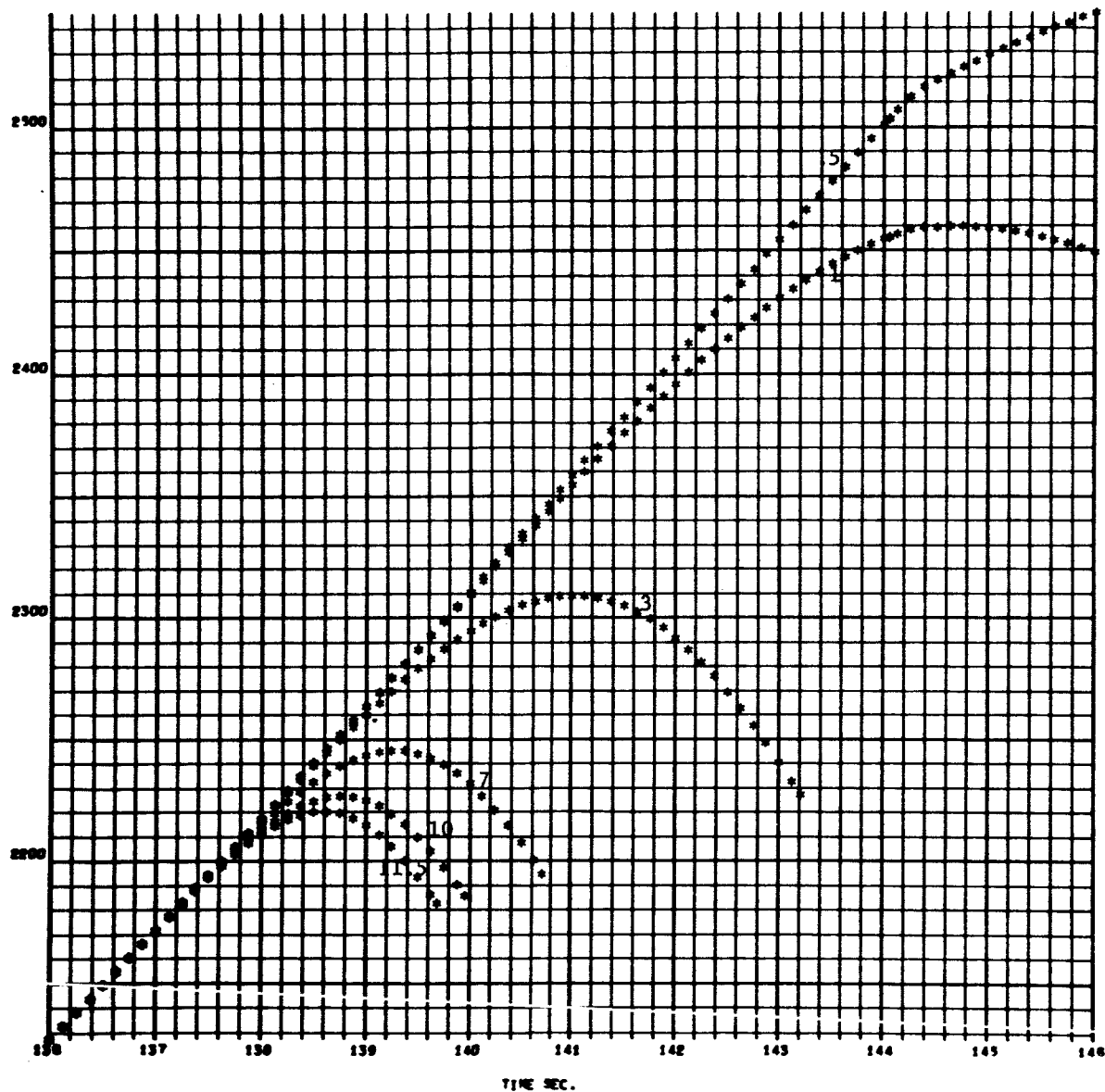($-\beta_y$ of 11.5, 10, 7, 3, 1, .5) at $T_o = 28$

FIGURE 76

TIME SEC.

EARTH-FIXED VELOCITY AS A FUNCTION OF TIME FOR MALFUNCTION
$(-\beta_y$ of 11.5, 10, 7, 3, 1, .5) at T_o = 32   FIGURE 77

TIME SEC.

EARTH-FIXED VELOCITY AS A FUNCTION OF TIME FOR MALFUNCTION
$(-\beta_y$ of 11.5, 10, 7, 3, 1, .5) at $T_o = 36$ FIGURE 78
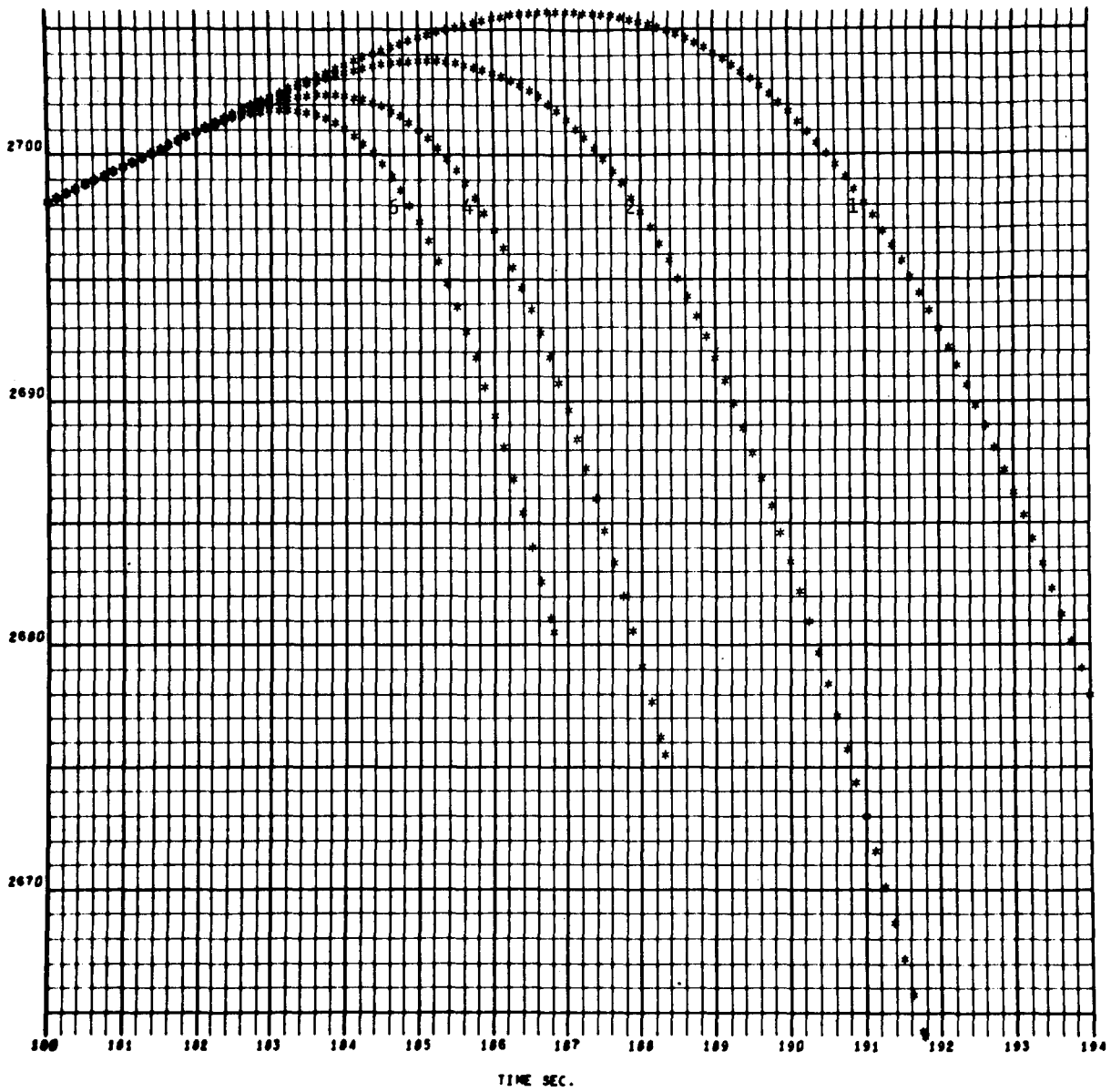

TIME SEC.

TIME SEC.

EARTH-FIXED VELOCITY AS A FUNCTION OF TIME FOR MALFUNCTION
$(-\beta_y$ of 11.5, 10, 7, 3, 1, .5) at $T_o = 44$ FIGURE 80

TIME SEC.

EARTH-FIXED VELOCITY AS A FUNCTION OF TIME FOR MALFUNCTION
$(-\beta_y$ of 11.5, 10, 7, 3, 1, .5) at $T_o = 52$

FIGURE 82

TIME SEC.

EARTH-FIXED VELOCITY AS A FUNCTION OF TIME FOR MALFUNCTION
$(-\beta_y$ of 11.5, 10, 7, 3, 1, .5) at $T_o = 56$ FIGURE 83

TIME SEC.

EARTH-FIXED VELOCITY AS A FUNCTION OF TIME FOR MALFUNCTION
$(-\beta_y$ of 11.5, 10, 7, 3, 1, .5) at $T_o = 60$ FIGURE 84

TIME SEC.

EARTH-FIXED VELOCITY AS A FUNCTION OF TIME FOR MALFUNCTION
$(-\beta_y$ of 11.5, 10, 7, 3, 1, .5) at $T_o = 64$ FIGURE 85

TIME SEC.

EARTH-FIXED VELOCITY AS A FUNCTION OF TIME FOR MALFUNCTION
$(-\beta_y$ of 11.5, 10, 7, 3, 1, .5) at $T_o = 68$ FIGURE 86

TIME SEC.

TIME SEC.

EARTH-FIXED VELOCITY AS A FUNCTION OF TIME FOR MALFUNCTION
$(-\beta_y$ of 11.5, 10, 7, 3, 1, .5) at $T_o = 76$ FIGURE 88

TIME SEC.
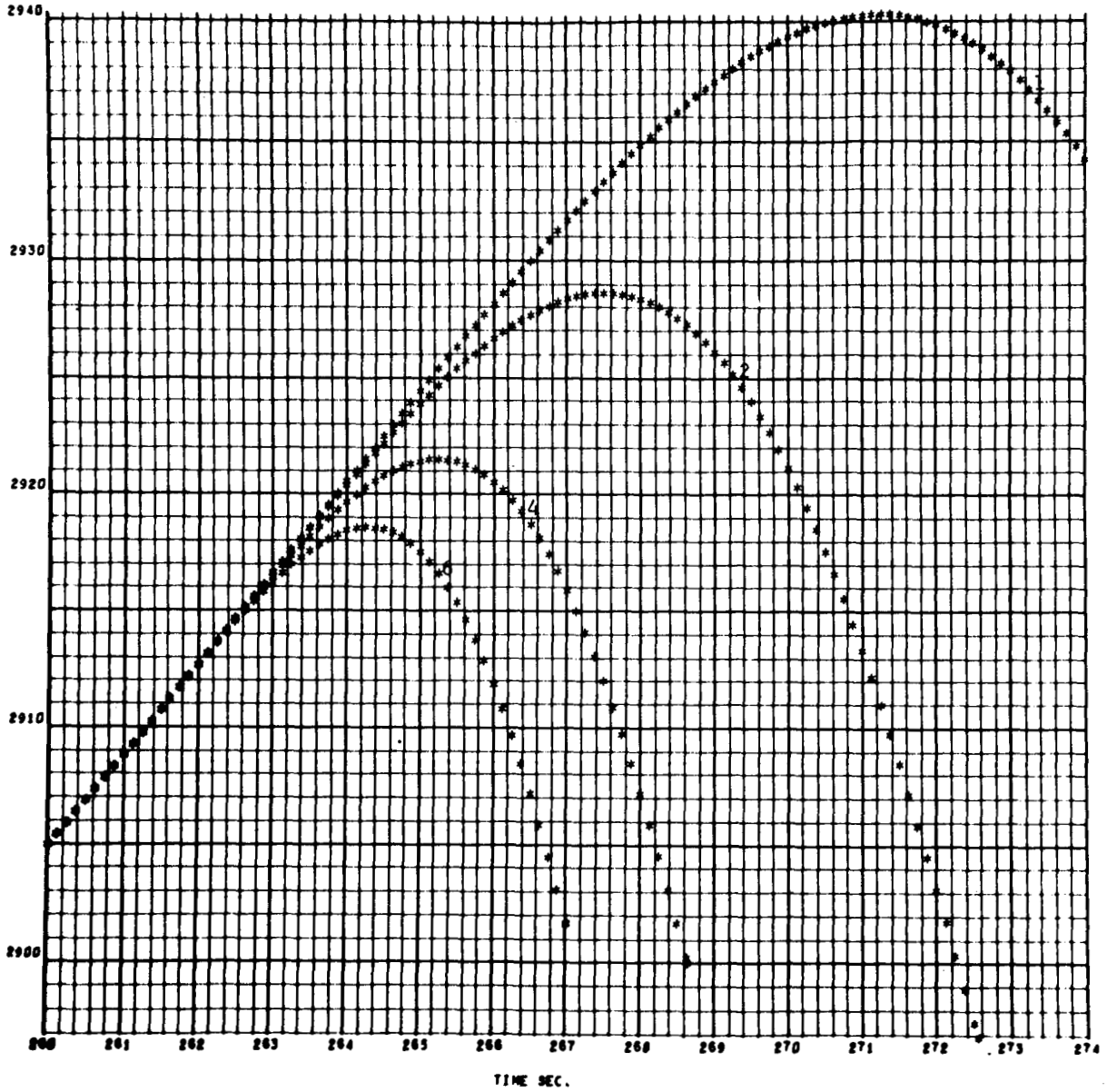
EARTH-FIXED VELOCITY AS A FUNCTION OF TIME FOR MALFUNCTION
$(-\beta_y$ of 11.5, 10, 7, 3, 1, .5) at $T_o = 80$ FIGURE 89

139

EARTH-FIXED VELOCITY AS A FUNCTION OF TIME FOR MALFUNCTION
$(-\beta_y$ of 11.5, 10, 7, 3, 1, .5) at T_o = 84   FIGURE 90

TIME SEC.

EARTH-FIXED VELOCITY AS A FUNCTION OF TIME FOR MALFUNCTION
$(-\beta_y$ of 11.5, 10, 7, 3, 1, .5) at $T_o = 88$ FIGURE 91

TIME SEC.

EARTH-FIXED VELOCITY AS A FUNCTION OF TIME FOR MALFUNCTION
$(-\beta_y$ of 11.5, 10, 7, 3, 1, .5) at T_o = 92   FIGURE 92

TIME SEC.

EARTH-FIXED VELOCITY AS A FUNCTION OF TIME FOR MALFUNCTION
$(-\beta_y$ of 11.5, 10, 7, 3, 1, .5) at T_o = 96   FIGURE 93

143

EARTH-FIXED VELOCITY AS A FUNCTION OF TIME FOR MALFUNCTION
$(-\beta_y$ of 11.5, 10, 7, 3, 1, .5) at $T_o = 100$ FIGURE 94

TIME SEC.

EARTH-FIXED VELOCITY AS A FUNCTION OF TIME FOR MALFUNCTION

$(-\beta_y$ of 11.5, 10, 7, 3, 1, .5) at $T_o = 104$ 　　　FIGURE 95

TIME SEC.

EARTH-FIXED VELOCITY AS A FUNCTION OF TIME FOR MALFUNCTION
$(-\beta_y$ of 11.5, 10, 7, 3, 1, .5) at $T_o = 108$ FIGURE 96

TIME SEC.

EARTH-FIXED VELOCITY AS A FUNCTION OF TIME FOR MALFUNCTION
($-\beta_y$ of 11.5, 10, 7, 3, 1, .5) at T_o = 112   FIGURE 97

TIME SEC.

EARTH-FIXED VELOCITY AS A FUNCTION OF TIME FOR MALFUNCTION
$(-\beta_y$ of 11.5, 10, 7, 3, 1, .5) at T_o = 116   FIGURE 98

148

EARTH-FIXED VELOCITY AS A FUNCTION OF TIME FOR MALFUNCTION
$(-\beta_y$ of 11.5, 10, 7, 3, 1, .5) at $T_o = 120$ FIGURE 99

149

EARTH-FIXED VELOCITY AS A FUNCTION OF TIME FOR MALFUNCTION
$(-\beta_y$ of 11.5, 10, 7, 3, 1, .5) at T_o = 124   FIGURE 100

TIME SEC.

EARTH-FIXED VELOCITY AS A FUNCTION OF TIME FOR MALFUNCTION
$(-\beta_y$ of 11.5, 10, 7, 3, 1, .5) at $T_o = 132$ FIGURE 102

152

TIME SEC.

EARTH-FIXED VELOCITY AS A FUNCTION OF TIME FOR MALFUNCTION
$(-\beta_y$ of 11.5, 10, 7, 3, 1, .5) at T_o = 136   FIGURE 103

TIME SEC.

EARTH-FIXED VELOCITY AS A FUNCTION OF TIME FOR MALFUNCTION
$(-\beta_y$ of 6, 4, 2, 1) at $T_o = 180$ FIGURE 104

TIME SEC.

EARTH-FIXED VELOCITY AS A FUNCTION OF TIME FOR MALFUNCTION
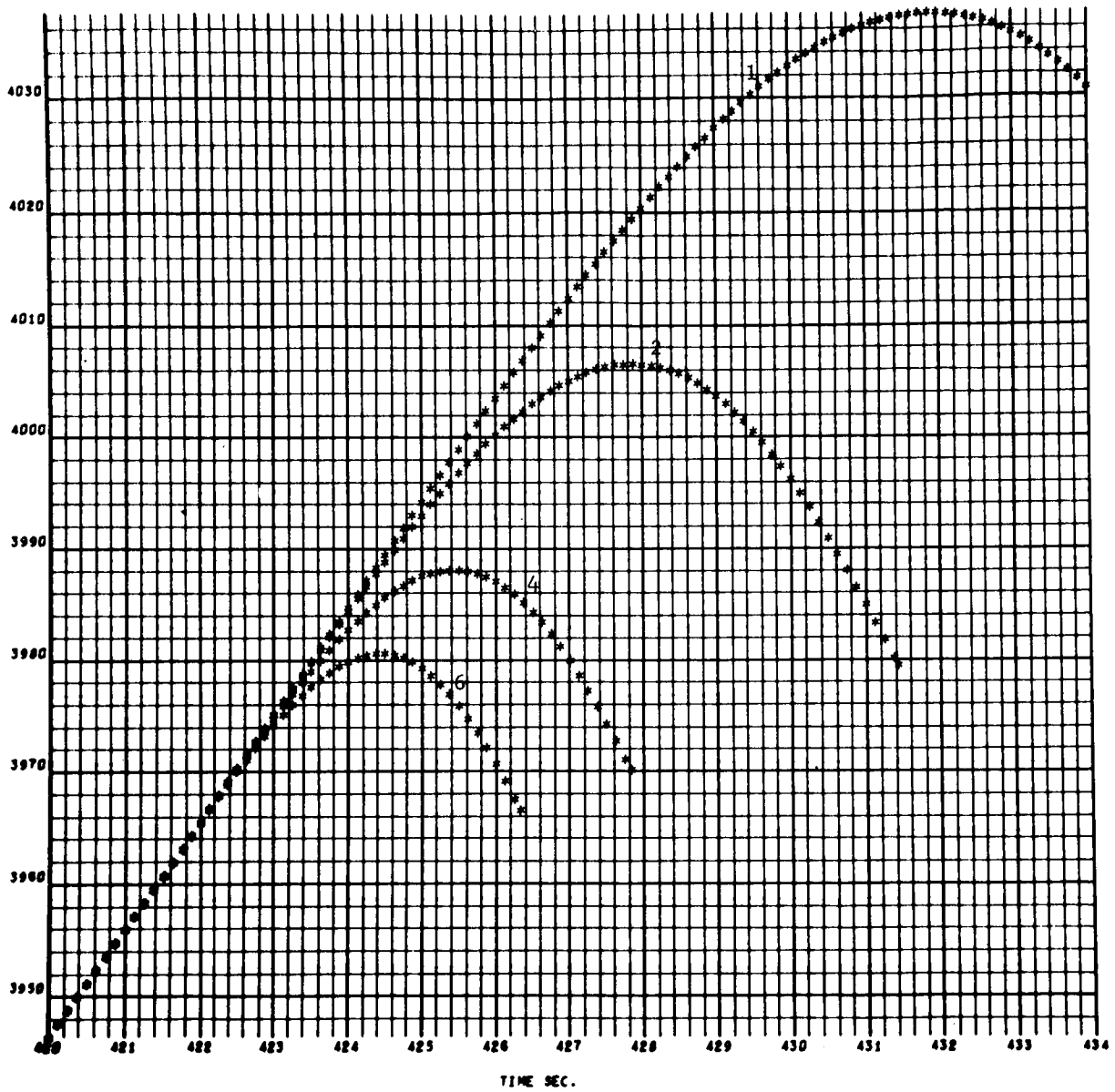$(-\beta_y$ of 6, 4, 2, 1) at T_o = 200

FIGURE 105

EARTH-FIXED VELOCITY AS A FUNCTION OF TIME FOR MALFUNCTION
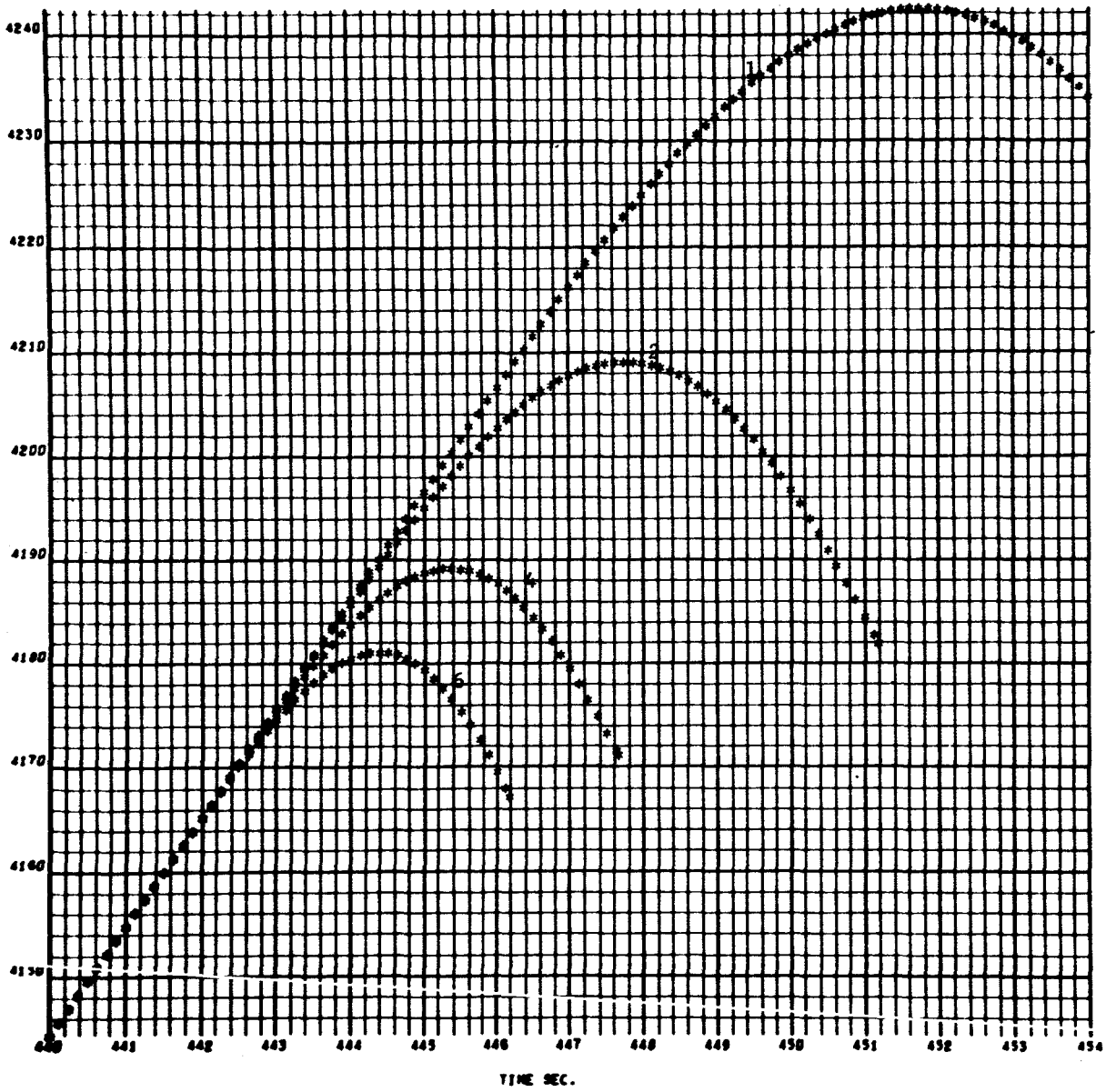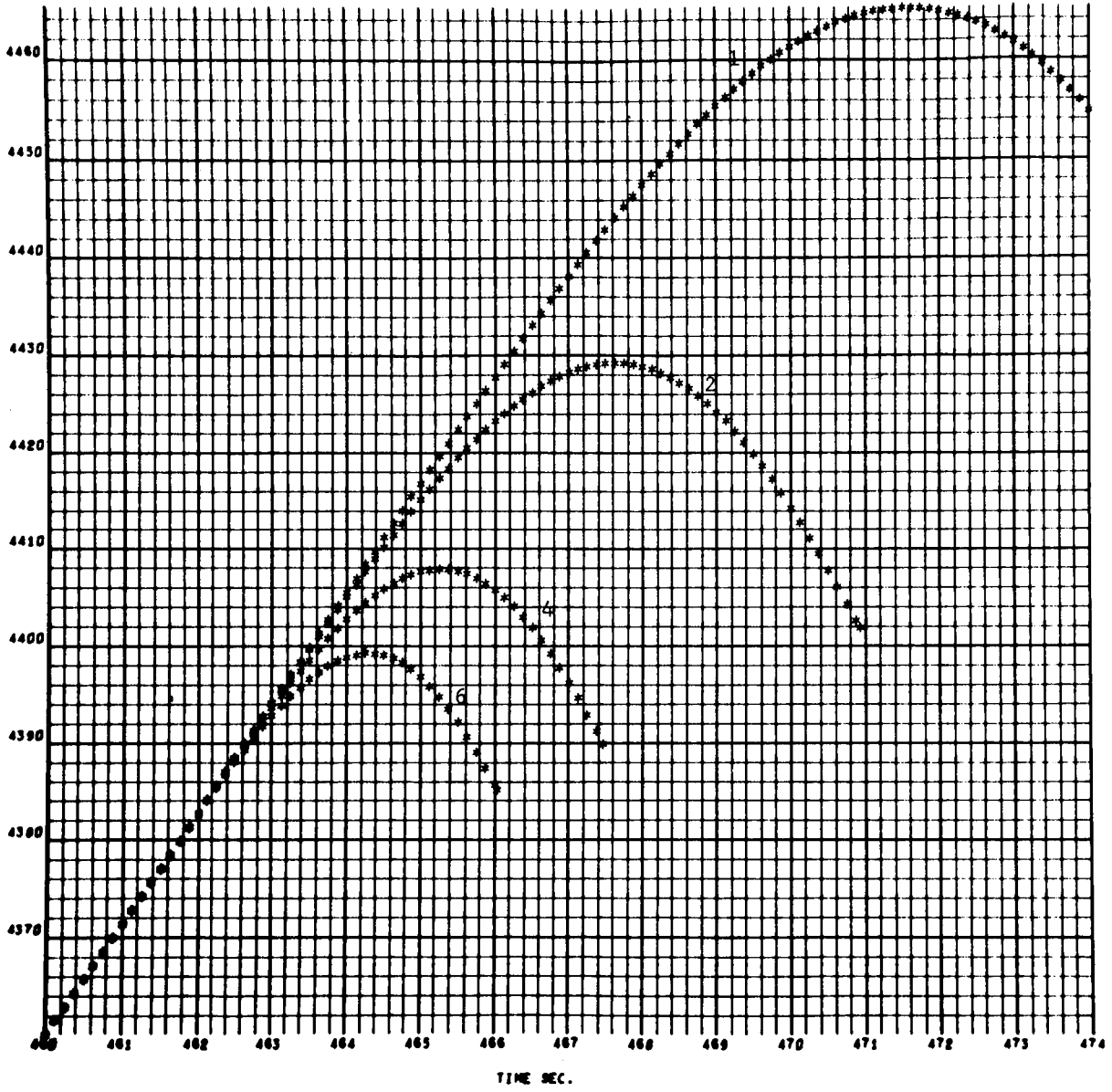$(-\beta_y$ of 6, 4, 2, 1) at $T_o = 220$ FIGURE 106

TIME SEC.

TIME SEC.

EARTH-FIXED VELOCITY AS A FUNCTION OF TIME FOR MALFUNCTION
($-\beta_y$ of 6, 4, 2, 1) at T_o = 280   FIGURE 109

TIME SEC.

EARTH-FIXED VELOCITY AS A FUNCTION OF TIME FOR MALFUNCTION
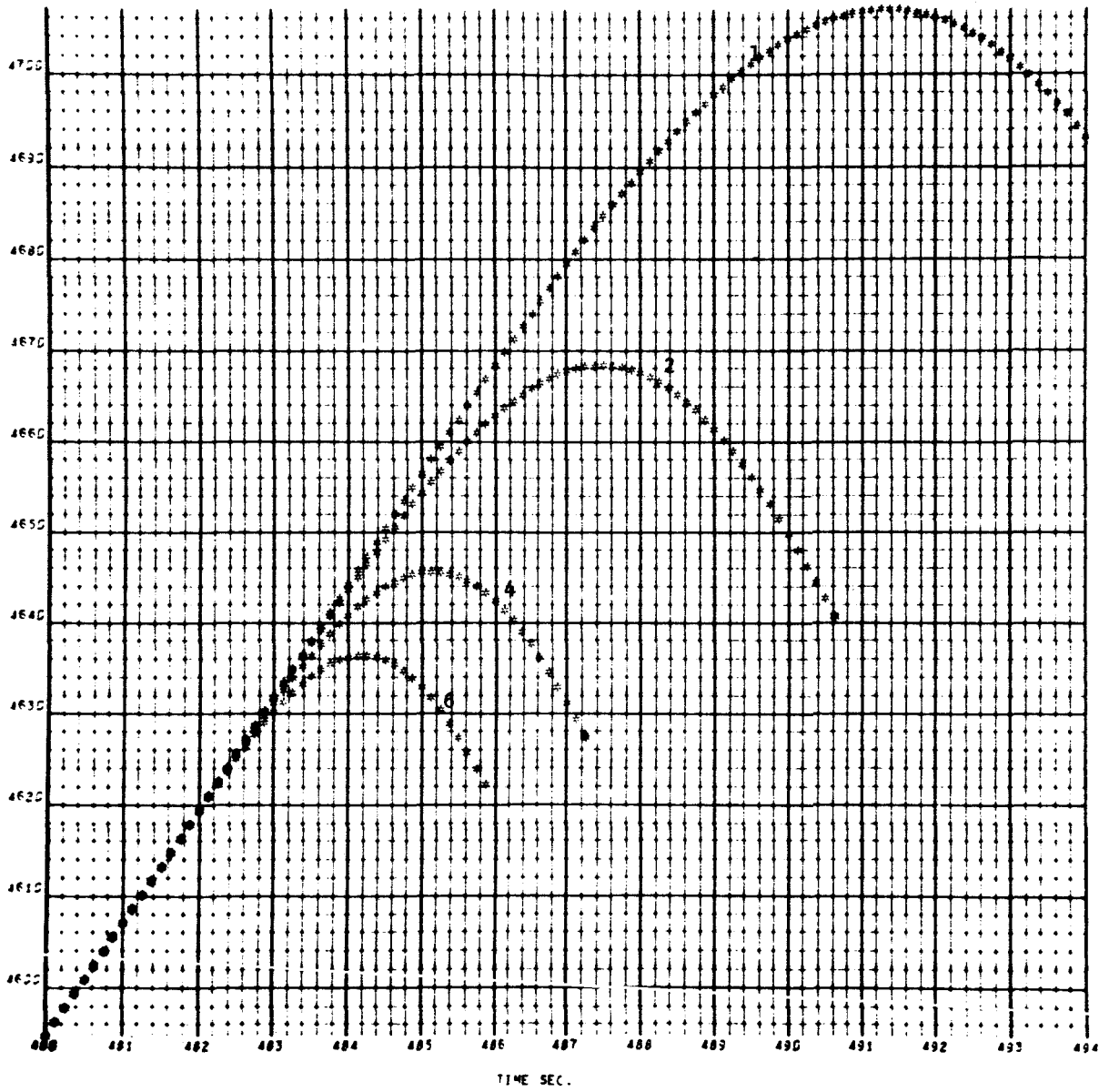$(-\beta_y$ of 6, 4, 2, 1) at $T_o = 300$ FIGURE 110

TIME SEC.

162

TIME SEC.

EARTH-FIXED VELOCITY AS A FUNCTION OF TIME FOR MALFUNCTION
$(-\beta_y$ of 6, 4, 2, 1) at T_o = 360

FIGURE 113

TIME SEC.

EARTH-FIXED VELOCITY AS A FUNCTION OF TIME FOR MALFUNCTION
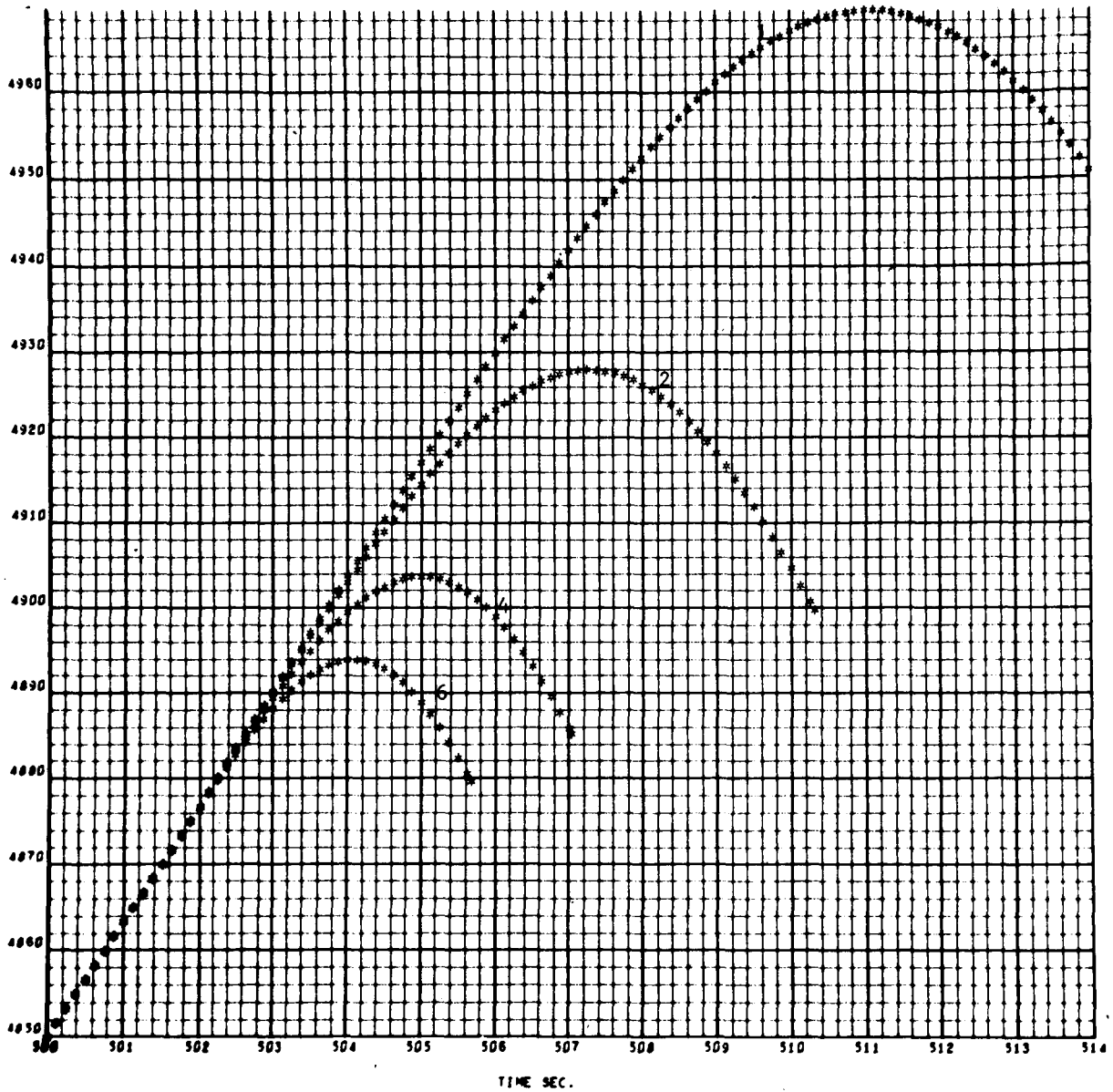($-\beta_y$ of 6, 4, 2, 1) at T_o = 380

FIGURE 114

TIME SEC.

TIME SEC.

EARTH-FIXED VELOCITY AS A FUNCTION OF TIME FOR MALFUNCTION
($-\beta_y$ of 6, 4, 2, 1) at T_o = 420   FIGURE 116

EARTH-FIXED VELOCITY AS A FUNCTION OF TIME FOR MALFUNCTION
$(-\beta_y$ of 6, 4, 2, 1) at $T_o = 440$ FIGURE 117
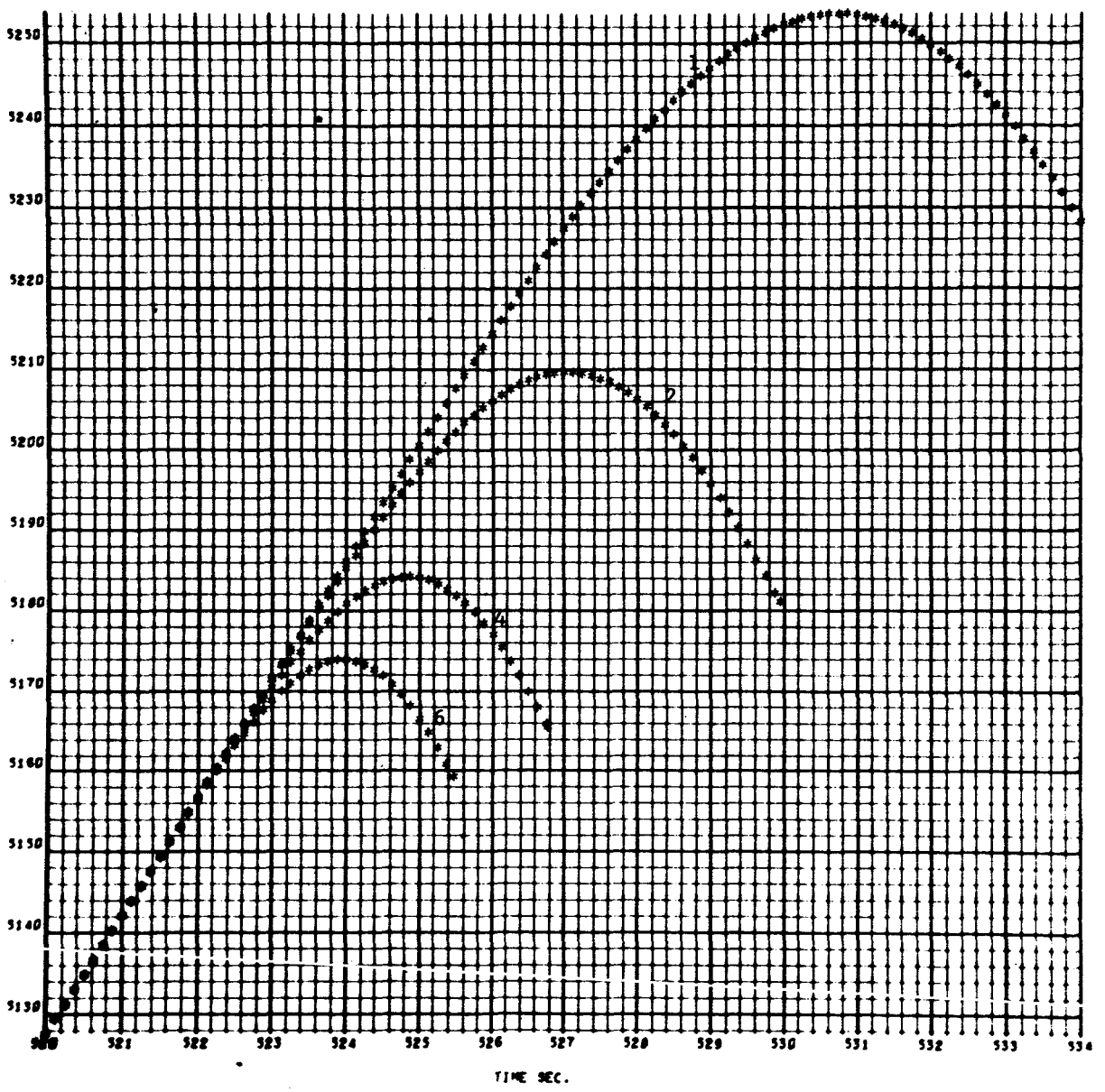
TIME SEC.

EARTH-FIXED VELOCITY AS A FUNCTION OF TIME FOR MALFUNCTION
($-\beta_y$ of 6, 4, 2, 1) at T_o = 460

FIGURE 118

TIME SEC.

TIME SEC.

EARTH-FIXED VELOCITY AS A FUNCTION OF TIME FOR MALFUNCTION
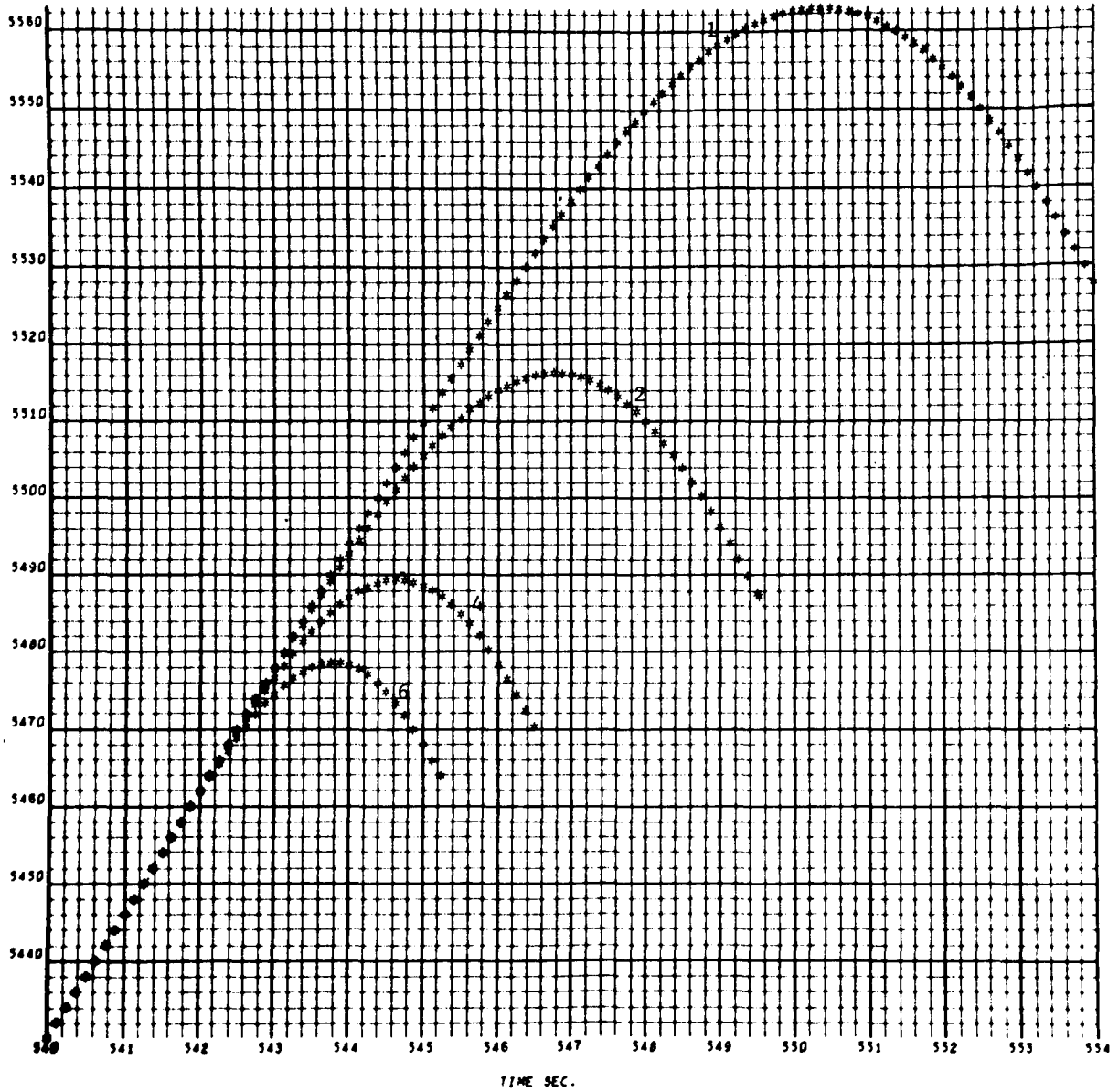($-\beta_y$ of 6, 4, 2, 1) at T_o = 500   FIGURE 120

TIME SEC.

TIME SEC.

EARTH-FIXED VELOCITY AS A FUNCTION OF TIME FOR MALFUNCTION
$(-\beta_y$ of 6, 4, 2, 1) at T_o = 540

FIGURE 122

TIME SEC.

EARTH-FIXED VELOCITY AS A FUNCTION OF TIME FOR MALFUNCTION
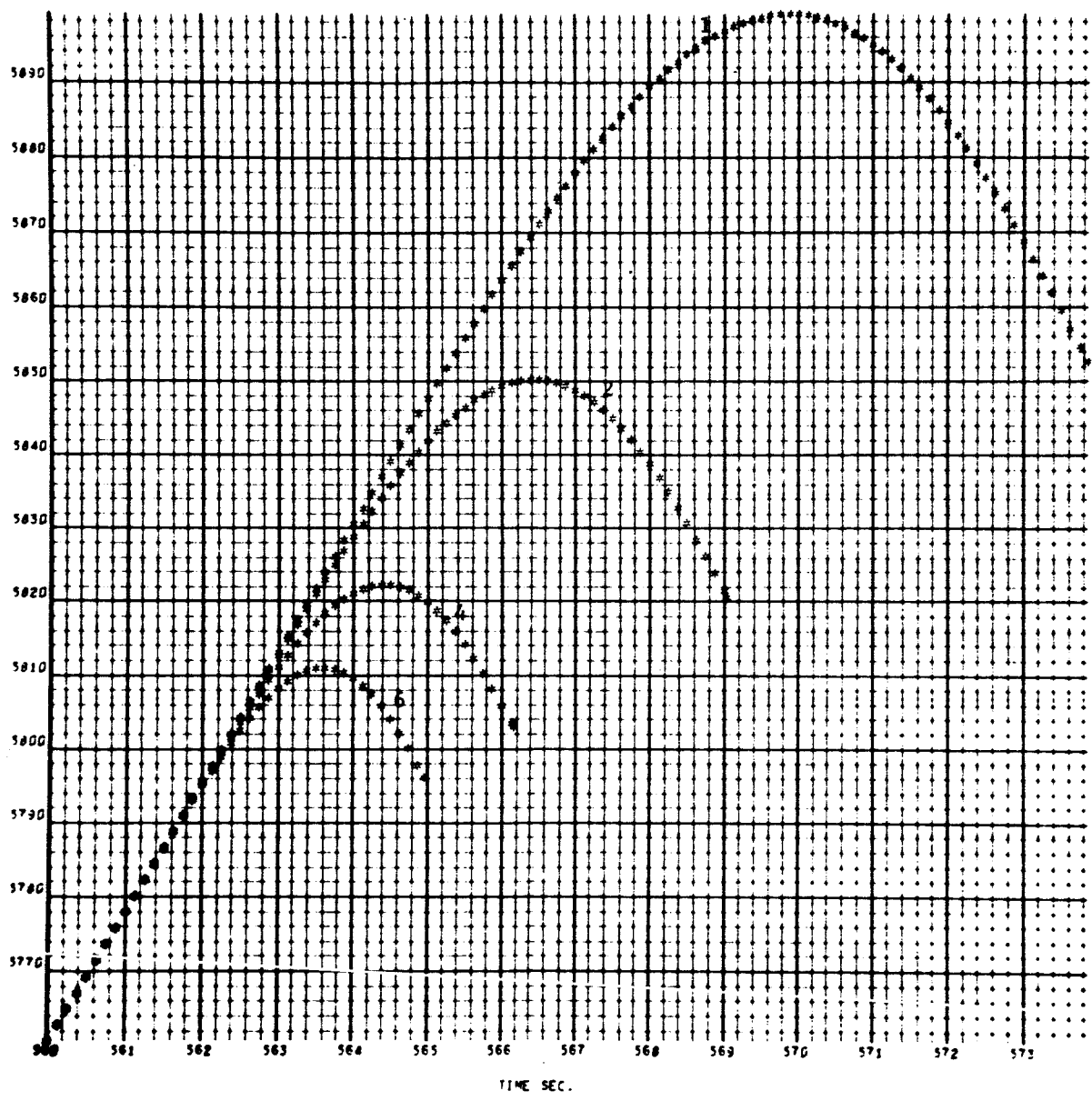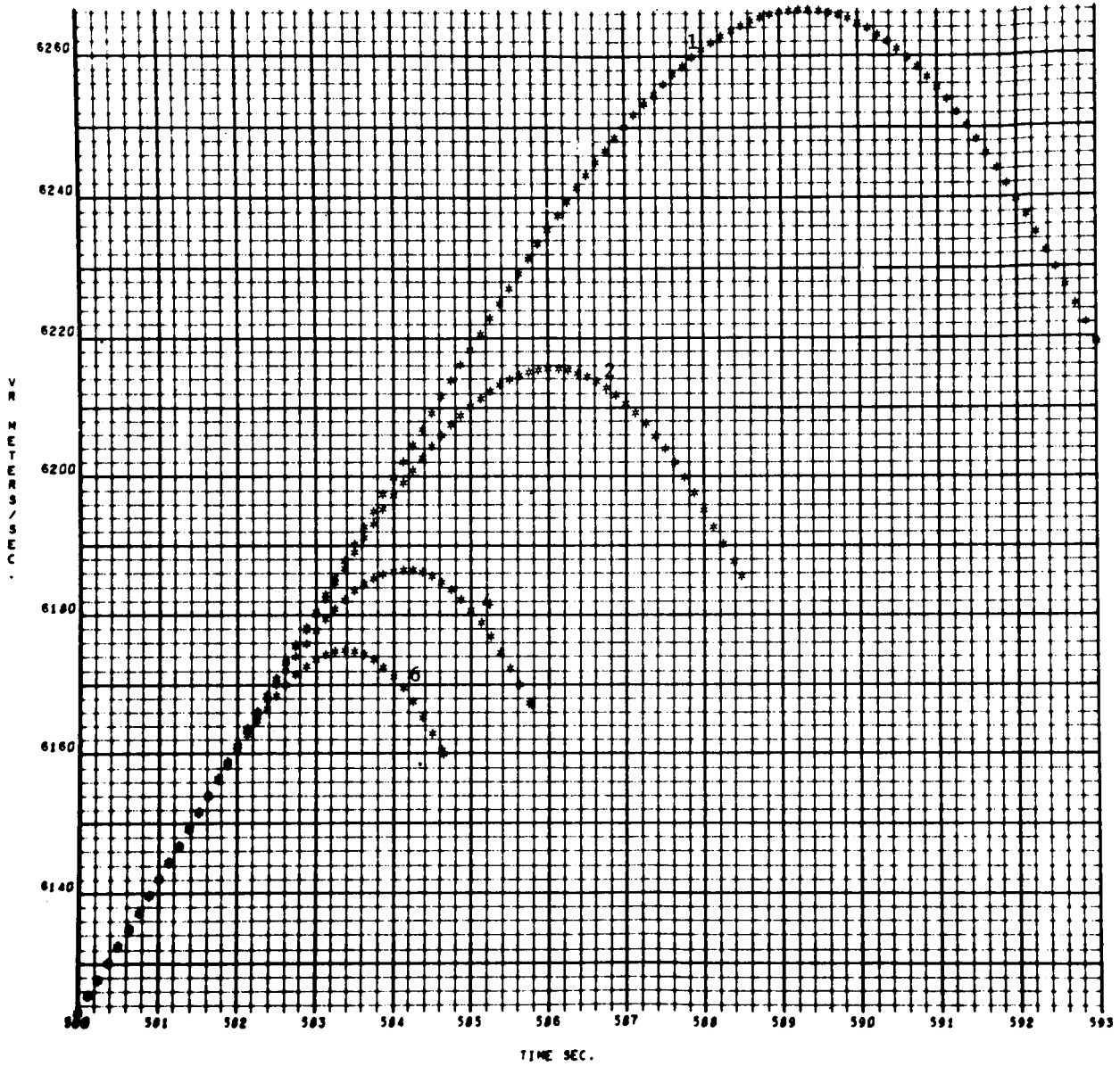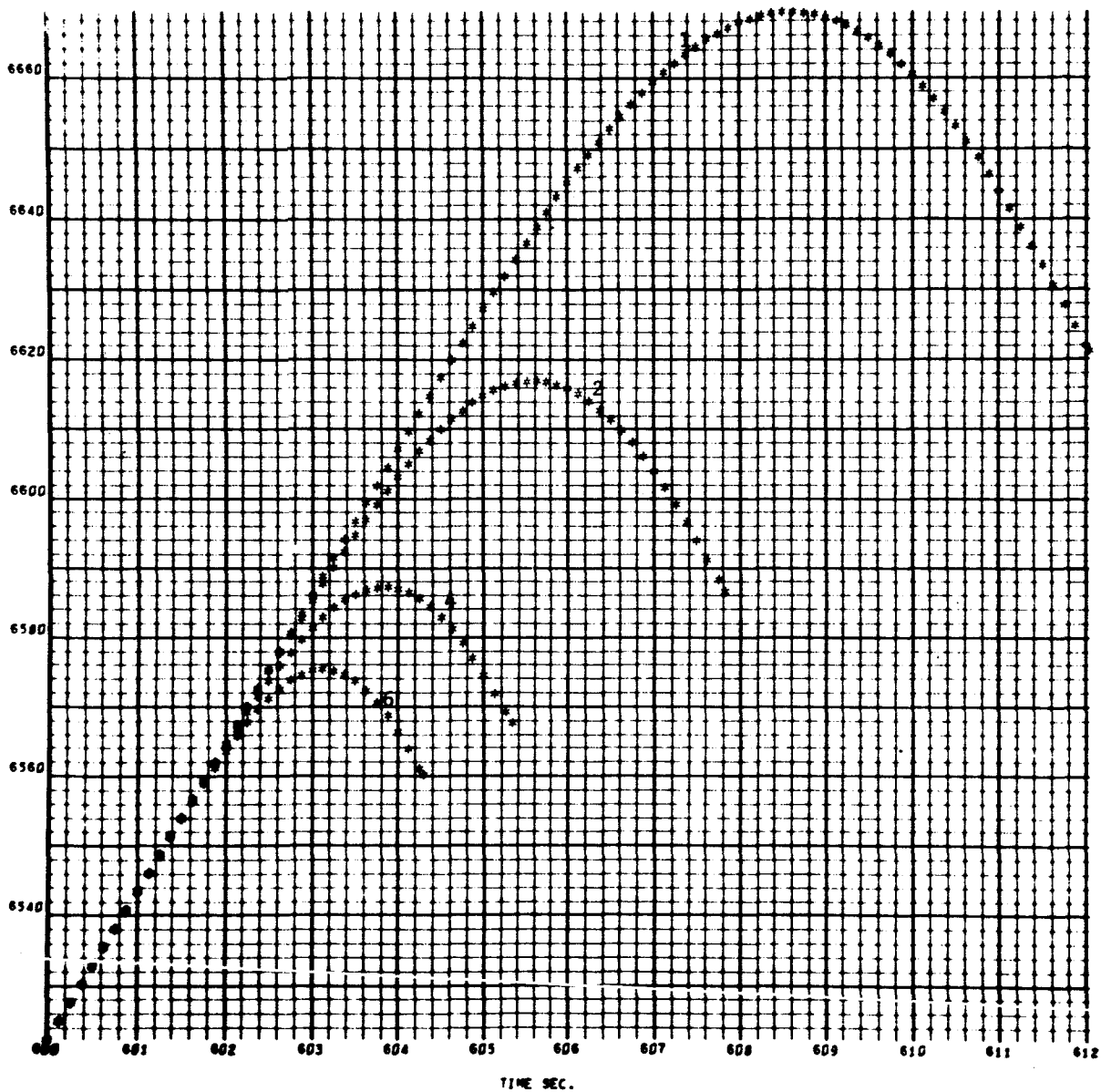(-β$_y$ of 6, 4, 2, 1) at T$_o$ = 560   FIGURE 123

TIME SEC.

EARTH-FIXED VELOCITY AS A FUNCTION OF TIME FOR MALFUNCTION
$(-\beta_y$ of 6, 4, 2, 1) at $T_o = 580$ FIGURE 124

EARTH-FIXED VELOCITY AS A FUNCTION OF TIME FOR MALFUNCTION ($-\beta_y$ of 6, 4, 2, 1) at T_o = 600
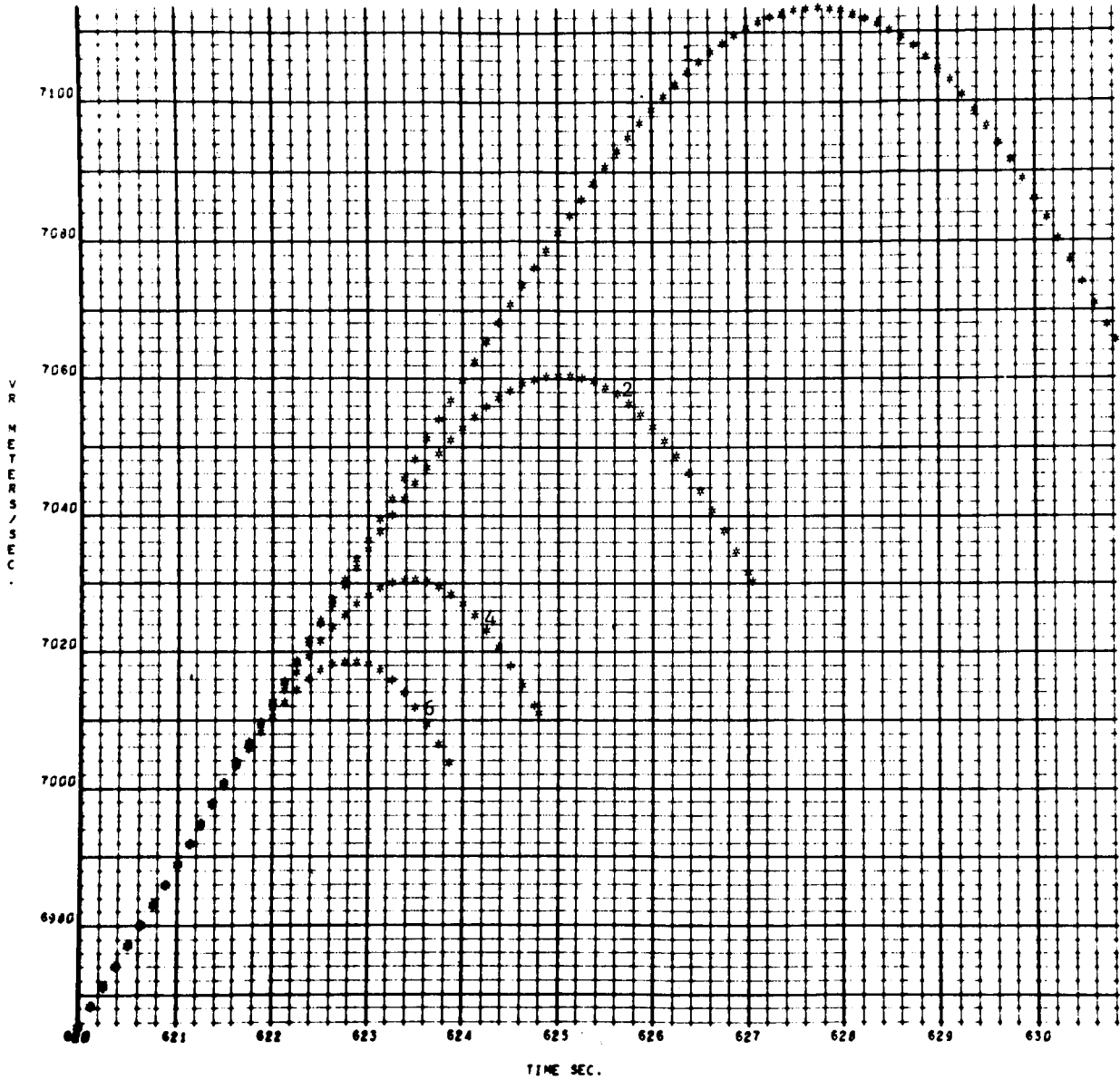
EARTH-FIXED VELOCITY AS A FUNCTION OF TIME FOR MALFUNCTION
($-\beta_y$ of 6, 4, 2, 1) at T_o = 620   FIGURE 126

TIME SEC.

REFERENCES

1. "Range Safety Aerodynamic Characteristics of Saturn I, Block II Vehicle Consisting of the SA-5, SA-6, and SA-7," M-AERO-AA, July 19, 1963.

2. "Cape Canaveral, Florida, Wind Profile Envelopes for Selected Flight Azimuths," Office Memorandum No. M-AERO-G-53-63, March 28, 1963, W. W. Vaughan.

3. SA-10 Predicted Trajectory to be published by R-AERO-FM.
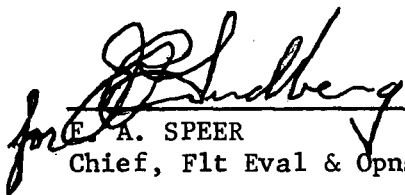
APPROVAL

RANGE SAFETY DATA FOR SATURN SA-10

by

G. W. Solmon and E. L. Leonard

The information in this report has been reviewed for security classification. Review of any information concerning Department of Defense or Atomic Energy Commission programs has been made by the MSFC Security Classification Officer. This report, in its entirety, has been determined to be unclassified.

L. O. STONE
Chief, Flight Mechanics Branch

E. A. SPEER
Chief, Flt Eval & Opns Studies Division

E. D. GEISSLER
Director, Aero-Astrodynamics Laboratory

DISTRIBUTION

R-DIR, Mr. Weidner
I-I/IB-SIV, Mr. Gerguson
MS-IPL (8)
V, Dr. Gruene
PF, Mr. Bishop
ED, Dr. Bruns
VG3, Mr. Chambers
ET, Mr. Collins
VE, Mr. Davidson
L, Mr. Gorman
PE, Major Hock
ED4, Mr. Jelen
VG4, Mr. Jenke
SF, Mr. Moore
T, Dr. Knothe (3)
VT, Mr. Moser
P, Colonel Petrone
GT, Mr. Russo
E, Mr. Sendler
VG4, Mr. Whiteside
VE, Mr. Williams
GTO2
GAO2
R-P&VE-AAL, Mr. Stafford
R-P&VE-VSA, Mr. Beck
CC-P, Mr. Wofford
R-AERO-DIR, Dr. Geissler
R-AERO-DIR, Mr. Jean
R-AERO-P, Mr. McNair
R-AERO-P, Mr. Teague (7)
R-AERO-P, Mr. Thionnet (6)
R-AERO-AD, Mr. Nash
R-AERO-Y, Mr. Vaughan
R-AERO-F, Dr. Speer
R-AERO-FM, Mr. Stone
R-AERO-FM, Mr. Leonard (8)
R-AERO-FM, Mr. Solmon
R-AERO-FM, Mr. Crafts

MSC

MSC-PT6, Mr. R. E. McKann
MSC-PS-3, Mr. C. H. Perrine, Jr.
MSC-FM, Mr. J. P. Mayer

MSC-FM, Mr. D. J. Incerto
MSC-STO, Mr. J. Funk
MSC-ASPO-SCE, Mr. T. H. Skopinski (4)
MSC-ASPO-SCE, Mr. Clay Hicks